Destabilization mechanisms of periodic pulse patterns near a homoclinic limit

Arjen Doelman[*], Jens Rademacher[†], Björn de Rijk[‡], Frits Veerman[§]

Abstract

It has been observed in the Gierer-Meinhardt equations that destabilization mechanisms are rather complex when spatially periodic pulse patterns approach a homoclinic limit. In this paper we show that this holds in much broader generality. While decreasing the wave number k, the character of destabilization alternates between two kinds of Hopf instabilities. In the first kind, a conjugated pair of so-called 1-eigenvalues crosses the imaginary axis exciting perturbations that are in phase with the periodic solution. In the second kind, a pair of -1-eigenvalues crosses the imaginary axis exciting anti-phase perturbations. In (parameter, wave number)-space, the curves $\mathcal{H}_{\pm 1}$ corresponding to ± 1-Hopf instabilities intersect infinitely often as they oscillate about each other, while both converging to the Hopf destabilization point of the homoclinic limit on the line $k = 0$, i.e. they perform a 'Hopf dance'. In an appropriate singular limit, the curves $\mathcal{H}_{\pm 1}$ generate the boundary of the region of stable pulse solutions – the so-called Busse balloon. The Busse-balloon boundary is non-smooth at intersections of $\mathcal{H}_{+1}$ and $\mathcal{H}_{-1}$ due to a surprisingly correlated higher order phenomenon: the 'belly dance'. In this paper, we employ recently developed spectral methods to show that both the Hopf and belly dance are persistent mechanisms that occur in a general class of singularly perturbed reaction-diffusion systems beyond the 'slowly linear' Gierer-Meinhardt equations. Moreover, we establish an explicit sign criterion to determine whether the homoclinic limit is the last or the first 'periodic' solution to destabilize. We illustrate our results by explicit calculations in a slowly nonlinear model system.

1 Introduction

The process of pattern formation is typically initiated by the appearance of spatially periodic patterns from a homogeneous state. In the setting of reaction-diffusion systems – which is the setting of the present paper – these patterns are most often generated by a Turing bifurcation, as a system parameter μ crosses through a critical value μ_T at which a spatially homogeneous state $\bar{u}_0$ becomes unstable [41]. While Turing's original work was restricted to linear reaction-diffusion systems, later a fully nonlinear treatment of this pattern generating mechanism has been embedded in the near-equilibrium theory of modulation equations. This theory has its origin in fluid mechanics and is applicable to the initiation of patterns in general classes of evolutionary partial differential equations on (unbounded) cylindrical domains. The evolution of small perturbations of the basic state $\bar{u}_0$ (measured in a well-chosen Banach space) is captured for μ sufficiently close to μ_T and for a finite, but asymptotically large, time by a modulation equation – typically a (complex) Ginzburg-Landau equation [24]. Through this Ginzburg-Landau approach it can be established that, if the bifurcation is supercritical, a one-parameter family of spatial patterns is generated as μ crosses through μ_T, typically with a subfamily of stable periodic patterns. In a graphical representation in the (μ, k)-plane – where k is the wave number (i.e. the reciprocal of the period) of the stable periodic pattern – the family of stable patterns corresponds to an (asymptotically small) open region, bounded by a curve that is at leading order given by the so-called Eckhaus parabola which has its extremum at (μ_T, k_T), where k_T is the critical wave number associated with the Turing instability in the setting of reaction-diffusion systems [12, 24].

The asymptotic theory is only valid for $|\mu - \mu_T|$ sufficiently small and it is natural to wonder how this asymptotically small region extends beyond the domain of validity of the modulation equations approach. A first continuation – in the context of convective roll patterns – has been explored in [2]. By direct numerical simulations, a balloon-shaped region in (parameter, wave number)-space was found within which stable roll patterns can be observed. This motivated the definition of the *Busse balloon* in the setting of evolutionary systems on unbounded domains: it is the region in (parameter, wave number)-space in which stable *wave trains* – i.e. spatially periodic patterns that travel with constant, often zero, speed – exist. In the context of fluid mechanics, the Busse balloon serves as the important first step towards turbulence. In

---

[*]Mathematisch Instituut, Universiteit Leiden, Niels Bohrweg 1, 2333 CA Leiden, The Netherlands

[†]Universität Bremen, Fachbereich Mathematik & Informatik, Bibliotheksstraße 5, 28359 Bremen

[‡]Institut für Analysis, Dynamik und Modellierung, Universität Stuttgart, Pfaffenwaldring 57, 70569 Stuttgart, Germany

[§]School of Mathematics, University of Edinburgh, James Clerk Maxwell Building, Peter Guthrie Tait Road, Edinburgh EH9 3FD, United Kingdom
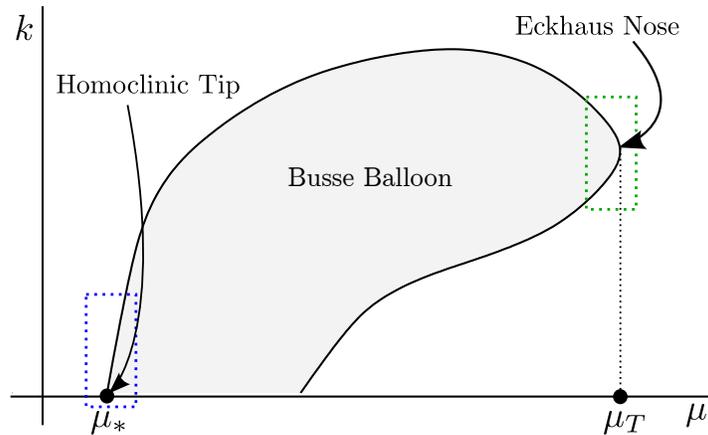
Figure 1: A sketch of a Busse balloon in (μ, k)-space. The underlying system undergoes a Turing bifurcation at $\mu = \mu_T$ yielding the onset of pattern formation with associated critical wave number k_T. In a neighborhood (in green) of the 'Eckhaus nose' (μ_T, k_T) analytic control over the Busse balloon is provided by the modulation equations approach. The Busse balloon closes at $(\mu_*, 0)$ at which a homoclinic limit pattern undergoes a Hopf destabilization. In this paper, we study the Busse balloon – and in particular its boundary – both analytically and numerically in a neighborhood (in blue) of the 'homoclinic tip' $(\mu_*, 0)$.

general, the Busse balloon is expected to play a similar role in related pattern forming systems. In fact, it appears as a central concept in the study of desertification processes in semi-arid ecosystems. Desertification is in its most simple form modeled by the Klausmeier [21, 37, 38] or the extended Klausmeier-Gray-Scott system [39, 40, 43], which are singularly perturbed 2-component reaction-diffusion systems of the type considered in the present work (if the ecosystem dynamics take place on a flat terrain). Stable spatially periodic vegetation patterns – i.e. patterns 'inside the Busse balloon' – bridge the gap between the fertile homogeneously vegetated state that is exhibited by the model if the rainfall parameter is sufficiently high and the bare soil state that appears as this parameter drops below a certain critical value. The (PDE) simulations of [37, 39, 40] show that these periodic vegetation patterns trace an intriguing path through the Busse balloon as the rainfall parameter changes (slowly) in time: as a pattern reaches the boundary of the Busse balloon, it 'bounces back' by an ecological 'mini-catastrophe' in which typically roughly half of the patterns simultaneously 'disappear'. Moreover, recent analysis and simulations of interacting pulse patterns in the same extended Klausmeier model [1] show that irregular patterns evolve towards spatially periodic patterns and that these are 'the most stable patterns', indicating that the Busse balloon acts as an attractor for pattern dynamics. Interpreting results in the literature on pulse dynamics in classical singularly perturbed systems as the Gray-Scott [27] and Gierer-Meinhardt [16] equations – see for instance [3, 47] and the references therein – strongly suggest that this phenomenon may be quite generic: irregular multi-pulse patterns naturally evolve towards regularity, i.e. the Busse balloon indeed seems to be an attractor in many singularly perturbed reaction-diffusion equations.

Nevertheless, there is remarkably little general insight in the nature of the Busse balloon – and especially in its boundary at which periodic patterns lose their stability – beyond the onset of pattern formation at its 'Eckhaus nose' – see Figure 1. In [31], co-dimension one instabilities of wave trains in reaction-diffusion systems on the real line are classified, thus providing insight in the possible nature of the boundary of a Busse balloon. The numerical analyses in [10, 39, 40, 43] indicate that such a classification only provides a very first glimpse into the realm of possible pattern destabilization mechanisms.

The Busse balloons presented in [10, 39, 40, 43] are all determined for the aforementioned two-component extended Klausmeier systems on the real line. For decreasing μ, each Busse balloon 'opens' at the 'Eckhaus nose' associated with a Turing bifurcation. Each balloon also 'closes' at a 'homoclinic tip' $(\mu, k) = (\mu_*, 0)$, at which a localized homoclinic pattern – that must be seen as the long-wavelength limit of a family of spatially periodic patterns as the wave number $k \downarrow 0$ – is the last pattern to become unstable; see the sketches in Figures 1 and 2(a). These observations confirmed earlier findings in the literature on the nature of the Busse balloon – and especially on the appearance of the 'homoclinic tip' – in the Gray-Scott and Gierer-Meinhardt models – see [10, 42] and Remark 1.2. Moreover, the desertification simulations of [37, 39, 40] also indicate that the homoclinic tip has a direct ecological relevance: it is found that the final collapse of the ecosystem into the bare soil state takes place very close to this homoclinic tip – which in ecological terms corresponds to an 'oasis state'.
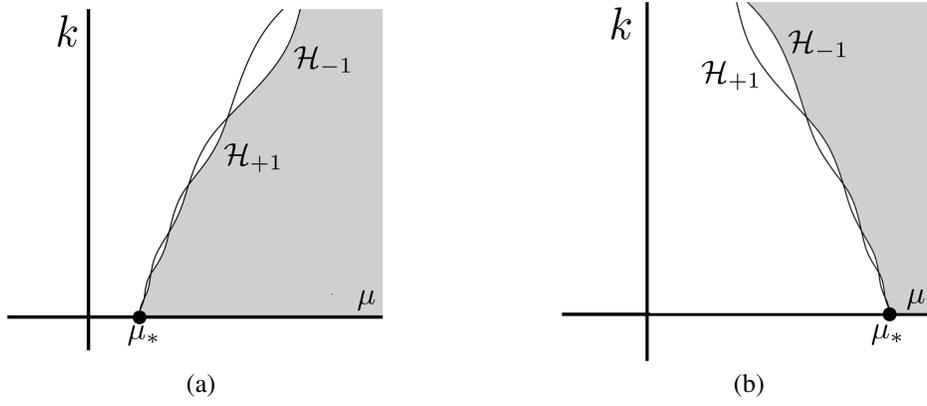
Figure 2: A zoomed-in sketch of a part of a Busse balloon (in gray) near a homoclinic tip $(\mu_*, 0)$ at which a homoclinic limit pattern undergoes a Hopf destabilization. In (a), the homoclinic pattern is the last 'periodic' pattern to become unstable as the parameter μ is decreased, i.e. Ni's conjecture is satisfied. The homoclinic pattern already destabilizes before its adjacent long-wavelength periodic patterns as μ decreases in (b), i.e. Ni's conjecture does not hold. In both cases, the boundary of the Busse balloon is (in an appropriate singular limit) determined by two intertwining Hopf destabilization curves, $\mathcal{H}_{+1}$ and $\mathcal{H}_{-1}$. At the intersection points, the boundary of the Busse balloon is non-smooth.

In all cases considered in the aforementioned literature, the tip of the Busse balloon on the line $k = 0$ corresponds to a homoclinic pulse (a localized 1-pulse) that is the last of all 'periodic' patterns to become unstable. In fact, it is always destabilized by a Hopf mechanism, i.e. the spectrum associated with the linearization of the system about the homoclinic pulse pattern contains a pair of (non-zero) complex conjugate eigenvalues crossing the imaginary axis at $\mu = \mu_*$. Although not formulated in the terminology of Busse balloons, a similar observation was already made by Wei-Ming Ni in [25] in the form of a conjecture about spatially periodic patterns in the (generalized) Gierer-Meinhardt equation – see Remark 1.1. Here, we formulate the conjecture as follows:

Ni's conjecture: *the homoclinic limit pattern is the most stable pattern within the family of (long-wavelength) spatially periodic patterns, in the sense that it is the last pattern to become unstable – or the first to become stable – as a parameter is varied. Moreover, the (de)stabilization is of Hopf type.*

A priori, there is no obvious argument to support Ni's conjecture (except for the observations in numerical simulations of example systems): near a homoclinic tip $(\mu_*, 0)$, the boundary of a Busse balloon could in principle also be oriented in such a way that (long-wavelength) periodic patterns may be stable while their homoclinic limit is not – see Figure 2(b).

Although there seem to be some similarities between the distinction 'Ni' vs. 'no-Ni' as depicted in Figure 2 and the distinction sub- vs. supercritical bifurcation, the situation is much more subtle. For instance, families of long-wavelength periodic patterns and their homoclinic limits may exist both for $\mu > \mu_*$ and for $\mu < \mu_*$. More importantly, near the homoclinic tip $(\mu_*, 0)$, the boundaries of the Busse balloons in [10, 43] also exhibit an intricate and non-smooth structure induced by two intertwining curves of two types of Hopf destabilizations, $\mathcal{H}_{+1}$ and $\mathcal{H}_{-1}$. At a +1-Hopf destabilization a conjugated pair of so-called 1-eigenvalues crosses the imaginary axis exciting perturbations that are in phase with the periodic solution. At a −1-Hopf destabilization a pair of −1-eigenvalues crosses the imaginary axis exciting anti-phase perturbations. Although the numerical analyses in [10, 43] only yield a limited number of such intersections of $\mathcal{H}_{+1}$ and $\mathcal{H}_{-1}$, it is strongly suggested – and in fact confirmed analytically in [10] in the context of Gierer-Meinhardt systems (see Remark 1.2) – that there is a countably infinite number of such intersections that converge to the critical value $(\mu_*, 0)$ as $k \downarrow 0$, at which the homoclinic pattern destabilizes – see again Figure 2 for a sketch. We emphasize that, although the curves $\mathcal{H}_{+1}$ and $\mathcal{H}_{-1}$ are well-defined beyond the homoclinic tip $(\mu_*, 0)$, they might diverge from the boundary of the Busse balloon sufficiently far away from the tip, which is observed in simulations in [10], where the curves $\mathcal{H}_{\pm 1}$ are traced globally.

Long-wavelength periodic patterns limiting on a homoclinic pattern provide a 'far-from-equilibrium' setting within which a general analysis of the boundary of the Busse balloon may be developed in the spirit of the near-equilibrium modulation equations approach – at least, in the setting of reaction-diffusion systems on the real line. Based on [14], it is shown in [15, 35] that the spectral curves associated with the stability of long-wavelength periodic patterns converge to the spectrum of the homoclinic limit as $k \downarrow 0$. If the homoclinic pulse undergoes a Hopf destabilization, i.e. if the system is near a homoclinic tip of the Busse balloon as in Figure 2, then the spectrum associated with a nearby periodic pulse pattern –

i.e. a long-wavelength solution with wave number $|k| \ll 1$ – crosses the imaginary axis at some $\mu = \mu(k)$-value close to μ_* (which not necessarily yields the destabilization of the pattern – see below). However, the insights of [15, 35] are not sufficiently refined to unravel the structure of the boundary of the Busse balloon near the tip $(\mu_*, 0)$.

In this paper, we will determine the fine-structure of the Busse balloon near a homoclinic tip of Hopf type as sketched in Figure 2. We will do so by employing the recently developed spectral methods of [5, 6, 7, 11] for the stability of spatially periodic and homoclinic (pulse) patterns to a general class of *singularly perturbed* two-component reaction-diffusion systems

$$\begin{cases} u_t &= u_{\check{x}\check{x}} - H_1(u, v, \varepsilon) - \varepsilon^{-1} H_2(u, v) \\ v_t &= \varepsilon^2 v_{\check{x}\check{x}} - G(u, v, \varepsilon) \end{cases} , \quad u \in \mathbb{R}, v \in \mathbb{R}, \tag{1.1}$$

or, in the 'fast' spatial scale $x = \varepsilon^{-1}\check{x}$,

$$\begin{cases} \varepsilon^2 u_t &= u_{xx} - \varepsilon^2 H_1(u, v, \varepsilon) - \varepsilon H_2(u, v) \\ v_t &= v_{xx} - G(u, v, \varepsilon) \end{cases} , \quad u \in \mathbb{R}, v \in \mathbb{R}, \tag{1.2}$$

where $0 < \varepsilon \ll 1$, H_1, H_2 and G are smooth functions of ε at $\varepsilon = 0$, and H_2 and G vanish at $v = 0$. The term $\varepsilon^{-1} H_2$ in (1.1) guarantees the possibility of having stable localized pulse patterns in semi-strong interaction [7, 11]. Here, the concept of 'semi-strong interactions' refers to the fact that localized structures in singularly perturbed reaction-diffusion equations typically interact 'strongly' through their slow components – u in (1.1)/(1.2) – while their fast components only interact 'exponentially weakly' (i.e. the fast components are exponentially close to the (fast reduced) stable background state – $v \equiv 0$ in (1.1)/(1.2) – in between two fast excursions) [8, 29]. We refer to Section 2 for more assumptions on the interaction terms (and their motivation). This class (1.1)/(1.2) significantly extends the aforementioned specific Gray-Scott and Gierer-Meinhardt models, most importantly since it is in general *slowly nonlinear*. This terminology refers to the nonlinear nature of the slow-reduced scalar u-equation

$$u_t = u_{\check{x}\check{x}} - H_1(u, 0, 0), \quad u \in \mathbb{R}, \tag{1.3}$$

that governs the leading-order flow of (1.1) outside the asymptotically small $\check{x}$-regions in which the v-component of the spatially periodic and homoclinic pulse patterns is *not* exponentially small – see Figure 3. Note that all the aforementioned Gray-Scott-/Gierer-Meinhardt-type models considered in the literature are *slowly linear* (i.e. these models correspond to explicit versions of (1.1) in which $H_1(u, 0, 0)$ is a linear function of u). The concept of *slowly nonlinear* singularly perturbed reaction-diffusion systems was introduced in [11, 46]. Apart from the fact that the spectral analysis associated with pulse patterns, which was developed in the context of slowly linear models, had to be rigorously re-developed – see [5, 6, 7, 11] – slowly nonlinear models are also particularly interesting from the original fluid mechanical point of view of the Busse balloon as the first step from a homogeneous basic state towards turbulence [2]. So far, numerical simulations of slowly linear (two-component, singularly perturbed, reaction-diffusion) systems in the literature indicate that there are no stable spatial patterns of increased complexity beyond the boundary of the Busse balloon. For instance, Hopf destabilizations at the boundary of the Busse balloon that are encountered (numerically) in the literature known to the authors seem to be sub-critical: the destabilized pulse oscillates and 'disappears'. In fact, one could say that the success of the Klausmeier-Gray-Scott model as conceptual model for the process of desertification [21, 40, 43] is directly related to this – especially from the mathematical point of view – very intriguing feature: once the homogeneously vegetated state has become unstable with respect to a Turing bifurcation, the homogeneous bare soil desert state appears to be the only attractor beyond the boundary of the Busse balloon of stable vegetation patterns [40, 43]. Thus, in these systems, the Busse balloon seems to describe both the first and the final step in the pattern forming process. The simulations presented in [46] – which exhibit stable periodically, quasi-periodically and chaotically oscillating pulses – indicate that this is certainly not the case for slowly nonlinear models: here, the Busse balloon indeed seems to be the first step in the transition from trivial to complex spatio-temporal dynamics. This is supported analytically by the results in [45], in which it is established – in the context of a slowly nonlinear system – that the Hopf destabilization of a homoclinic pulse pattern in (1.1) may change its nature from sub-critical to supercritical. Moreover, it is confirmed in [45] that the Hopf destabilization is sub-critical in the classical/canonical (slowly linear) Gierer-Meinhardt system.

Although our main goal is to obtain a general, analytical grip on aspects of the far-from-equilibrium boundary of a Busse balloon, we have chosen – unlike [15, 35] – to study the structure of a Busse balloon near a homoclinic tip $(\mu_*, 0)$ in the setting of a special kind of reaction-diffusion systems: (1.1) is singularly perturbed (since we assume $0 < \varepsilon \ll 1$). Such systems appear naturally in many applications. More importantly, while exhibiting behavior of a richness comparable to general reaction-diffusion systems, the singularly perturbed nature of (1.1) provides a framework by which this behavior
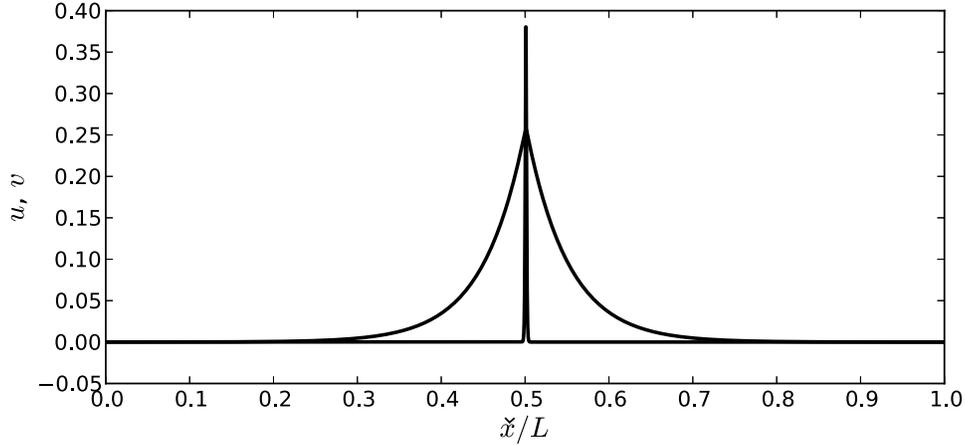
Figure 3: A numerically obtained profile of one period of a typical spatially periodic, nearly homoclinic, long-wavelength solution to the weakly nonlinear system (1.2), for a specific choice of $H_{1,2}$ and G. The v-component is strongly localized, the u-component is a solution to (1.3) in the region in which v is exponentially small. More specifically, the profile is a marginally stable solution to the basic model (1.4) scaled in the slow spatial variable $\check{x}$ as in (1.2) with $\varepsilon \approx 0.015$, $\nu_1 \approx -1.04$, $\nu_2 \approx 0.49$, $\mu_1 \approx 0.44$, $\mu_2 = 0$, $\mu_3 = 1$ and with wavelength $L = 20$.

can be unraveled by exploiting the small parameter ε.

Based on the methods developed in [5, 6, 7, 11], we will show that we can go beyond the leading-order – but non-singularly perturbed – results of [15, 35] and indeed establish the fine-structure of Busse balloons near a homoclinic tip as sketched in Figure 2. To do so, we restrict ourselves to stationary, reversibly symmetric, patterns – see Sections 2 and 7. We suppose that system (1.1) depends on a parameter μ and that a (non-degenerate) Hopf destabilization of a stable homoclinic pulse solution occurs at $\mu = \mu_*$. Thus, two simple conjugate eigenvalues, $\lambda_{\infty,\mu}$ and $\bar{\lambda}_{\infty,\mu}$, corresponding to the homoclinic pulse, cross the imaginary axis away from the origin at $\mu = \mu_*$. We know from [7, 11] that these homoclinic pulses can be seen as limit states of a family of stationary, reversibly symmetric, spatially periodic patterns (in the limit $\ell \to \infty$, where ℓ is a measure for the wavelength) – see Theorem 4.1. We also know by combining the reversibility symmetry of the patterns with Floquet theory, that the homoclinic eigenvalues $\lambda_{\infty,\mu}$ and $\bar{\lambda}_{\infty,\mu}$ are approximated (in the limit $\ell \to \infty$) by two critical pieces of spectral curves $\{\lambda_{\ell,\mu}(\gamma_r); \gamma_r \in [-1, 1]\}$ and $\{\bar{\lambda}_{\ell,\mu}(\gamma_r); \gamma_r \in [-1, 1]\}$ associated with the stability of the long-wavelength pattern – see [7, 10, 15, 35] and Theorem 4.5 for the quantitative details. We will see that the nature of the boundary of the Busse balloon – as sketched in Figure 2 – is controlled by the behavior of the critical spectral curve $\lambda_{\ell,\mu}(\gamma_r)$ as function of μ and ℓ ($\gg 1$).

However, there is another spectral curve that may be decisive for the stability of the long-wavelength patterns: the (real) spectral curve $\lambda^s_{\ell,\varepsilon}(\nu), \nu \in [0, 2\pi]$ of 'small spectrum' [18, 42] that is attached to the origin $\lambda = 0$ and that shrinks to the origin as $\varepsilon \to 0$ – see Figure 4. The position of this curve can be controlled by the methods recently developed in [5, 6] – see Section 3.3.1 and especially Theorem 3.4 (which is proven in [5, 6]). It also follows from [5, 6] that the position of $\lambda^s_{\ell,\varepsilon}(\nu)$ with respect to the imaginary axis – i.e. Figure 4(a) vs. 4(b) and (c) – does not change in the homoclinic limit (i.e. as $\ell \to \infty$) and is determined by the sign of certain explicit quantities (that only need the asymptotic profile of the homoclinic pulse as input – see [5, 6, 36] and Theorem 4.3). This leads to a sign condition that guarantees that the curve of small spectrum does not enter the right-half plane, provided the wavelength is sufficiently large. Consequently, one can test whether the stability properties of the limiting homoclinic are inherited by the nearby periodic pulse solutions – or not, as in Figure 4(a) – see Theorem 4.7.

The core of this paper concerns the analysis – and numerical validation – of the precise location of the critical spectral curve $\lambda_{\ell,\mu}(\gamma_r)$ for long-wavelength patterns beyond the leading-order result $\lambda_{\ell,\mu}(\gamma_r) \to \lambda_{\infty,\mu}$ as $\ell \to \infty$ of [15, 35]. Based on [7, 11], we derive explicit expansions of $\lambda_{\ell,\mu}(\gamma_r)$ in ℓ (in the limit $\varepsilon \to 0$) that – again – only need the input from the homoclinic limit. The outcome of our analysis is presented graphically in Figure 4: $\lambda_{\ell,\mu}(\gamma_r)$ is at leading order (in ℓ) an exponentially short straight line segment. The distance between this segment and $\lambda_{\infty,\mu}$ is given by another – larger – exponentially small term (in ℓ) multiplied by an ℓ-independent complex number L_0 that can be determined explicitly: L_0 determines the direction (in $\mathbb{C}$) of the translation of the segment with respect to $\lambda_{\infty,\mu}$ – see Figure 4(b), respectively 4(c), in
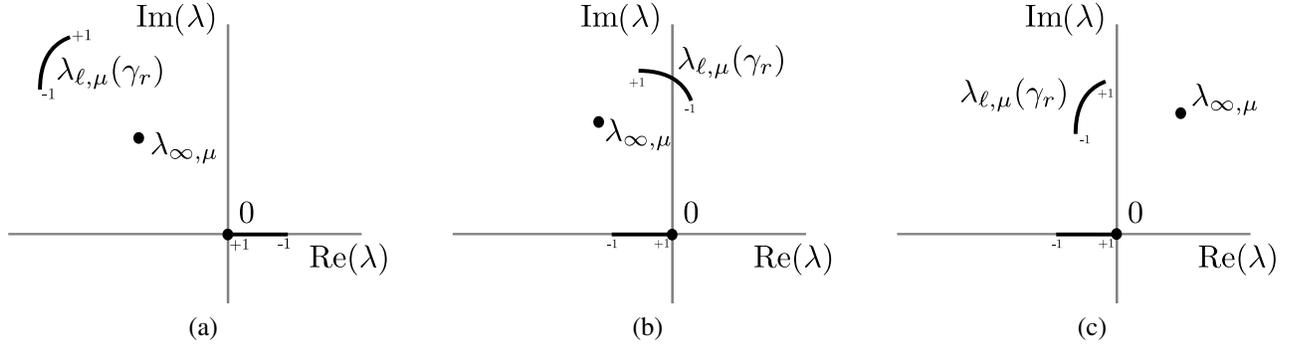
Figure 4: Three sketches of the critical spectrum associated with a long-wavelength periodic pulse pattern near a Hopf type homoclinic tip of a Busse balloon, i.e. the parameter μ is close to the Hopf destabilization value μ_* of the homoclinic limit and the wavelength ℓ is sufficiently large. The spectral curve $\lambda_{\ell,\mu}(\gamma_r)$ converges to the critical eigenvalue $\lambda_{\infty,\mu}$ of the homoclinic limit as $\ell \to \infty$, whereas the curve of small spectrum $\lambda_{\ell,\varepsilon}^s(\nu)$ converges to the origin as $\ell \to \infty$. In panel (a), the homoclinic limit is stable and the spectral curve $\lambda_{\ell,\mu}(\gamma_r)$ also is in the stable half plane. However, the small spectrum $\lambda_{\ell,\varepsilon}^s(\nu)$ is unstable. In panel (b), the homoclinic limit is stable and Ni's conjecture holds: the small spectrum $\lambda_{\ell,\varepsilon}^s(\nu)$ is stable but the segment $\lambda_{\ell,\mu}(\gamma_r)$ is (partly) unstable. In panel (c), both $\lambda_{\ell,\varepsilon}^s(\nu)$ and $\lambda_{\infty,\mu}(\gamma_r)$ are in the stable half plane. The long-wavelength pattern is stable, however, its homoclinic limit is unstable: Ni's conjecture is violated.

which $\mathrm{Re}(L_0) > 0$, respectively $\mathrm{Re}(L_0) < 0$, and Theorem 4.5 for the details. The orientation of the line segment $\lambda_{\ell,\mu}(\gamma_r)$ is determined by the argument of an expression $L_1 e^{-2\omega_\infty \ell}$, where both $L_1, \omega_\infty \in \mathbb{C}$ can again be determined explicitly (Theorem 4.5). The facts that $\mathrm{Re}(\omega_\infty) > 0$ and $\mathrm{Im}(\omega_\infty) \neq 0$ imply that $\lambda_{\ell,\mu}(\gamma_r)$ not only shrinks as $\ell \to \infty$, but that it also rotates (with (asymptotically) constant speed) as a function of ℓ (while it approaches $\lambda_{\infty,\mu}$).

Under the assumption that the aforementioned sign condition is satisfied such that the small spectrum $\lambda_{\ell,\varepsilon}^s(\nu)$ does not enter the unstable half plane, we may conclude from the above results that the boundary of the Busse balloon (in the limit $\varepsilon \to 0$) near a homoclinic tip associated with a Hopf destabilization must indeed be as sketched in Figures 2(a) or (b). The sign of $\mathrm{Re}(L_0)$ determines whether the homoclinic pattern is the last or the first 'periodic' pulse to become unstable as μ decreases. If $\mathrm{Re}(L_0) > 0$ as in Figure 4(b), Ni's conjecture holds – i.e. $\lambda_{\infty,\mu}$ only passes through the imaginary axis (for decreasing μ) after all $\lambda_{\ell,\mu}(\gamma_r)$-segments (for ℓ sufficiently large) – and the orientation of the boundary of the Busse balloon is as in Figure 2(a). If Ni's conjecture does not hold – Figure 4(c) with $\mathrm{Re}(L_0) < 0$ – then the boundary of the Busse balloon is oriented as in Figure 2(b). A non-degenerate first intersection of a straight segment crossing through the imaginary axis must occur at its endpoints. Therefore, the boundary of the Busse balloon is (in the limit $\varepsilon \to 0$) described by the two curves $\mathcal{H}_{\pm 1}$ determined by those values of μ and ℓ, or equivalently the wave number k, for which $\lambda_{\ell,\mu}(\pm 1) \in i\mathbb{R}$ – see also Figure 5. Thus, the long-wavelength pattern is (to leading order) either destabilized by a perturbation with approximately the same wavelength, which corresponds to $\lambda_{\ell,\mu}(1) \in i\mathbb{R}$, or a perturbation with approximately twice its wavelength, that is, $\lambda_{\ell,\mu}(-1) \in i\mathbb{R}$. The sign of the oscillating expression $\mathrm{Re}(L_1 e^{-2\omega_\infty \ell})$ (as a function of ℓ) determines which of these two cases hold. Hence, it follows that the boundary of the Busse balloon (in the limit $\varepsilon \to 0$) near a homoclinic tip of Hopf type must indeed have a fine-structure of two intertwining curves with countably many intersections that limit on $\lambda_{\infty,\mu}$ as sketched in Figures 2 (a) and (b). This was called the *Hopf dance* in [10] (see also Remark 1.2).

However, the segment $\lambda_{\ell,\mu}(\gamma_r)$ cannot be expected to be perfectly straight. A further perturbation analysis confirms that this segment is (slightly) parabolically deformed – see Theorem 4.5 and Corollary 4.8. The orientation of this parabolic 'belly' determines the nature of the boundary of the Busse balloon near the intersections of $\mathcal{H}_{+1}$ and $\mathcal{H}_{-1}$, i.e. near situations where $\mathrm{Re}(L_1 e^{-2\omega_\infty \ell}) = 0$ so that the line segment $\lambda_{\ell,\mu}(\gamma_r)$ is (to leading order) vertical at its passage through the imaginary axis. If the belly points into the unstable half plane for a solution on $\mathcal{H}_{+1} \cap \mathcal{H}_{-1}$, then there is a small piece of the boundary of the Busse balloon near, but away from, $\mathcal{H}_{+1} \cap \mathcal{H}_{-1}$ that is determined by curves $\mathcal{H}_{\gamma_r^{in}}$ with $-1 < \gamma_r^{in} < 1$ (i.e. the first point that hits the imaginary axis is given by $\lambda_{\ell,\mu}(\gamma_r^{in}) \in i\mathbb{R}$ for some $\gamma_r^{in} \neq \pm 1$). As a consequence, the local boundary of the Busse balloon is smooth (in the limit $\varepsilon \to 0$) without any co-dimension 2 points. This is not the case if the belly points into the stable half plane. Then, $\mathcal{H}_{+1}$ and $\mathcal{H}_{-1}$ indeed cover the boundary of the Busse balloon (in the limit $\varepsilon \to 0$), including the co-dimension 2 points in $\mathcal{H}_{+1} \cap \mathcal{H}_{-1}$ where the endpoints of the segment $\lambda_{\ell,\mu}(\gamma_r)$ pass simultaneously through the imaginary axis (thus where $\lambda_{\ell,\mu}(\pm 1) \in i\mathbb{R}$ for the same – critical – value of μ). Perhaps the most surprising outcome of our analysis is that, within the full class of slowly nonlinear systems (1.1), the parabolic belly always points into the left-half plane and thus only the second type of intersections can occur (for ℓ sufficiently large) – see Corollary 4.8 and
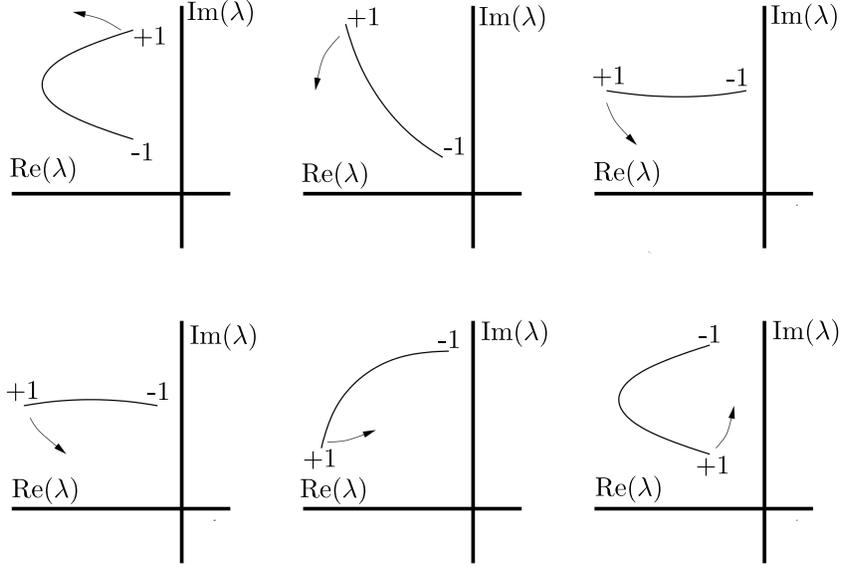
Figure 5: The belly dance as a series of sketches of the rotating spectral curve $\lambda_{\ell,\mu}(\gamma_r)$ for increasing ℓ. The sketches are corrected for exponential shrinking and the parabolic deformations are exaggerated. If $\lambda_{\ell,\mu}(\gamma_r)$ is vertical the 'belly' always points to the left: the point on the curve with largest real part must be one of the endpoints $\lambda_{\ell,\mu}(\pm 1)$.

Remark 1.2. Like in the Gray-Scott and Gierer-Meinhardt models [10], $\lambda_{\ell,\mu}(\gamma_r)$ performs a *belly dance* as ℓ increases. This 'dance' is sketched in Figure 5: while the line segment $\lambda_{\ell,\mu}(\gamma_r)$ makes half a turn, the parabolic deformation moves from one side of the straight connection between $\lambda_{\ell,\mu}(+1)$ and $\lambda_{\ell,\mu}(-1)$ to the other. Thus, we may conclude that the boundary of the Busse balloon (in the limit $\varepsilon \to 0$) near a homoclinic tip of Hopf type is given *exactly* by the non-smooth union of countably many successive pieces of the intertwining curves $\mathcal{H}_{+1}$ and $\mathcal{H}_{-1}$, including the intermediate co-dimension 2 intersection points $\mathcal{H}_{+1} \cap \mathcal{H}_{-1}$ – as was already sketched in Figure 2. Furthermore, we establish that the non-smoothness of the boundary of the Busse balloon persists for sufficiently small $\varepsilon > 0$.

As a second (sub)theme of this paper, we present a detailed analysis of an *explicit* slowly nonlinear model,

$$\begin{cases} \varepsilon^2 u_t &= u_{xx} - \varepsilon^2 \mu_1 \sin u - \varepsilon \nu_1 \left(v^2 - \nu_2 v^3 \right) \\ v_t &= v_{xx} - v + \frac{v^2}{\mu_2 + \mu_3 \sin u} \end{cases} , \quad u \in \mathbb{R}, v \in \mathbb{R}, \tag{1.4}$$

given in the form of (1.2) with nonlinearities $H_{1,2}$ and G and parameters $\mu_{1,2}$ and $\nu_{1,2,3}$ specified as,

$$\begin{aligned} H_1(u,v,\varepsilon) &= \mu_1 \sin u, & \mu_1 > 0, \\ H_2(u,v) &= \nu_1 \left(v^2 - \nu_2 v^3 \right), & \nu_1 > 0, \nu_2 \geq 0, \\ G(u,v,\varepsilon) &= v - \frac{v^2}{\mu_2 + \mu_3 \sin u}, & \mu_2 \geq 0, \mu_3 >, 0 \end{aligned} \tag{1.5}$$

see Section 2.1 for more details on (1.5) and its relation to (the conditions on) (1.2). In Section 2.1, we explicitly study the existence problem associated with (1.4) and explain the richness of potential stationary patterns exhibited by the model – see for instance Figure 7. In Section 3.4, we follow the general approach developed in [7] to obtain explicit control over the spectrum associated with the stability of spatially periodic pulse patterns to (1.4). The critical spectral curve $\lambda_{\ell,\mu}(\gamma_r)$ is determined by the outcome of this analysis – see (3.50). Moreover, we numerically determine the spectra associated with several (numerical) solutions of (1.4) (for various specified choices of parameters). We present examples in which Ni's conjecture hold and examples where it does not hold, and confirm (the first stages of) the Hopf and belly dances numerically. Finally, we compare the numerics with the outcome to the explicit stability analysis of patterns in (1.4) of Section 3.4.

The set-up of the paper is as follows. In Sections 2 and 3 we present overviews of the existence and stability analysis of patterns in (1.2) (and (1.4)) based on [7, 11]. Our main results – which establish the Hopf and belly dance and thus the structure of the Busse balloon near a homoclinic tip of Hopf type sketched in Figure 2 – are presented in full quantitative detail in Section 4. The proofs of these results are postponed until Section 6. In Section 5, we compare our analytical findings with numerical approximations. We end with a short discussion and outlook in Section 7.

Remark 1.1. In his 1988 review paper [25], Wei-Ming Ni considered the stability of a 'boundary-peak' as a solution to the generalized (and singularly perturbed) Gierer-Meinhardt equation on a bounded interval. Theorem 2 in [25] establishes that this 1-pulse pattern – or better: 1/2-pulse pattern, since the singular pulse sits at the boundary of the domain – is stable in the shadow system limit of the Gierer-Meinhardt system. The shadow system corresponds to the limit $d_2 \to \infty$, where d_2 is the diffusion coefficient of the slow component (since (1.1) is considered on the unbounded domain $\mathbb{R}$, d_2 is scaled to 1 in the present paper). This stability result is confirmed by numerical simulations of the Gierer-Meinhardt system itself with d_2 'sufficiently big'. Ni conjectures in the discussion of this result and these simulations (2nd column on page 14 of [25]), '*It is conjectured that as d_2 decreases, more and more multi-peak spike-layer steady states become stable. Heuristically, since the rapidly diffusing inhibitor suppresses the formation of new spikes close to the existing ones, the larger d_2 becomes, the fewer stable spikes are expected.*' Transferring this statement to spatially unbounded domains $\mathbb{R}$, brings us to 'Ni's conjecture' as formulated in this paper. Thus, we interpret this stament as the first observation of the 'homoclinic tip' of a Busse balloon associated to a system of reaction-diffusion equations.

Remark 1.2. The analysis [42] of spatially periodic pulse patterns in the (slowly linear, two-component) generalized Gierer-Meinhardt equation can be seen as a predecessor of the existence and stability analysis of spatially periodic pulse patterns in the general class of singularly perturbed $(m + n)$-component slowly nonlinear reaction-diffusion systems – where m is the number of slow and n of fast components – in [7]. In [42], the rotating behavior of critical spectral curves $\lambda_{\ell,\mu}(\gamma_r)$ in the long-wavelength limit was observed but was not interpreted in terms of a fine-structure of the boundary of an associated Busse balloon. This behavior was first observed numerically in the context of the Gray-Scott model and established analytically in the Gierer-Meinhardt model (both in [10]). The belly dance mechanism was also first observed in [10] and established for the Gierer-Meinhardt model. It was conjectured in the discussion of [10] that the Hopf dance is a generic mechanism; our present results confirm this. However, the analysis of the Gierer-Meinhardt models in [10] suggested that the belly dance is driven by the – in the present terminology – slow linearity of these models. Thus it was – as we now know incorrectly – conjectured that the belly dance would disappear in slowly nonlinear models.

2   Review of existence results

In this section, we review existence results for periodic pulse patterns and homoclinic pulses in (1.1)/(1.2), in a unified way. A new result for a one-parameter family of long-wavelength periodic pulses that converge to a homoclinic pulse will be given in §4.1. We are interested in stationary, reversibly symmetric, periodic pulse solutions of system (1.1)/(1.2) that approach a homoclinic limit. As mentioned in §1, we impose the following assumptions on the interaction terms of (1.1)/(1.2).

(S1)   *Conditions on the interaction terms*
There exists open, connected sets $U, V, I \subset \mathbb{R}$ with $0 \in V, I$ such that H_1, G and H_2 are C^3 on their domains $U \times V \times I$ and $U \times V$, respectively. Moreover, we have $H_2(u, 0) = 0$ and $G(u, 0, \varepsilon) = 0$ for all $u \in U$ and $\varepsilon \in I$.

Stationary solutions to (1.2) satisfy

$$\begin{cases} u_x &= \varepsilon p \\ p_x &= \varepsilon H_1(u, v, \varepsilon) + H_2(u, v) \\ v_x &= q \\ q_x &= G(u, v, \varepsilon) \end{cases} \quad , \quad u \in U, p \in \mathbb{R}, v \in V, q \in \mathbb{R}. \tag{2.1}$$

The pulse solutions under consideration in this paper arise from a concatenation of solutions to a series of reduced subsystems of (2.1) in the singular limit $\varepsilon \to 0$. If we take $\varepsilon = 0$ in (2.1), the dynamics is given by the *fast reduced system*,

$$\begin{cases} u_x &= 0 \\ p_x &= H_2(u, v) \\ v_x &= q \\ q_x &= G(u, v, 0) \end{cases} \quad , \quad u \in U, p \in \mathbb{R}, v \in V, q \in \mathbb{R}. \tag{2.2}$$

We observe that the manifold $\mathcal{M} = \{(u, p, 0, 0) : u \in U, p \in \mathbb{R}\}$ consists entirely of equilibria of (2.2) by **(S1)**. We require $\mathcal{M}$ to be normally hyperbolic.

(S2)   *Normal hyperbolicity*
There exists a lower bound $G_0 > 0$ such that for each $u \in U$ it holds $\partial_v G(u, 0, 0) \geq G_0$.

When $\varepsilon > 0$, the manifold $\mathcal{M}$ consists no longer of equilibria, but remains invariant. The flow restricted to $\mathcal{M}$ is to leading order governed by the so-called *slow reduced system*,

$$\begin{cases} u_{\check{x}} & = & p \\ p_{\check{x}} & = & H_1(u, 0, 0) \end{cases}, \quad u \in U, p \in \mathbb{R}. \tag{2.3}$$

System (2.3) is R_s-reversible, where $R_s \colon \mathbb{R}^2 \to \mathbb{R}^2$ is the reflection in the line $p = 0$.

It is well known that the dynamics around such a normally hyperbolic manifold $\mathcal{M}$ is captured by Fenichel's geometric singular perturbation theory [13]. Suppose we have obtained a so-called singular orbit by piecing together orbit segments of the fast and slow reduced systems. Although this singular orbit is not a solution to the full system, one can prove in some cases, with the aid of Fenichel's theory, that an actual orbit lies in the vicinity of the singular one, provided $\varepsilon > 0$ is sufficiently small.

In this paper we are interested in solutions to (2.1) that are close to singular orbits that consist of a pulse satisfying the fast reduced system (2.2) and a segment on the invariant manifold $\mathcal{M}$, satisfying the slow reduced system (2.3). The following assumption ensures the existence of a pulse in the fast reduced system.

(E1) *Existence of a pulse solution to the fast reduced system*
There exists $u_\diamond \in U$ such that system,

$$\begin{cases} v_x & = & q \\ q_x & = & G(u, v, 0) \end{cases}, \quad v \in V, q \in \mathbb{R}, \tag{2.4}$$

has for fixed $u = u_\diamond$ a solution $\kappa_h(x, u_\diamond) = (v_h(x, u_\diamond), q_h(x, u_\diamond))$ homoclinic to 0 with $q_h(0, u_\diamond) = 0$.

Since system (2.4) is R_f-reversible, where $R_f \colon \mathbb{R}^2 \to \mathbb{R}^2$ is the reflection in the line $q = 0$, assumption **(E1)** implies the existence of a neighborhood $U_h \subset U$ of $u_\diamond$ such that for every $u \in U_h$ there exists a homoclinic solution $\kappa_h(x, u)$ to (2.4) with $q_h(0, u) = 0$. It holds $\kappa_h(x, u) = R_f \kappa_h(-x, u)$ for $x \in \mathbb{R}$. The homoclinics $\kappa_h(x, u)$ yield pulse solutions

$$\phi_h(x, u) := \left(u, \int_0^x H_2(u, v_h(z, u)) dz, v_h(x, u), q_h(x, u) \right),$$

to (2.2), which are homoclinic to $\mathcal{M}$. The limits $\lim_{x \to \pm\infty} \phi_h(x, u)$ give rise to the so-called *take-off* and *touch-down curves* on $\mathcal{M}$. For that reason, we define the mapping $\mathcal{J} \colon U_h \to \mathbb{R}$ by

$$\mathcal{J}(u) = \int_0^\infty H_2(u, v_h(z, u)) dz. \tag{2.5}$$

The graphs $T_\pm := \{(u, \pm\mathcal{J}(u)) : u \in U_h\}$ represent the take-off and touch-down curves. Indeed, it holds $\lim_{x \to \pm\infty} \phi_h(x, u) = (u, \pm\mathcal{J}(u), 0, 0)$. Having defined these curves, we are able to the state the existence result for periodic and homoclinic pulse solutions to (2.1).

Theorem 2.1. *[7, Theorem 2.11], [11, Theorem 2.1] Assume* **(S1)**-**(S2)** *and* **(E1)** *hold true. Suppose there exists a solution $\psi_\ell(\check{x}) = (u_\ell(\check{x}), p_\ell(\check{x}))$ to (2.3), that intersects the touch-down curve T_+ transversally at $\check{x} = 0$ and satisfies $\lim_{\check{x} \to \ell} p_\ell(\check{x}) = 0$ for some $0 < \ell \leq \infty$. Then, for any $\delta > 0$ there exists $\varepsilon_\delta > 0$ such that for each $\varepsilon \in (0, \varepsilon_\delta)$ there exists a solution $\phi_{\ell,\varepsilon}(x)$ to (2.1) satisfying the following assertions*

1. *Character of solution*
   If $0 < \ell < \infty$, then $\phi_{\ell,\varepsilon}$ is $2L_{\ell,\varepsilon}$-periodic, where $|\varepsilon L_{\ell,\varepsilon} - \ell| \leq C\varepsilon$ for some ε-independent constant $C > 0$. If $\ell = \infty$, then $\phi_{\ell,\varepsilon}$ is a homoclinic solution.

2. *Singular limit*
   The Hausdorff distance between the orbit of $\phi_{\ell,\varepsilon}$ in $\mathbb{R}^4$ and the singular orbit

$$\{(u_\ell(\check{x}), \pm p_\ell(\check{x}), 0, 0) : \check{x} \in [0, \ell]\} \cup \{\phi_h(x, u_\ell(0)) : x \in \mathbb{R}\},$$

   is smaller than δ.

3. *Reversibility*
   The solution $\phi_{\ell,\varepsilon}(x)$ is reversibly symmetric about the hyperplane $\{p = q = 0\}$: it holds $\phi_{\ell,\varepsilon}(x) = \mathcal{R}\phi_{\ell,\varepsilon}(-x)$ for $x \in \mathbb{R}$, where $\mathcal{R} \colon \mathbb{R}^4 \to \mathbb{R}^4$ is the reflection in the hyperplane $\{p = q = 0\}$.

It should be remarked that the solutions established by Theorem 2.1 are the most simple stationary, reversible, solutions: the associated homoclinic and periodic orbits in (2.1) only make one single 'jump' through the fast field. Following the approach of [7, 11], orbits that combine various different kinds of jumps can be constructed. Based on the Evans function approach of [7, 11], the spectral stability of the corresponding patterns can also be established – see also [9, 42].

2.1 Existence of pulse solutions in the model equation

We apply the analysis developed in the current paper – and the preceding papers [7, 11] – to the explicit, slowly nonlinear system (1.4). Note that the nonlinearities (1.5) clearly satisfy assumptions **(S1)** (we choose $U = (0, 2\pi)$). Moreover, we have $\partial_v G(u, 0, 0) = 1$, thereby satisfying assumption **(S2)**. A priori, system (1.4) could be singular in u, however, we will only consider patterns with u-components such that $\mu_2 + \mu_3 \sin u$ remains bounded away from 0.

The slow reduced (existence) system is given by

$$\begin{cases} u_{\check{x}} &= p \\ p_{\check{x}} &= \mu_1 \sin u \end{cases} , \quad u \in U, p \in \mathbb{R}, \tag{2.6}$$

widely known as the model for the mathematical (nonlinear) pendulum. The system (2.6) is Hamiltonian, and can be integrated to obtain the relation

$$\frac{1}{2\mu_1} u_{\check{x}}^2 + \cos u = 2\kappa^2 - 1. \tag{2.7}$$

The level sets of (2.7), parameterized by κ, characterize the solutions of (2.6). The level set $\kappa = 0$ is equal to the set of equilibria of (2.6), while the level set $\kappa = 1$ contains the two heteroclinic orbits connecting the saddles at $u = 0$ and $u = 2\pi$. All bounded (periodic) orbits, which lie within the bounded region 'in between' the two heteroclinics, are concentrically parameterized by $0 < \kappa < 1$, see also Figure 6. The 'bottom' heteroclinic orbit, which converges to $u = 0$ as $\check{x} \to \infty$, is given by

$$u_\infty(\check{x}; \check{x}_0) = 4 \arctan e^{-\sqrt{\mu_1}(\check{x}+\check{x}_0)}, \tag{2.8}$$

while the periodic orbits, parameterized by $0 < \kappa < 1$, can be expressed in terms of the Jacobi elliptic function $\mathrm{cd}(z, \kappa)$ [32, §22.2], yielding

$$u_\ell(\check{x}; \kappa, \pm) = \pi \pm 2 \arcsin\left(\kappa \, \mathrm{cd}(\sqrt{\mu_1}(\check{x} - \ell), \kappa)\right), \quad 0 < \ell < 2K(\kappa), \tag{2.9}$$

where $K(\kappa)$ is the complete elliptic integral of the first kind [32, §19.1]. For $u_\ell(\check{x}; \kappa, \pm)$ as in (2.9), we have $\lim_{\check{x} \to \ell} \partial_{\check{x}} u_\ell(\check{x}; \kappa, \pm) = 0$. As $u_\ell(\check{x}; \kappa, \pm)$ is periodic in $\check{x}$ with period $\frac{4}{\sqrt{\mu_1}} K(\kappa)$, we have $u_\ell(\check{x} + \frac{2}{\sqrt{\mu_1}} K(\kappa); \kappa, +) = u_\ell(\check{x}; \kappa, -)$. The reason for making the distinction between $u_\ell(\check{x}; \kappa, +)$ and its $\frac{2}{\sqrt{\mu_1}} K(\kappa)$-shifted counterpart $u_\ell(\check{x}; \kappa, -)$ is that, due to its periodicity, p_ℓ vanishes twice during one period. The $\pm$ sign in $u_\ell(\check{x}; \kappa, \pm)$ indicates the sign of the initial value $p_\ell(0; \kappa, \pm)$; this implies that $\check{x} = \ell$ is always the *first* point where $\partial_{\check{x}} u_\ell(\check{x}; \kappa, \pm)$ vanishes.

The fast reduced system is given by

$$\begin{cases} v_x &= q \\ q_x &= v - \frac{v^2}{\mu_2 + \mu_3 \sin u} \end{cases} , \quad v \in V, q \in \mathbb{R}. \tag{2.10}$$

System (2.10) has a R_f-reversible solution homoclinic to 0 for any $u = u_\diamond \in U$, its first component given by

$$v_h(x, u_\diamond) = \frac{3}{2}(\mu_2 + \mu_3 \sin u_\diamond) \operatorname{sech}^2 \frac{x}{2}, \tag{2.11}$$

with $\partial_x v_h(0, u_\diamond) = 0$, thereby satisfying assumption **(E1)**. The function $v_h(x, u_\diamond)$ (2.11) can be used to obtain an explicit expression for $\mathcal{J}(u)$ (2.5), yielding

$$\mathcal{J}(u) = \nu_1 \int_0^\infty v_h(z, u)^2 - \nu_2 v_h(z, u)^3 \, dz = 3\nu_1(\mu_2 + \mu_3 \sin u)^2 \left(1 - \frac{6}{5}\nu_2(\mu_2 + \mu_3 \sin u)\right). \tag{2.12}$$

The phase plane of the slow reduced system (2.6), including the graphs of the take-off and touchdown curves $T_\pm = \{(u, \pm \mathcal{J}(u))\}$ are shown in Figure 6.
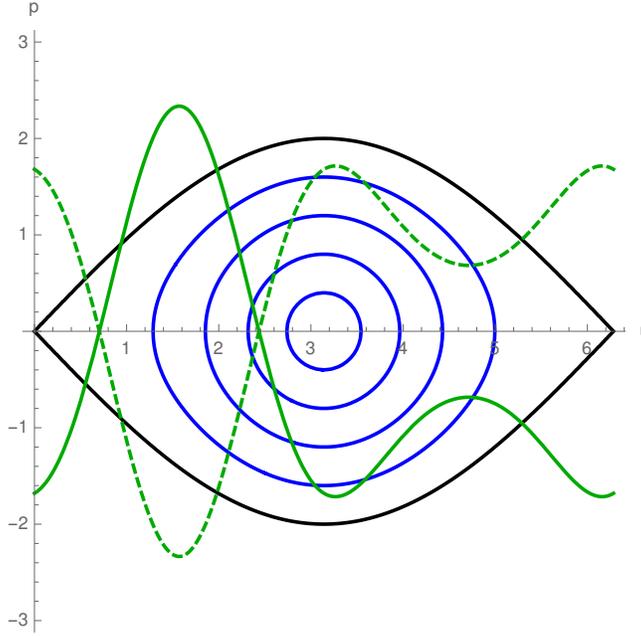
Figure 6: The phase plane of (2.6) for $0 < u < 2\pi$. The heteroclinic orbits, where $\kappa = 1$ (c.f. (2.7)), are drawn in black. Several periodic orbits, parameterized by $0 < \kappa < 1$, are drawn in blue. The take-off curve $T_- = \{(u, -\mathcal{J}(u))\}$ (2.12) is drawn in green, solid; the touchdown curve $T_+ = \{(u, \mathcal{J}(u))\}$ is drawn in green, dashed. Here, $\nu_1 = 2$, $\mu_2 = 1$ and $\nu_2 = \frac{3}{5} = \mu_3$.

The intersections of the touchdown curve T_+ with the orbits of the slow system (2.6) can be calculated using the conserved quantity (2.7), yielding,

$$\frac{1}{2\mu_1}\mathcal{J}(u)^2 + \cos u = 2\kappa^2 - 1. \tag{2.13}$$

Nondegenerate solutions of (2.13) correspond to transversal intersections of the touchdown curve T_+ with the orbits of the slow system (2.6). The assumptions of Theorem 2.1 are satisfied if $u_\infty(0; \check{x}_0)$ (2.8) solves (2.13) for $\kappa = 1$ (the case $\ell = \infty$), or if $u_\ell(0; \kappa, \pm)$ (2.9) solves (2.13) for $0 < \kappa < 1$ (the case $0 < \ell < \infty$); see also Figure 7.

3 Overview of spectral analysis

In order to study the destabilization mechanisms of periodic pulse solutions to (1.2) as these approach a homoclinic limit, we need detailed analytical properties of the spectra of the linearizations about these periodic pulse solutions. The (critical) spectra in both the homoclinic and periodic case are given by the zero sets of analytic functions, the so-called *Evans functions*. Thus, the Evans function is a tool to locate the spectrum. The passage to the singular limit $\varepsilon \to 0$ of the Evans function $\mathcal{E}_\varepsilon$ – associated to patterns in singularly perturbed reaction-diffusion systems – is well understood. In fact, there exists an explicit *reduced Evans function* $\mathcal{E}_0$, whose zeros approximate those of $\mathcal{E}_\varepsilon$. This reduced Evans function admits a factorization in a slow and a fast component that correspond to properly scaled, lower-dimensional, slow respectively fast eigenvalue problems. In this section, we define these Evans functions and provide their explicit reductions in the singular limit for both the homoclinic and periodic case as obtained in [7, 11].

Assume we satisfy the conditions for Theorem 2.1. Let $\phi_{\ell,\varepsilon}(x)$, for $\varepsilon > 0$ sufficiently small, be the pulse solution to (2.1) as described in Theorem 2.1. Denote by $\check{\phi}_{\ell,\varepsilon}(\check{x})$ the corresponding solution to the PDE (1.1). We linearize system (1.1) about $\check{\phi}_{\ell,\varepsilon}$ and obtain a differential operator $\mathcal{L}_{\ell,\varepsilon}$ on the space $C_{ub}(\mathbb{R}, \mathbb{R}^2)$ of bounded and uniformly continuous functions. We are interested in the spectrum of $\mathcal{L}_{\ell,\varepsilon}$ and consider the eigenvalue problem $\mathcal{L}_{\ell,\varepsilon}\varphi = \lambda\varphi$ for $\lambda \in \mathbb{C}$. This eigenvalue problem can be written as a first order system,

$$\varphi_x = \mathcal{A}_{\ell,\varepsilon}(x, \lambda)\varphi, \quad \varphi \in \mathbb{R}^4. \tag{3.1}$$

In the next two subsections, we analyze the cases $\ell = \infty$ and $0 < \ell < \infty$ separately.
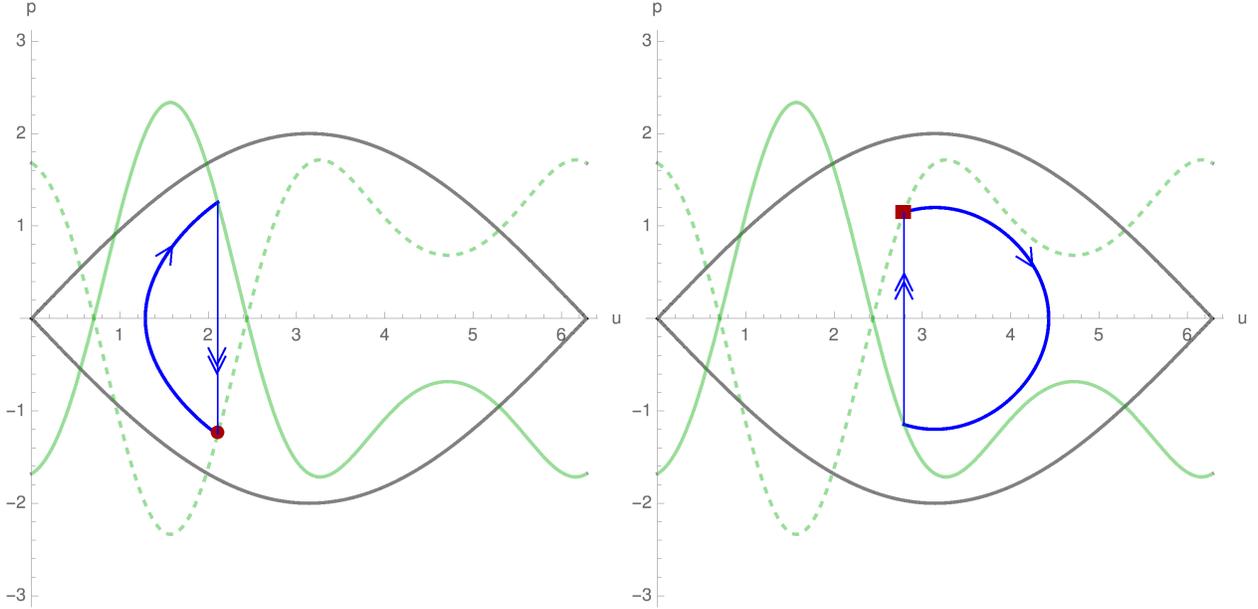
Figure 7: Two possible singular orbits in the phase plane of (2.6) for $0 < u < 2\pi$. The parameter values are as in Figure 6. As in Figure 6, the take-off curve T_- is drawn in green, solid, and the touchdown curve T_+ in green, dashed. Left, the initial point of the slow orbit, indicated by a red dot, is in the lower half plane; its coordinates are $(u_\ell(0; \frac{4}{5}, -), p_\ell(0; \frac{4}{5}, -))$. Right, the initial point of the slow orbit, indicated by a red square, is in the upper half plane; its coordinates are $(u_\ell(0; \frac{3}{5}, +), p_\ell(0; \frac{3}{5}, +))$.

3.1 Evans function for homoclinic pulse solutions

First we consider the case $\ell = \infty$ in Theorem 2.1. Since the solution $\phi_{\infty,\varepsilon}(x)$ is homoclinic, the limits $\lim_{x \to \pm\infty} \mathcal{A}_{\infty,\varepsilon}(x, \lambda) = \mathcal{A}_{*,\varepsilon}(\lambda)$ exist [11]. Write $u_* = \lim_{\check{x} \to \infty} u_\infty(\check{x})$. Because $(u_*, 0)$ must be a hyperbolic saddle in system (2.3), we have $\min\{G_0, \partial_u H_1(u_*, 0, 0)\} > 0$, where G_0 is as in (S2). In the following we choose any $\Lambda \in (-\min\{G_0, \partial_u H_1(u_*, 0, 0)\}, 0)$. Then the matrix $\mathcal{A}_{*,\varepsilon}(\lambda)$ is hyperbolic on the half plane

$$C_\Lambda := \{\lambda \in \mathbb{C} : \operatorname{Re}(\lambda) > \Lambda\}. \tag{3.2}$$

Hence, by Lemma A.3, system (3.1) admits for $\lambda \in C_\Lambda$ exponential dichotomies on both half lines $[0, \infty)$ and $(-\infty, 0]$ such that the associated projections are analytic in λ. Denote by $\varphi_{1,\varepsilon}^s(x, \lambda)$ and $\varphi_{2,\varepsilon}^s(x, \lambda)$ two solutions to (3.1) that span the stable subspaces of the dichotomy on $[0, \infty)$ and are analytic in $\lambda \in C_\Lambda$. Similarly, let $\varphi_{1,\varepsilon}^u(x, \lambda)$ and $\varphi_{2,\varepsilon}^u(x, \lambda)$ span the unstable subspaces on $(-\infty, 0]$. The critical spectrum in C_Λ is located by the analytic Evans function $\mathcal{E}_{\infty,\varepsilon} : C_\Lambda \to \mathbb{C}$, given by

$$\mathcal{E}_{\infty,\varepsilon}(\lambda) = \det\left(\varphi_{1,\varepsilon}^s(0, \lambda) \mid \varphi_{2,\varepsilon}^s(0, \lambda) \mid \varphi_{1,\varepsilon}^u(0, \lambda) \mid \varphi_{2,\varepsilon}^u(0, \lambda)\right). \tag{3.3}$$

More precisely, a point $\lambda \in C_\Lambda$ is in the spectrum $\sigma(\mathcal{L}_{\infty,\varepsilon})$ if and only if we have $\mathcal{E}_{\infty,\varepsilon}(\lambda) = 0$. We emphasize that the spectrum of $\mathcal{L}_{\infty,\varepsilon}$ in C_Λ consists of point spectrum only.

3.2 Evans function for periodic pulse solutions

We shift our attention to the case $0 < \ell < \infty$. Since $\mathcal{A}_{\ell,\varepsilon}(\cdot, \lambda)$ is $2L_{\ell,\varepsilon}$-periodic, bounded solutions to (3.1) must satisfy $\varphi(-L_{\ell,\varepsilon}) = \gamma \varphi(L_{\ell,\varepsilon})$ for some γ in the unit circle S^1 by Floquet theory. This gives rise to the analytic Evans function $\mathcal{E}_{\ell,\varepsilon} : \mathbb{C}^2 \to \mathbb{C}$, given by

$$\mathcal{E}_{\ell,\varepsilon}(\lambda, \gamma) := \det(T_{\ell,\varepsilon}(0, -L_{\ell,\varepsilon}, \lambda) - \gamma T_{\ell,\varepsilon}(0, L_{\ell,\varepsilon}, \lambda)), \tag{3.4}$$

where $T_{\ell,\varepsilon}(x, y, \lambda)$ denotes the evolution operator of (3.1). The spectrum of $\mathcal{L}_{\ell,\varepsilon}$ is parameterized by $\gamma \in S^1$ via the discrete zero sets $\{\lambda \in \mathbb{C} : \mathcal{E}_\varepsilon(\lambda, \gamma) = 0\}$. Note that the spectrum of $\mathcal{L}_{\ell,\varepsilon}$ consists of essential spectrum only. We refer to the isolated roots of $\mathcal{E}_\varepsilon(\cdot, \gamma)$ as γ-eigenvalues.

3.3 The Evans function in the singular limit

We construct the reduced Evans functions $\mathcal{E}_{\infty,0}\colon C_\Lambda \to \mathbb{C}$ and $\mathcal{E}_{\ell,0}\colon C_\Lambda \times \mathbb{C} \to \mathbb{C}$ $(0 < \ell < \infty)$, whose zeros approximate the zeros of the Evans functions $\mathcal{E}_{\infty,\varepsilon}$ (3.3) and $\mathcal{E}_{\ell,\varepsilon}$ (3.4), provided that $\varepsilon > 0$ is sufficiently small. The slow-fast structure of the eigenvalue problem (3.1) is reflected by the fact that the analytic maps $\mathcal{E}_{\infty,0}$ and $\mathcal{E}_{\ell,0}$ can be factorized as

$$\mathcal{E}_{\infty,0}(\lambda) = \mathcal{E}_{\infty,f}(\lambda)\mathcal{E}_{\infty,s}(\lambda),$$
$$\mathcal{E}_{\ell,0}(\lambda, \gamma) = -\gamma\mathcal{E}_{\ell,f}(\lambda)\mathcal{E}_{\ell,s}(\lambda, \gamma), \quad 0 < \ell < \infty. \tag{3.5}$$

Here, the analytic map $\mathcal{E}_{\ell,f}\colon C_\Lambda \to \mathbb{C}$ for $0 < \ell \le \infty$ is called the *fast Evans function*. It locates the eigenvalues $\lambda \in C_\Lambda$ of the *homogeneous fast eigenvalue problem*,

$$\varphi_x = \mathcal{B}(x, u, \lambda)\varphi, \quad \varphi \in \mathbb{C}^2, \qquad \mathcal{B}(x, u, \lambda) := \begin{pmatrix} 0 & 1 \\ \partial_v G(u, v_h(x, u), 0) + \lambda & 0 \end{pmatrix}, \tag{3.6}$$

where $u \in U_h$ functions as a parameter. More precisely, the zeros of $\mathcal{E}_{\ell,f}$ are the eigenvalues in C_Λ of (3.6) for $u = u_\ell(0)$. Since $\kappa_h(\cdot, u)$ is a homoclinic orbit in system (2.4), one deduces with Lemma A.3 and **(S2)** that (3.6) admits, for each $\lambda \in C_\Lambda$, solutions that decay as $x \to \infty$ and ones that decay as $x \to -\infty$. Moreover, these solutions can be chosen to be analytic in λ. Now, the fast Evans function is given by the λ-dependent Wronskian of two such non-trivial analytic solutions: one that decays in forward time and one in backward time.

The meromorphic *slow Evans functions* $\mathcal{E}_{\infty,s}\colon C_\Lambda \setminus \mathcal{E}_{\infty,f}^{-1}(0) \to \mathbb{C}$ and $\mathcal{E}_{\ell,s}\colon [C_\Lambda \setminus \mathcal{E}_{\ell,f}^{-1}(0)] \times \mathbb{C} \to \mathbb{C}$ $(0 < \ell < \infty)$ are determined by two eigenvalue problems. The first is the *inhomogeneous fast eigenvalue problem*,

$$\varphi_x = \mathcal{B}(x, u, \lambda)\varphi + \mathcal{F}(x, u), \quad \varphi \in \mathbb{C}^2, \qquad \mathcal{F}(x, u) := \begin{pmatrix} 0 \\ \partial_u G(u, v_h(x, u), 0) \end{pmatrix}, \tag{3.7}$$

for $u \in U_h$. The second is the *slow eigenvalue problem*,

$$\varphi_{\check{x}} = \mathcal{A}_\ell(\check{x}, \lambda)\varphi, \quad \varphi \in \mathbb{C}^2, \qquad \mathcal{A}_\ell(\check{x}, \lambda) := \begin{pmatrix} 0 & 1 \\ \partial_u H_1(u_\ell(\check{x}), 0, 0) + \lambda & 0 \end{pmatrix}. \tag{3.8}$$

Note that the coefficient matrix $\mathcal{A}_\ell$ in (3.8) for $\ell = \infty$ converges, as $\check{x} \to \infty$, to the asymptotic matrix

$$\mathcal{A}_*(\lambda) := \begin{pmatrix} 0 & 1 \\ \partial_u H_1(u_*, 0, 0) + \lambda & 0 \end{pmatrix}, \tag{3.9}$$

which is hyperbolic on C_Λ with eigenvalues $\pm\sqrt{\partial_u H_1(u_*, 0, 0) + \lambda}$. An application of Proposition A.1 yields a unique analytic solution $\varphi_\infty(\check{x}, \lambda) = (\hat{u}_\infty(\check{x}, \lambda), \hat{p}_\infty(\check{x}, \lambda))$ to (3.8) for $\ell = \infty$ that satisfies

$$\lim_{\check{x}\to\infty} \hat{u}_\infty(\check{x}, \lambda)e^{\check{x}\sqrt{\partial_u H_1(u_*,0,0)+\lambda}} = 1, \quad \lambda \in C_\Lambda. \tag{3.10}$$

The slow Evans functions are now explicitly given by

$$\mathcal{E}_{\infty,s}(\lambda) = \det\left(\varphi_\infty(0, \lambda) \mid \Upsilon(u_\infty(0), \lambda)R_s\varphi_\infty(0, \lambda)\right), \tag{3.11}$$
$$\mathcal{E}_{\ell,s}(\lambda, \gamma) = \det\left(\Upsilon(u_\ell(0), \lambda)T_\ell(2\ell, 0, \lambda) - \gamma I\right), \quad 0 < \ell < \infty, \tag{3.12}$$

where $T_\ell(\check{x}, \check{y}, \lambda)$ is the evolution of (3.8) for $0 < \ell < \infty$ and the term $\Upsilon(u, \lambda)$ is given by

$$\Upsilon(u, \lambda) := \begin{pmatrix} 1 & 0 \\ \mathcal{G}(u, \lambda) & 1 \end{pmatrix},$$
$$\mathcal{G}(u, \lambda) := \int_{-\infty}^{\infty} [\partial_u H_2(u, v_h(x, u)) + \partial_v H_2(u, v_h(x, u))\mathcal{V}_{in}(x, u, \lambda)]dx, \qquad u \in U_h. \tag{3.13}$$

Here $\mathcal{V}_{in}(x, u, \lambda)$ denotes the v-component of the unique bounded solution to the inhomogeneous fast eigenvalue problem (3.7). We emphasize that the slow Evans functions $\mathcal{E}_{\infty,s}$ and $\mathcal{E}_{\ell,s}(\cdot, \gamma)$ are meromorphic on C_Λ such that the products $\mathcal{E}_{\infty,0}$ and $\mathcal{E}_{\ell,0}(\cdot, \gamma)$ given in (3.5) are analytic on C_Λ for each $\gamma \in S^1$.

Having defined the reduced Evans functions $\mathcal{E}_{\infty,0}$ and $\mathcal{E}_{\ell,0}$, we are able to state the precise approximation result.

13

Theorem 3.1. *[11, Section 4] Let Γ be a simple closed curve, contained in $C_\Lambda \setminus \mathcal{E}_{\infty,0}^{-1}(0)$. For $\varepsilon > 0$ sufficiently small, the number of zeros of $\mathcal{E}_{\infty,\varepsilon}$ interior to Γ equals the number (including multiplicity) of zeros of $\mathcal{E}_{\infty,0}$ interior to Γ.*

Theorem 3.2. *[7, Theorem 3.8] Let $\gamma \in S^1$. Define $\mathcal{E}_{\ell;\gamma} := \mathcal{E}_{\ell,0}(\cdot, \gamma)$. Take a simple closed curve Γ in $C_\Lambda \setminus \mathcal{E}_{\ell;\gamma}^{-1}(0)$. For $\varepsilon > 0$ sufficiently small, the number (including multiplicity) of zeros of $\mathcal{E}_{\ell,\varepsilon}(\cdot, \gamma)$ interior to Γ equals the number of zeros of $\mathcal{E}_{\ell;\gamma}$ interior to Γ.*

Due to the translational invariance of system (1.1)/(1.2), we must take special care of the case $\lambda = 0$. On the one hand, the fast eigenvalue problem (3.6) admits at $\lambda = 0$ a one-dimensional space of exponentially localized solutions spanned by the derivative $\partial_x \kappa_{\mathrm{h}}(x, u_\ell(0))$, which implies that $\lambda = 0$ is a simple root of the fast Evans function $\mathcal{E}_{\ell,f}$ for $0 < \ell \leq \infty$. On the other hand, the derivative $\psi_\ell'(\check{x}) = (u_\ell'(\check{x}), p_\ell'(\check{x}))$ of the solution $\psi_\ell(\check{x})$ to the slow reduced system (2.3) is a solution to the slow eigenvalue problem (3.8) for $\lambda = 0$. This leads to the following expansion of $\mathcal{E}_{\ell,s}(\lambda, \gamma)$ at $\lambda = 0$.

Proposition 3.3. *[11, Lemma 5.9], [7, Proposition 4.4] For any $\gamma \in S^1$ and $0 < \ell < \infty$ it holds*

$$\mathcal{E}_{\ell,s}(0, \gamma) = \gamma^2 + 2(1 + 2\mathfrak{a}_\ell \mathfrak{b}_\ell)\gamma + 1,$$

with

$$\mathfrak{a}_\ell := \mathcal{J}'(u_\ell(0))\mathcal{J}(u_\ell(0)) - H_1(u_\ell(0), 0, 0),$$

$$\mathfrak{b}_\ell := \mathcal{J}(u_\ell(0)) \int_0^\ell \frac{(\partial_u H_1(u_\ell(\check{x}), 0, 0) + 1)[(p_\ell(\check{x}))^2 - (H_1(u_\ell(\check{x}), 0, 0))^2]}{[(p_\ell(\check{x}))^2 + (H_1(u_\ell(\check{x}), 0, 0))^2]^2} d\check{x} + \frac{H_1(u_\ell(0), 0, 0)}{(\mathcal{J}(u_\ell(0)))^2 + (H_1(u_\ell(0), 0, 0))^2}. \tag{3.14}$$

Moreover, we have

$$\mathcal{E}_{\infty,s}(0) = -2\mathfrak{j}_\infty \mathfrak{a}_\infty,$$

with

$$\mathfrak{j}_\infty := -\mathcal{J}(u_\infty(0)), \quad \mathfrak{a}_\infty := \mathcal{J}'(u_\infty(0))\mathcal{J}(u_\infty(0)) - H_1(u_\infty(0), 0, 0). \tag{3.15}$$

Since 0 is a simple zero of the fast Evans function $\mathcal{E}_{\ell,f}$, Proposition 3.3 yields that the root 0 of the reduced Evans function $\mathcal{E}_{\ell,0}$ is simple unless $\mathfrak{a}_\ell \mathfrak{b}_\ell \in [-1, 0]$ for $0 < \ell < \infty$ or $\mathfrak{a}_\infty \mathfrak{j}_\infty = 0$ for $\ell = \infty$. For $0 < \ell \leq \infty$, the quantity $\mathfrak{a}_\ell$ measures the transversality of the intersection between $\psi_\ell(\check{x}) = (u_\ell(\check{x}), p_\ell(\check{x}))$ and the touch-down curve $T_+ = \{(u, \mathcal{J}(u)) : u \in U_{\mathrm{h}}\}$ at $\check{x} = 0$. So, $\mathfrak{a}_\ell$ is non-zero by assumption – see Theorem 2.1. Moreover, $\mathfrak{j}_\infty = -\mathcal{J}(u_\infty(0))$ is the jump between the take-off and touch-down curves $T_\pm$. If $\mathfrak{j}_\infty$ equals zero, then there is no leading-order coupling between the u- and v-component of the periodic pulse solution. This leads to an extra degree of freedom and produces a *double* eigenvalue $\lambda = 0$ – see [11, Corollary 5.8]. The quantity $\mathfrak{b}_\ell$ equals the value at $\check{x} = 0$ of the solution to the slow eigenvalue problem (3.8) for $\lambda = 0$ and $0 < \ell < \infty$ that is perpendicular to the solution $\psi_\ell'(\check{x})$ at $\check{x} = \ell$ – we refer to [6, Remark 3.30] for further interpretation of the quantity $\mathfrak{b}_\ell$.

3.3.1 Spectrum induced by the fast Evans function

Let $0 < \ell \leq \infty$. The zeros of the fast Evans function $\mathcal{E}_{\ell,f}$ correspond to the eigenvalues $\lambda \in C_\Lambda$ for which (3.6) admits an exponentially localized solution. By Sturm-Liouville theory [20, Theorem 2.3.3], all eigenvalues of (3.6) are simple and real. In particular, $\lambda = 0$ is an eigenvalue of (3.6) with corresponding eigenfunction $\partial_x \kappa_{\mathrm{h}}(x, u_\ell(0))$. Moreover, there is precisely one positive eigenvalue $\lambda_{1,\ell} > 0$. Let $(v_{1,\ell}(x), q_{1,\ell}(x))$ be the eigenfunction of (3.6) for $\lambda_{1,\ell}$. By [7, Proposition 6.10], the slow Evans function $\mathcal{E}_{\ell,s}$ has a pole at $\lambda_{1,\ell}$ if and only if the generic condition $\mathfrak{i}_\ell \neq 0$ is satisfied, where

$$\mathfrak{i}_\ell := \lim_{\check{x} \to 2\ell} u_{1,\ell}(\check{x}) \int_{-\infty}^\infty v_{1,\ell}(x)\partial_v H_2(u_\ell(0), v_{\mathrm{h}}(x, u_\ell(0)))dx \int_{-\infty}^\infty v_{1,\ell}(x)\partial_u G(u_\ell(0), v_{\mathrm{h}}(x, u_\ell(0)), 0)dx, \tag{3.16}$$

with $\varphi_{1,\ell}(\check{x}) = (u_1(\check{x}), p_1(\check{x}))$ the solution to (3.8) for $\lambda = \lambda_1$ with initial condition $\varphi_{1,\ell}(0) = (0, 1)$. Thus, due to zero-pole cancelation, the reduced Evans function $\mathcal{E}_{\ell,0}$ has a zero at λ_1 if and only if $\mathfrak{i}_\ell = 0$.

Using Theorem 3.1 and 3.2, we conclude that the fast Evans function $\mathcal{E}_{\ell,f}$ can only produce unstable spectrum close to its roots 0 and $\lambda_1 > 0$. If $\mathfrak{i}_\ell \neq 0$, there is no unstable spectrum close to λ_1. In addition, due to translational invariance, we

know that 0 is in the spectrum [45]. Therefore, in the case $\ell = \infty$, we know that all spectrum in $\{\lambda \in \mathbb{C} : \mathrm{Re}(\lambda) \geq 0\} \setminus \{0\}$ must be produced by the slow Evans function $\mathcal{E}_{\infty,s}$, provided $\mathfrak{i}_\infty \neq 0$.

In the case $0 < \ell < \infty$, we have to be more careful: by Theorem 3.2, there is a curve of spectrum attached to 0 that shrinks to 0 as $\varepsilon \to 0$. Therefore, knowledge of the spectrum in the case $\ell \to \infty$ is insufficient to determine the position of this critical spectral curve with respect to the imaginary axis. Therefore, a separate leading-order analysis of this curve is necessary to control the spectrum induced by the fast Evans function $\mathcal{E}_{\ell,f}$. In [5, 6], the following result is proven.

Theorem 3.4. *[5], [6, Proposition 3.29] Let $0 < \ell < \infty$ and suppose $\mathcal{E}_{\ell,s}(0, \gamma) \neq 0$ for each $\gamma \in S^1$. Then, provided $\varepsilon > 0$ is sufficiently small, the there exists a 2π-periodic, even, analytic map $\lambda^s_{\ell,\varepsilon} : \mathbb{R} \to \mathbb{R}$ such that for any $v \in \mathbb{R}$ there is a unique (simple) root $\lambda^s_{\ell,\varepsilon}(v)$ of $\mathcal{E}_{\ell,\varepsilon}(\cdot, e^{iv})$ converging to 0 as $\varepsilon \to 0$. The critical spectral curve $\{\lambda^s_{\ell,\varepsilon}(v)\}$ is approximated as*

$$\left| \lambda^s_{\ell,\varepsilon}(v) - \varepsilon^2 \lambda^s_{\ell,0}(v) \right| \leq C \varepsilon^3 |\log(\varepsilon)|^5, \tag{3.17}$$

where $C > 0$ is a constant independent of ε, ℓ and v, and $\lambda^s_{\ell,0} : \mathbb{R} \to \mathbb{R}$ is given by

$$\lambda^s_{\ell,0}(v) = \mathfrak{a}_\ell \mathfrak{w}_\ell \frac{\cos(v) - 1}{1 + \cos(v) + 2\mathfrak{a}_\ell \mathfrak{b}_\ell}, \tag{3.18}$$

where $\mathfrak{a}_\ell, \mathfrak{b}_\ell$ are defined in (3.14) and $\mathfrak{w}_\ell$ is given by

$$\mathfrak{w}_\ell = -\frac{\int_{-\infty}^{\infty} \frac{\partial G}{\partial u}(u_\ell(0), v_h(x, u_\ell(0)), 0)\partial_x v_h(x, u_\ell(0))x\,dx}{\int_{-\infty}^{\infty} (\partial_x v_h(x, u_\ell(0)))^2\,dx}. \tag{3.19}$$

3.4 Stability of pulse solutions in the model equation

In order to construct the reduced Evans function for the periodic ($0 < \ell < \infty$) and homoclinic ($\ell = \infty$) solutions to the model system (1.4), we first study the homogeneous fast limit problem (3.6), where the matrix $\mathcal{B}(x, u, \lambda)$ for $v_h(u, x)$ as in (2.11) takes the form

$$\mathcal{B}(x, u, \lambda) = \begin{pmatrix} 0 & 1 \\ 1 + \lambda - 3\,\mathrm{sech}^2 \frac{x}{2} & 0 \end{pmatrix}, \tag{3.20}$$

and is in particular independent of u. The homogeneous fast limit problem of the form (3.6) with $\mathcal{B}(x, u, \lambda)$ as specified in (3.20) was studied in [46]. There, it was found that the eigenvalues of this problem are $\frac{5}{4}$, 0 and $-\frac{3}{4}$. The solution space is spanned by $w(\pm x, \lambda)$, which are given in terms of associated Legendre functions [32, §14.3] as

$$w(x, \lambda) = P_3^{-2\sqrt{1+\lambda}}\left(\tanh\frac{x}{2}\right). \tag{3.21}$$

The fast Evans function, which is equal to the Wronskian of $w(\pm x, \lambda)$, is therefore given by [32, §14.2(iv)]

$$\mathcal{E}_{\ell,f}(\lambda) = \frac{1}{\Gamma(-3 + 2\sqrt{1 + \lambda})\Gamma(4 + 2\sqrt{1 + \lambda})}. \tag{3.22}$$

The zeroes of the fast Evans function (3.22) are given by the eigenvalues of the homogeneous fast limit problem (3.6), which means that $\mathcal{E}_{\ell,f}^{-1}(0) = \left\{-\frac{3}{4}, 0, \frac{5}{4}\right\}$ for $0 < \ell \leq \infty$.

The inhomogeneous term $\mathcal{F}(x, u)$ in the inhomogeneous fast limit problem (3.7) takes the form

$$\mathcal{F}(x, u) = \begin{pmatrix} 0 \\ \frac{9}{4}\mu_3 \cos u\,\mathrm{sech}^4 \frac{x}{2} \end{pmatrix}. \tag{3.23}$$

We can again use the results in [46] to express the v-component of the solution to the inhomogeneous fast limit problem (3.6), with matrix $\mathcal{B}$ and inhomogeneous term $\mathcal{F}$ given by (3.20) respectively (3.23), as

$$\mathcal{V}_{\mathrm{in}}(x, u, \lambda) = -\frac{\frac{9}{4}\mu_3 \cos u}{\mathcal{E}_{\ell,f}(\lambda)}\left[w(x, \lambda)\int_{-\infty}^{x} w(-y, \lambda)\,\mathrm{sech}^4\frac{y}{2}\,dy + w(-x, \lambda)\int_{x}^{\infty} w(y, \lambda)\,\mathrm{sech}^4\frac{y}{2}\,dy\right]. \tag{3.24}$$

This is used as input for the function $\mathcal{G}(u, \lambda)$ (3.13), which in the case of the model system (1.4) takes the form

$$
\begin{aligned}
\mathcal{G}(u, \lambda) &= \nu_1 \int_{-\infty}^{\infty} (2 - 3\nu_2 v_h(x, u)) \, v_h(x, u) \, \mathcal{V}_{in}(x, u, \lambda) \, dx \\
&= 3\nu_1(\mu_2 + \mu_3 \sin u) \int_{-\infty}^{\infty} \left(1 - \frac{9}{4} \nu_2(\mu_2 + \mu_3 \sin u) \operatorname{sech}^2 \frac{x}{2} \right) \operatorname{sech}^2 \frac{x}{2} \, \mathcal{V}_{in}(x, u, \lambda) \, dx \\
&= -\frac{\frac{27}{2} \nu_1 \mu_3 \cos u}{\mathcal{E}_{\ell, f}(\lambda)} (\mu_2 + \mu_3 \sin u) \int_{-\infty}^{\infty} \left(1 - \frac{9}{4} \nu_2(\mu_2 + \mu_3 \sin u) \operatorname{sech}^2 \frac{x}{2} \right) \operatorname{sech}^2 \frac{x}{2} \, w(x, \lambda) \int_{-\infty}^{x} w(-y, \lambda) \operatorname{sech}^4 \frac{y}{2} \, dy \, dx.
\end{aligned}
\tag{3.25}
$$

For the slow limit problem (3.8), we treat the homoclinic and periodic cases separately. For clarity of exposition, we focus our attention on the saddle point at the origin of the slow phase plane, see Figure 6. Therefore, we restrict the analysis of the periodic orbits to those whose slow segment has a 'c'-shape, i.e. whose intersection with the u-axis tends to the origin as $\ell \to \infty$; for an example of such an orbit, see Figure 7, left. The analysis of the complementary type of periodic orbits, as shown in Figure 7, right, is analogous.

In the homoclinic case ($\ell = \infty$), with the homoclinic orbit u_∞ as given in (2.8) (for which $\lim_{\check{x} \to \infty} u_\infty(\check{x}) = u_* = 0$), the matrix $\mathcal{A}$ in (3.8) takes the form

$$
\mathcal{A}_\infty(\check{x}, \lambda) = \begin{pmatrix} 0 & 1 \\ \lambda + \mu_1 \cos u_\infty(\check{x}; \check{x}_0) & 0 \end{pmatrix} = \begin{pmatrix} 0 & 1 \\ \lambda + \mu_1 - 2\mu_1 \operatorname{sech}^2 \sqrt{\mu_1}(\check{x} + \check{x}_0) & 0 \end{pmatrix}.
\tag{3.26}
$$

The unique analytic solution to the homoclinic slow limit problem that satisfies (3.10) is found to be

$$
\varphi_\infty(\check{x}, \lambda) = \begin{pmatrix} \hat{u}_\infty(\check{x}, \lambda) \\ \hat{p}_\infty(\check{x}, \lambda) \end{pmatrix} = \frac{e^{-\sqrt{\lambda + \mu_1} \check{x}}}{\sqrt{\mu_1} + \sqrt{\lambda + \mu_1}} \begin{pmatrix} \sqrt{\lambda + \mu_1} + \sqrt{\mu_1} \tanh \sqrt{\mu_1}(\check{x} + \check{x}_0) \\ -\lambda - \mu_1 + \mu_1 \operatorname{sech}^2 \sqrt{\mu_1}(\check{x} + \check{x}_0) - \sqrt{\mu_1} \sqrt{\lambda + \mu_1} \tanh \sqrt{\mu_1}(\check{x} + \check{x}_0) \end{pmatrix}.
\tag{3.27}
$$

The slow Evans function for the homoclinic case (3.3) can then be calculated as

$$
\mathcal{E}_{\infty, s}(\lambda) = \hat{u}_\infty(0, \lambda)^2 \left[\mathcal{G}(u_\infty(0; \check{x}_0), \lambda) - 2 \frac{\hat{p}_\infty(0, \lambda)}{\hat{u}_\infty(0, \lambda)} \right].
\tag{3.28}
$$

Moreover, from the fact that we consider the saddle point at the origin of the slow system (2.6), we infer that

$$
C_\Lambda \subset \{\lambda \in \mathbb{C} \ : \ \operatorname{Re}(\lambda) > \min(-1, -\mu_1)\},
\tag{3.29}
$$

see (3.2).

In the periodic case ($0 < \ell < \infty$), with the bounded slow part of the orbit u_ℓ as given in (2.9), the matrix $\mathcal{A}$ in (3.8) takes the form

$$
\mathcal{A}_\ell(\check{x}, \lambda) = \begin{pmatrix} 0 & 1 \\ \lambda + \mu_1 \cos u_\ell(\check{x}; \kappa, \pm) & 0 \end{pmatrix} = \begin{pmatrix} 0 & 1 \\ \lambda - \mu_1 + 2\kappa^2 \mu_1 \operatorname{cd}^2\left(\sqrt{\mu_1}(\check{x} - \ell), \kappa \right) & 0 \end{pmatrix}.
\tag{3.30}
$$

Using the coordinate $z = \operatorname{cd}\left(\sqrt{\mu_1}(\check{x} - \ell), \kappa \right)$, the periodic slow limit problem (3.8) can be written as a second order ODE in z of the form $y_{zz} + a\,y_z + b\,y = 0$, where a and b are rational functions of z, yielding

$$
y_{zz} + \left(-\frac{z}{1 - z^2} - \frac{\kappa^2 z}{1 - \kappa^2 z^2} \right) y_z + \frac{1 - \frac{\lambda}{\mu_1} - 2\kappa^2 z^2}{(1 - z^2)(1 - \kappa^2 z^2)} y = 0.
\tag{3.31}
$$

The coefficient of y_z can be eliminated by introducing $\eta(z) = (1 - z^2)^{\frac{1}{4}} (1 - \kappa^2 z^2)^{\frac{1}{4}} y(z)$, yielding

$$
\eta_{zz} - r\eta = 0,
\tag{3.32}
$$

with

$$
\begin{aligned}
r(z) = &-\frac{3}{16} \left(\frac{1}{(1 - z)^2} + \frac{1}{(1 + z)^2} + \frac{\kappa^2}{(1 - \kappa z)^2} + \frac{\kappa^2}{(1 + \kappa z)^2} \right) \\
&- \frac{9 - 21\kappa^2 - 8\frac{\lambda}{\mu_1}}{16(1 - \kappa^2)} \left(\frac{1}{1 - z} + \frac{1}{1 + z} \right) - \frac{13 - \kappa^2 + 8\frac{\lambda}{\mu_1}}{16(1 - \kappa^2)} \left(\frac{\kappa^2}{1 + \kappa z} + \frac{\kappa^2}{1 - \kappa z} \right).
\end{aligned}
\tag{3.33}
$$

16

To find a closed form solution to (3.32), we use the algorithm presented in [22], which is based on differential Galois theory. The algorithm distinguishes four mutually exclusive cases [22, Section 1.2], and equation (3.32) obeys all necessary conditions for Cases 1, 2 and 3 to hold [22, Section 2.1]. Execution of the algorithm for Case 1 [22, Section 3] yields no nontrivial solutions to (3.32). Subsequent application of the algorithm for Case 2 [22, Section 4] reveals that (3.32) admits a closed form solution of the form $\eta(z) = e^{\int^z \omega(\zeta)\,d\zeta}$, where ω can be found by solving the equation [1]

$$\omega^2 - \varphi\,\omega + \frac{1}{2}\varphi_z + \frac{1}{2}\varphi^2 - r = 0, \tag{3.34}$$

where

$$\varphi(z) = -\frac{z}{1-z^2} - \frac{\kappa^2 z}{1-\kappa^2 z^2} - \frac{2\kappa^2 z}{\kappa^2(1-z^2) + \frac{\lambda}{\mu_1}}. \tag{3.35}$$

This yields for ω

$$\omega(z) = \frac{1}{2}\frac{z}{1-z^2} + \frac{1}{2}\frac{\kappa^2 z}{1-\kappa^2 z^2} + \frac{\kappa^2 z}{\kappa^2(1-z^2) + \frac{\lambda}{\mu_1}} \pm \sqrt{\frac{\frac{\lambda}{\mu_1}\left(\frac{\lambda}{\mu_1} + \kappa^2\right)\left(\frac{\lambda}{\mu_1} + \kappa^2 - 1\right)}{(1-z^2)(1-\kappa^2 z^2)\left(\kappa^2(1-z^2) + \frac{\lambda}{\mu_1}\right)^2}}, \tag{3.36}$$

and hence

$$y(z) = (1-z^2)^{-\frac{1}{4}}(1-\kappa^2 z^2)^{-\frac{1}{4}}\eta(z) = \sqrt{\kappa^2(1-z^2) + \frac{\lambda}{\mu_1}}\,\exp\left[\pm\int^z \sqrt{\frac{\frac{\lambda}{\mu_1}\left(\frac{\lambda}{\mu_1} + \kappa^2\right)\left(\frac{\lambda}{\mu_1} + \kappa^2 - 1\right)}{(1-\zeta^2)(1-\kappa^2\zeta^2)\left(\kappa^2(1-\zeta^2) + \frac{\lambda}{\mu_1}\right)^2}}\,d\zeta\right]. \tag{3.37}$$

The integral in (3.37) can be expressed in terms of the incomplete (Legendre) elliptic integral of the third kind $\Pi(\varphi, \alpha^2, \kappa)$ [32, §19.2], as

$$\int^z \sqrt{\frac{\frac{\lambda}{\mu_1}\left(\frac{\lambda}{\mu_1} + \kappa^2\right)\left(\frac{\lambda}{\mu_1} + \kappa^2 - 1\right)}{(1-\zeta^2)(1-\kappa^2\zeta^2)\left(\kappa^2(1-\zeta^2) + \frac{\lambda}{\mu_1}\right)^2}}\,d\zeta = \sqrt{\frac{\frac{\lambda}{\mu_1}\left(\frac{\lambda}{\mu_1} + \kappa^2 - 1\right)}{\frac{\lambda}{\mu_1} + \kappa^2}}\,\Pi\left(-\arcsin z, \frac{\kappa^2}{\frac{\lambda}{\mu_1} + \kappa^2}, \kappa\right) \tag{3.38}$$

$$= \sqrt{\frac{\frac{\lambda}{\mu_1}\left(\frac{\lambda}{\mu_1} + \kappa^2 - 1\right)}{\kappa^2\left(\frac{\lambda}{\mu_1} + \kappa^2\right)}}\,\Pi\left(-\arcsin(\kappa z), \frac{1}{\frac{\lambda}{\mu_1} + \kappa^2}, \frac{1}{\kappa}\right). \tag{3.39}$$

We now can express the evolution of (3.8), $T_\ell(\check{x}, \check{y}, \lambda)$, for $\mathcal{A}_\ell$ as in (3.30), in terms of the fundamental matrix solution $\Phi(\check{x}, \lambda)$ of (3.8) as $T_\ell(\check{x}, \check{y}, \lambda) = \Phi(\check{x}, \lambda)\Phi^{-1}(\check{y}, \lambda)$. We write this fundamental matrix as $\Phi(\check{x}, \lambda) = (\tilde{\varphi}_1(\check{x}, \lambda)\,|\,\tilde{\varphi}_2(\check{x}.\lambda))$, where $\tilde{\varphi}_{1,2}(\check{x}, \lambda)$ are two linearly independent solutions to (3.8), which are gauged such that $\Phi(0, \lambda) = I$. In order to express these $\tilde{\varphi}_{1,2}(\check{x}, \lambda)$ in terms of the functions $y(z)$ (3.37), we have to realize that the coordinate change $\check{x} \to z = \mathrm{cd}\left(\sqrt{\mu_1}(\check{x} - \ell), \kappa\right)$ is one-to-one only for $\check{x} \in (0, \ell)$ or $\check{x} \in (\ell, 2\ell)$, as cd is an even function. Therefore, we split

$$T_\ell(2\ell, 0, \lambda) = T_\ell(2\ell, \ell, \lambda) \circ T_\ell(\ell, 0, \lambda). \tag{3.40}$$

We invoke the above results to express the first coordinates of $\tilde{\varphi}_{1,2} = (\tilde{u}_{1,2}, \tilde{p}_{1,2})^T$ as

$$\tilde{u}_1(\check{x}, \lambda) = \rho(\check{x}, \lambda)\left(\cosh\,\sigma(\check{x}, \lambda) - \frac{\partial_{\check{x}}\rho(0, \lambda)}{\partial_{\check{x}}\sigma(0, \lambda)}\,\sinh\,\sigma(\check{x}, \lambda)\right), \tag{3.41}$$

$$\tilde{u}_2(\check{x}, \lambda) = \frac{\rho(\check{x}, \lambda)}{\partial_{\check{x}}\sigma(0, \lambda)}\,\sinh\,\sigma(\check{x}, \lambda), \tag{3.42}$$

where

$$\rho(\check{x}, \lambda) = \sqrt{\frac{\frac{\lambda}{\mu_1} + \kappa^2 - \kappa^2\mathrm{cd}\left(\sqrt{\mu_1}(\check{x} - \ell), \kappa\right)}{\frac{\lambda}{\mu_1} + \kappa^2 - \kappa^2\mathrm{cd}\left(\sqrt{\mu_1}(-\ell), \kappa\right)}} \tag{3.43}$$

$$= \sqrt{\frac{\frac{\lambda}{\mu_1} + \kappa^2 - \cos^2\frac{u_\ell(\check{x})}{2}}{\frac{\lambda}{\mu_1} + \kappa^2 - \cos^2\frac{u_\ell(0)}{2}}} \tag{3.44}$$

$$= \sqrt{\frac{4\lambda + \partial_{\check{x}}u_\ell(\check{x})^2}{4\lambda + \partial_{\check{x}}u_\ell(0)^2}} \tag{3.45}$$

---

[1]Note that [22] contains a typographical error on p. 18, last equation, where "$+\varphi\omega$" is written. From the proof on p. 19-22 therein, it is clear that this should be replaced by "$-\varphi\omega$".

and

$$\sigma(\check{x},\lambda) = \sqrt{\frac{\frac{\lambda}{\mu_1}\left(\frac{\lambda}{\mu_1}+\kappa^2-1\right)}{\frac{\lambda}{\mu_1}+\kappa^2}}\ \Pi\left(-\arcsin\operatorname{cd}\left(\sqrt{\mu_1}(\check{x}-\ell),\kappa\right),\frac{\kappa^2}{\frac{\lambda}{\mu_1}+\kappa^2},\kappa\right) \tag{3.46}$$

$$= \sqrt{\frac{\frac{\lambda}{\mu_1}\left(\frac{\lambda}{\mu_1}+\kappa^2-1\right)}{\kappa^2\left(\frac{\lambda}{\mu_1}+\kappa^2\right)}}\ \Pi\left(\frac{u_\ell(\check{x})-\pi}{2},\frac{1}{\frac{\lambda}{\mu_1}+\kappa^2},\frac{1}{\kappa}\right), \tag{3.47}$$

using (2.9) and (2.7). Now, the slow Evans function $\mathcal{E}_{\ell,s}(\lambda,\gamma)$ (3.4) can be written as

$$\mathcal{E}_{\ell,s}(\lambda,\gamma) = \det\Phi(2\ell,\lambda) - \gamma\left[\tilde{u}_1(2\ell,\lambda)+\partial_{\check{x}}\tilde{u}_2(2\ell,\lambda)+\tilde{u}_2(2\ell,\lambda)\,\mathcal{G}(u_\ell(0),\lambda)\right] + \gamma^2. \tag{3.48}$$

Since $u_\ell(2\ell) = u_\ell(0)$ and $\partial_{\check{x}}u_\ell(2\ell) = -\partial_{\check{x}}u_\ell(2\ell)$ (which follows from the $\mathbb{R}_s$-reversibility of (2.3), combined with the fact that $\lim_{\check{x}\to\ell}\partial_{\check{x}}u_\ell(\check{x}) = 0$), we see that

$$\det\Phi(2\ell,\lambda) = \tilde{u}_1(2\ell,\lambda)\,\partial_{\check{x}}\tilde{u}_2(2\ell,\lambda) - \tilde{u}_2(2\ell,\lambda)\,\partial_{\check{x}}\tilde{u}_1(2\ell,\lambda) = \rho(2\ell,\lambda)^2\frac{\partial_{\check{x}}\sigma(2\ell,\lambda)}{\partial_{\check{x}}\sigma(0,\lambda)} = -1, \tag{3.49}$$

using (3.41) and (3.42). Moreover, from (3.47) we infer that $\sigma(2\ell,\lambda) = \sigma(0,\lambda)$, and from (3.45) follows that $\rho(2\ell,\lambda) = 1$. Therefore, the slow Evans function (3.48) simplifies to

$$\mathcal{E}_{\ell,s}(\lambda,\gamma) = \gamma^2 - \gamma\frac{\sinh\sigma(0,\lambda)}{\partial_{\check{x}}\sigma(0,\lambda)}\left[\mathcal{G}(u_\ell(0),\lambda) - 2\partial_{\check{x}}\rho(0,\lambda)\right] - 1, \tag{3.50}$$

with

$$\partial_{\check{x}}\rho(0,\lambda) = \frac{\mu_1\,u_\ell'(0)\,\sin u_\ell(0)}{4\lambda + u_\ell'(0)^2}, \tag{3.51}$$

$$\partial_{\check{x}}\sigma(0,\lambda) = \operatorname{sgn}u_\ell'(0)\,\frac{4\sqrt{\lambda(\lambda+\kappa^2\mu_1)(\lambda+(\kappa^2-1)\mu_1)}}{4\lambda + u_\ell'(0)^2}, \tag{3.52}$$

and $\mathcal{G}(u_\ell(0),\lambda)$ as in (3.25).

4 Main results

Suppose system (1.2) depends on a parameter $\mu \in \mathbb{R}$. In this paper we are interested in destabilization mechanisms of long-wavelength periodic pulse solutions to (1.1)/(1.2), when the limiting homoclinic pulse undergoes a Hopf destabilization at $\mu = \mu_*$. As outlined in §1, this requires information on the structure of three critical spectral curves associated with the periodic pulse. First, we are interested in the (real) spectral curve attached to the origin – see §3.3.1. We will show that, generically, the relative location of this curve with respect to the imaginary axis does not change as the pattern wavelength tends to infinity. Second, there are two complex conjugate spectral curves that shrink to the critical eigenvalues associated with the limiting homoclinic as the wavelength tends to infinity – see [15, 35]. Assuming that the spectrum that is attached to the origin is not unstable, we derive the result that long-wavelength periodic pulse solutions also destabilize at some μ-value close to μ_*, by the transition of these two conjugate curves through the imaginary axis. The relative positions of these curves with respect to the critical eigenvalues of the homoclinic pulse determine whether the homoclinic is the last (or first) 'periodic' pattern to destabilize as we vary μ. Moreover, the orientation of the conjugate spectral curves as they pass through the imaginary axis, characterizes the type of instability that occurs as we vary μ.

This section is structured as follows. First, we extend the existence results by constructing a family of periodic pulse solutions to (2.1), parametrized by wavelength, that approach a homoclinic pulse as the pattern wavelength approaches infinity. Second, we study the geometry of the three critical spectral curves associated to the periodic pulse patterns in the long-wavelength limit. Third, we derive a sign criterion that determines whether the long-wavelength periodic pulse solutions also destabilize at some μ-value close to μ_*. Fourth, under the assumption that long-wavelength periodic pulses destabilize in this manner, we prove the occurrence of the Hopf and belly dance destabilization mechanisms, and we establish an explicit sign criterion to determine whether the homoclinic pulse solution is the last (or the first) 'periodic' pattern to destabilize. Finally, we draw the connection to the boundary of the Busse balloon – see §1.

4.1 Existence of a family of periodic pulse solutions approaching a homoclinic limit

With the aid of Theorem 2.1 we construct a family of periodic pulse solutions to (2.1) that approach a homoclinic pulse solution in the long-wavelength limit. Key to the construction of such a family is the existence of a saddle in the slow reduced system (2.3).

(E2) *Existence of saddle in the slow reduced system*
There exists $u_* \in U$ such that $\psi_* := (u_*, 0)$ is a hyperbolic saddle in (2.3). In addition, the touch-down curve $\mathcal{T}_+ = \{(u, \mathcal{J}(u)) : u \in U_{\mathrm{h}}\}$ intersects the stable manifold $W^s(\psi_*)$ transversally in some point ψ_0.

Theorem 4.1. *Assume (S1), (S2), (E1) and (E2) hold true. Let $\psi_\infty(\check{x})$ be the solution to (2.3) in $W^s(\psi_*)$ with initial condition $\psi_\infty(0) = \psi_0$. Then, there exist $\ell_0, \varepsilon_0 > 0$ such that the following assertions hold true:*

1. ***Saddle dynamics in slow reduced system***
   For $\ell \in (\ell_0, \infty)$, there exists a solution $\psi_\ell(\check{x}) = (u_\ell(\check{x}), p_\ell(\check{x}))$ to (2.3) that intersects $\mathcal{T}_+$ transversally at $\check{x} = 0$ and crosses the line $p = 0$ at $\check{x} = \ell$. In addition, $\psi_\ell(\check{x})$ converges, as $\ell \to \infty$, to $\psi_\infty(\check{x})$ for each $\check{x} \in [0, \ell]$.

2. ***Existence of family of periodic pulse solutions***
   For $(\ell, \varepsilon) \in (\ell_0, \infty) \times (0, \varepsilon_0)$ there exists a reversibly symmetric, $2L_{\ell,\varepsilon}$-periodic pulse solution $\phi_{\ell,\varepsilon}$ to (2.1), whose orbit converges in the Hausdorff distance to the singular orbit

$$\{(u_\ell(\check{x}), p_\ell(\check{x}), 0, 0) : \check{x} \in (0, 2\ell)\} \cup \{\phi_{\mathrm{h}}(x, u_\ell(0)) : x \in \mathbb{R}\} \tag{4.1}$$

   as $\varepsilon \to 0$, and whose period satisfies $\varepsilon L_{\ell,\varepsilon} \to \ell$ as $\varepsilon \to 0$.

3. ***Long-wavelength limit***
   For every $\varepsilon \in (0, \varepsilon_0)$ the family of solutions $\phi_{\ell,\varepsilon}$ converges pointwise on $[0, L_{\ell,\varepsilon}]$ to a reversibly symmetric, homoclinic pulse solution $\phi_{\infty,\varepsilon}$ to (2.1) as $\ell \to \infty$. Moreover, $\phi_{\infty,\varepsilon}$ converges in Hausdorff distance to the singular concatenation

$$\{(u_\infty(\check{x}), \pm p_\infty(\check{x}), 0, 0) : \check{x} \in (0, \infty)\} \cup \{\phi_{\mathrm{h}}(x, u_\infty(0)) : x \in \mathbb{R}\} \tag{4.2}$$

   as $\varepsilon \to 0$.
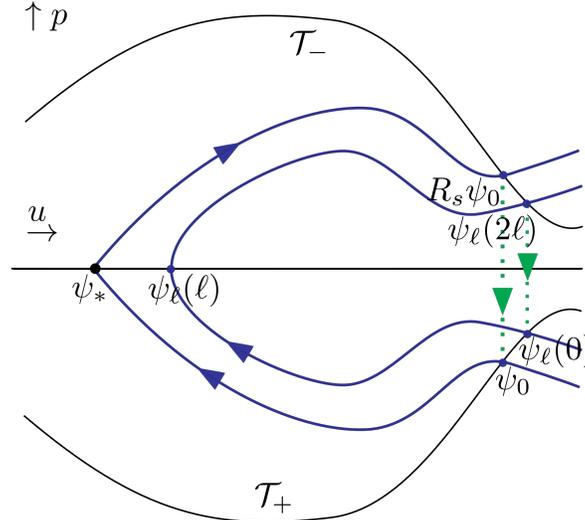
Figure 8: Depicted are the orthogonal projections of the singular periodic orbit (4.1) and the singular homoclinic orbit (4.2) onto the slow manifold $\mathcal{M}$ and the take-off and touch-down curves $\mathcal{T}_\pm$.

Proof. The first assertion is immediate by Hamiltonian nature of the planar system (2.3). For any fixed $\ell > \ell_0$ the existence of a periodic pulse solution $\phi_{\ell,\varepsilon}(x)$ for $0 < \varepsilon \ll 1$ follows from Theorem 2.1. Following the proof of Theorem 2.1, one observes that the ε-bound is in fact ℓ-uniform. This establishes the second assertion. The existence of the homoclinic pulse solution $\phi_{\infty,\varepsilon}(x)$ for $0 < \varepsilon \ll 1$ follows from Theorem 2.1. Now fix $\varepsilon \in (0, \varepsilon_0)$. From the proof of Theorem 2.1 we deduce

that the pointwise limits $\lim_{\ell\to\infty} \phi_{\ell,\varepsilon}(x)$ exist for each $x \in \mathbb{R}$ and must lie on the stable manifold $W^s(\phi_{*,\varepsilon})$ in (2.1), where $\phi_{*,\varepsilon} \in \mathcal{M}$ is a saddle converging to $(\psi_*, 0)$ as $\varepsilon \to 0$. Moreover, the limiting orbit $\{\lim_{\ell\to\infty} \phi_{\ell,\varepsilon}(x) : x \in \mathbb{R}\}$ is reversibly symmetric. On the other hand, the proof of Theorem 2.1 – see [11, Theorem 2.1] – shows that the 2-dimensional manifold $W^s(\phi_{*,\varepsilon})$ intersects the reversibility symmetry plane $p = q = 0$ transversally in $\phi_{\infty,\varepsilon}(0)$. This intersection point is locally unique in a small ε- and ℓ-independent neighborhood of $\phi_{\infty,\varepsilon}(0)$. Thus, we conclude that for $x \in [0, L_{\ell,\varepsilon}]$, the pointwise limits $\lim_{\ell\to\infty} \phi_{\ell,\varepsilon}(x)$ are given by the homoclinic $\phi_{\infty,\varepsilon}(x)$. $\qquad\square$

Remark 4.2. Theorem 4.1 states that for fixed $\varepsilon \in (0, \varepsilon_0)$, the orbit of the periodic pulse $\phi_{\ell,\varepsilon}$ converges to the orbit of the homoclinic $\phi_{\infty,\varepsilon}$ as $\ell \to \infty$. If we subsequently take the limit $\varepsilon \to 0$, we obtain the singular concatenation (4.2). On the other hand, the orbit of $\phi_{\ell,\varepsilon}$ converges to (4.1) in the limit $\varepsilon \to 0$. Taking subsequently the long-wavelength limit $\ell \to \infty$ again yields (4.2). Thus, we may conclude that the limits $\lim_{\varepsilon\to 0} \lim_{\ell\to\infty} \phi_{\ell,\varepsilon}$ and $\lim_{\ell\to\infty} \lim_{\varepsilon\to 0} \phi_{\ell,\varepsilon}$ with respect to Hausdorff metric on $\mathbb{R}^4$ are equal.

4.2 Spectral geometry of long-wavelength periodic pulse solutions

Assume **(S1)**, **(S2)**, **(E1)** and **(E2)** hold true. For fixed $\varepsilon \in (0, \varepsilon_0)$, Theorem 4.1 provides a family of periodic pulse solutions $\phi_{\ell,\varepsilon}(x)$ to (1.2) converging pointwise to a homoclinic pulse solution $\phi_{\infty,\varepsilon}(x)$ as $\ell \to \infty$.

We are interested in Hopf destabilization of long-wavelength periodic pulses $\phi_{\ell,\varepsilon}$, for $\ell \gg 1$. Such a destabilization is caused by two complex conjugate curves of spectrum moving through the imaginary axis, away from the origin. Since these spectral curves converge to the eigenvalues associated with the homoclinic limit as $\ell \to \infty$ [15, 35], Hopf destabilizations of $\phi_{\ell,\varepsilon}$ occur in the vicinity of a Hopf instability of $\phi_{\infty,\varepsilon}$ as long as the critical spectral curve is confined to the left half-plane – see §1. Recall that Hopf instabilities of the homoclinic pulse occur when a conjugate pair of roots $\lambda_{\infty,\pm}$ of $\mathcal{E}_{\infty,s}$ moves through the imaginary axis.

Thus, to understand the character of the Hopf destabilization of long-wavelength periodic pulses, we need to have information about three spectral curves. First, we are interested in the position of the critical spectral curve attached to the origin, for $\ell \gg 1$. Second, we need to understand the geometry of the spectral curves that shrink to the eigenvalues $\lambda_{\infty,\pm}$ of the limiting homoclinic as $\ell \to \infty$. The first curve is by Theorem 3.4 to leading order approximated by the quantity $\lambda_{\ell,0}^s(\nu)$, defined in (3.18). The other two curves will be embedded in the set $\{\lambda \in \mathbb{C} : \mathcal{E}_{\ell,s}(\lambda, \gamma) = 0, \gamma \in S^1\}$ as $\varepsilon \to 0$ by Theorem 3.2; see also the discussion in Section 3.3.1.

For the following we define and choose

$$\omega_* := \sqrt{\partial_u H_1(u_*, 0, 0)}, \tag{4.3}$$

$$\omega_\infty := \sqrt{\partial_u H_1(u_*, 0, 0) + \lambda_\infty}, \tag{4.4}$$

$$\varsigma_* \in (0, \omega_*). \tag{4.5}$$

Regarding the spectral curve that is attached to the origin, we have the following results.

Theorem 4.3. *Suppose that the quantities $\mathfrak{a}_\infty$ and $\mathfrak{j}_\infty$, defined in (3.15), are non-zero. Then, for $1 \ll \ell < \infty$, the analytic curve $\lambda_{\ell,0}^s(\nu)$, given by (3.18), can be expanded in terms of $e^{-2\omega_*\ell}$ as*

$$\left| \lambda_{\ell,0}^s(\nu) - \frac{2\mathfrak{w}_\infty \omega_* e^{-2\omega_*\ell}(\cos(\nu)-1)}{\mathfrak{j}_\infty} \right| \le C e^{-(2\omega_* + \varsigma_*)\ell}, \tag{4.6}$$

where $C > 0$ is independent of ℓ and ν and

$$\mathfrak{w}_\infty := -\frac{\int_{-\infty}^{\infty} \frac{\partial G}{\partial u}(u_\infty(0), v_h(x, u_\infty(0)), 0) \partial_x v_h(x, u_\infty(0)) x \, dx}{\int_{-\infty}^{\infty} (\partial_x v_h(x, u_\infty(0)))^2 \, dx}. \tag{4.7}$$

Remark 4.4. In [36], one studies the critical spectral curve associated with long-wavelength periodic solutions to reaction-diffusion systems without assuming the presence of a small parameter ε. Thus, the above result could also have been obtained by taking the singular limit $\varepsilon \to 0$ of the expansion in [36, Theorem 5.5]. However, we stress that, in that case, one should check whether the error estimates in [36] are in fact ε-uniform.

The second key result reveals the leading and next order geometry of the other two spectral curves converging to the critical eigenvalues $\lambda_{\infty,\pm}$ of the limiting homoclinic as $\ell \to \infty$.

Theorem 4.5. *Let $\lambda_\infty \in C_\Lambda \setminus \mathcal{E}_{\infty,f}^{-1}(0)$ be a simple zero of $\mathcal{E}_{\infty,s}$ satisfying*

$$-4\mathrm{Re}(\lambda_\infty)\omega_*^2 < \mathrm{Im}(\lambda_\infty)^2, \tag{4.8}$$

Take ς_∞ such that $\omega_* < \varsigma_\infty < \mathrm{Re}(\omega_\infty)$.
Then, for all $1 \ll \ell < \infty$ there exists an analytic curve $\lambda_\ell \colon [-1,1] \to \mathbb{C}$ satisfying the following assertions:

1. *For each $\gamma \in S^1$ the point $\lambda_\ell(\mathrm{Re}(\gamma))$ is the unique zero of $\mathcal{E}_{\ell,s}(\cdot,\gamma)$ converging to λ_∞ as $\ell \to \infty$.*

2. *The curve λ_ℓ can be expanded in terms of $e^{-2\omega_*\ell}$ as*

$$\lambda_\ell(\gamma_r) = \lambda_\infty + L_0 e^{-2\omega_*\ell} + \mathcal{R}_{2,\ell}(\gamma_r),$$

$$L_0 := \frac{2\left(\omega_* \lim_{\check{x}\to\infty} (u_\infty(\check{x}) - u_*)\, e^{\omega_*\check{x}}\right)^2}{\mathfrak{a}_\infty \mathcal{E}'_{\infty,s}(\lambda_\infty)} \left([\hat{u}_\infty(0,\lambda_\infty)]^2\, \partial_u \mathcal{G}(u_\infty(0),\lambda_\infty) \right. \tag{4.9}$$

$$\left. + 2\int_0^\infty \partial_{uu}H_1(u_\infty(\check{x}),0,0)\tilde{u}_\infty(\check{x})\, [\hat{u}_\infty(\check{x},\lambda_\infty)]^2\, d\check{x}\right),$$

where $\mathfrak{a}_\infty$ is defined in (3.15) and the remainder $\mathcal{R}_{2,\ell}(\gamma_r)$ is bounded as $|\mathcal{R}_{2,\ell}(\gamma_r)| \leq C\max\left\{e^{-3\varsigma_*\ell}, e^{-2\varsigma_\infty\ell}\right\}$ with $C > 0$ independent of ℓ and γ_r. Here, $\hat{u}_\infty(\check{x},\lambda)$ denotes the u-coordinate of the unique solution $\varphi_\infty(\check{x},\lambda)$ to the slow eigenvalue problem

$$\varphi_{\check{x}} = \mathcal{A}_\infty(\check{x},\lambda)\varphi, \quad \varphi \in \mathbb{C}^2, \qquad \mathcal{A}_\infty(\check{x},\lambda) := \begin{pmatrix} 0 & 1 \\ \partial_u H_1(u_\infty(\check{x}),0,0) + \lambda & 0 \end{pmatrix} \tag{4.10}$$

satisfying (3.10), and $\tilde{u}_\infty(\check{x})$ is the solution to the initial value problem

$$\tilde{u}_{\check{x}\check{x}} = \partial_u H_1(u_\infty(\check{x}),0,0)\tilde{u}, \qquad \tilde{u}(0) = 1, \quad \tilde{u}'(0) = \mathcal{J}'(u_\infty(0)).$$

3. *The derivatives of λ_ℓ at $\gamma_r \in [-1,1]$ are approximated by*

$$\left|\lambda_\ell'(\gamma_r) - L_1 e^{-2\varsigma_\infty\ell}\right| \leq Ce^{-(2\varsigma_\infty+\varsigma_*)\ell}, \qquad \left|\lambda_\ell''(\gamma_r) - L_{2,\ell}e^{-4\omega_\infty\ell}\right| \leq Ce^{-(4\varsigma_\infty+\varsigma_*)\ell}, \tag{4.11}$$

with $C > 0$ independent of ℓ and γ_r, and

$$L_1 := \frac{4\omega_\infty}{\mathcal{E}'_{\infty,s}(\lambda_\infty)}, \qquad L_{2,\ell} := L_1^2\left(\frac{-2\ell}{\omega_\infty} + \frac{1}{\omega_\infty^2} - \frac{\mathcal{E}''_{\infty,s}(\lambda_\infty)}{\mathcal{E}'_{\infty,s}(\lambda_\infty)}\right). \tag{4.12}$$

Remark 4.6. The quantities $\pm\omega_*$ in Theorems 4.3 and 4.5 correspond to the spatial eigenvalues of the linearization about the fixed point $(u_*,0)$ in the slow reduced system (2.3). Moreover, $\pm\omega_\infty$ are the spatial eigenvalues of the asymptotic system obtained by taking the limit $\check{x} \to \pm\infty$ in the slow eigenvalue problem (4.10) for $\lambda = \lambda_\infty$. Note that condition (4.8) is equivalent to $\omega_* < \mathrm{Re}(\omega_\infty)$. In particular, any $\lambda_\infty \in i\mathbb{R} \setminus \{0\}$ satisfies (4.8).

Theorem 4.5 provides an expansion of the coefficients of γ_r^0, γ_r^1 and γ_r^2 in the power series expansion of $\lambda_\ell(\gamma_r)$, yielding

$$\lambda_\ell(\gamma_r) = \left(\lambda_\infty + L_0 e^{-2\omega_*\ell} + O\left(e^{-3\varsigma_*\ell}, e^{-2\varsigma_\infty\ell}\right)\right)\gamma_r^0 + \left(L_1 e^{-2\omega_\infty\ell} + O\left(e^{-(2\varsigma_\infty+\varsigma_*)\ell}\right)\right)\gamma_r^1$$

$$+ \left(L_{2,\ell}e^{-4\omega_\infty\ell} + O\left(e^{-(4\varsigma_\infty+\varsigma_*)\ell}\right)\right)\gamma_r^2 + O\left(\gamma_r^3\right). \tag{4.13}$$

We emphasize that the coefficients in the power series (4.13) have very different magnitudes in ℓ. The distance $\lambda_\ell(\gamma_r) - \lambda_\infty$ is for example much larger than the distance between the end points $\lambda_\ell(\pm 1)$, since λ_∞ satisfies (4.8) – see also Figure 9.
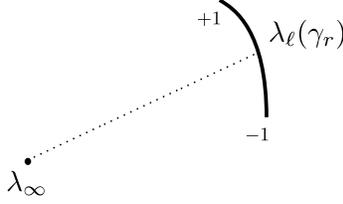
Figure 9: Depicted is the setting of Theorem 4.5. Notice that the translation $\lambda_\ell(\gamma_r) - \lambda_\infty$ is much larger than the distance between the end points $\lambda_\ell(\pm 1)$. Moreover, to leading order, the curve λ_ℓ is a straight line, because the quadratic deformation of the curve is of higher order than the distance between the end points $\lambda_\ell(\pm 1)$.

4.3 Spectral stability of long-wavelength periodic pulse solutions

Consider the family of periodic pulse solutions $\phi_{\ell,\varepsilon}(x)$, established in Theorem 4.1, converging pointwise to the homoclinic limit $\phi_{\infty,\varepsilon}(x)$ as $\ell \to \infty$. The fact that the spectral curves corresponding to $\phi_{\ell,\varepsilon}$ shrink to the eigenvalues associated with the homoclinic pulse $\phi_{\infty,\varepsilon}$ as $\ell \to \infty$, does not imply that spectral stability properties of the homoclinic pulse are inherited by the periodic pulses – see §1. This depends on the location of critical spectral curve attached to the origin.

By Theorem 4.3 the relative location of the critical curve with respect to the imaginary axis does not change as $\ell \to \infty$, under the generic assumption that the quantities $\mathfrak{a}_\infty$, $\mathfrak{j}_\infty$ and $\mathfrak{w}_\infty$, defined in (3.15) and (4.7), are non-zero. Depending on the sign of these quantities, long-wavelength periodic pulses inherit the (spectral) stability properties of the limiting homoclinic pulse.

Corollary 4.7. *Suppose that the slow Evans function $\mathcal{E}_{\infty,s}$ (3.11) has no roots $\lambda \in \mathbb{C}$ with $\mathrm{Re}(\lambda) \geq 0$ and that the quantities $\mathfrak{a}_\infty, \mathfrak{i}_\infty, \mathfrak{j}_\infty$ and $\mathfrak{w}_\infty$, defined in (3.15), (3.16) and (4.7), are non-zero. Then, there exists $\ell_0 > 0$ such that for each $\ell \in (\ell_0, \infty)$ the following holds true.*

1. *If $\mathfrak{j}_\infty$ and $\mathfrak{w}_\infty$ have the same sign, then the periodic pulse solution $\phi_{\ell,\varepsilon}$ to (1.2) is spectrally stable, provided $\varepsilon > 0$ is sufficiently small.*

2. *If $\mathfrak{j}_\infty$ and $\mathfrak{w}_\infty$ have different signs, then $\phi_{\ell,\varepsilon}$ is spectrally unstable, provided $\varepsilon > 0$ is sufficiently small.*

Proof. Observe that the quantity $\mathfrak{i}_\ell$, defined in (3.16), converges to $\mathfrak{i}_\infty$ as $\ell \to \infty$ by Theorem 4.1. Thus, by §3.3.1, $\mathcal{E}_{\ell,s}(\cdot, \gamma)$ has precisely one pole in the right half-plane for any $\gamma \in S^1$ and $\ell > 0$ sufficiently large. In addition, all roots of $\mathcal{E}_{\ell,s}(\cdot, \gamma)$ in the right half-plane converge to roots of $\mathcal{E}_{\infty,s}$ as $\ell \to \infty$ by Theorem 4.5. Therefore, we conclude that $\mathcal{E}_{\ell,0}(\cdot, \gamma)$ has no roots $\lambda \in \mathbb{C} \setminus \{0\}$ with $\mathrm{Re}(\lambda) \geq 0$ for any $\gamma \in S^1$ and $\ell > 0$ sufficiently large. In addition, 0 is a simple root of $\mathcal{E}_{\ell,f}$ and $\mathcal{E}_{\ell,s}(0, \gamma) \neq 0$ for each $\gamma \in S^1$ and $\ell > 0$ sufficiently large.

Hence, spectral stability is determined by the position of the critical spectral curve $\lambda_{\ell,\varepsilon}^s(\nu)$, which is approximated by the curve $\lambda_{\ell,0}^s(\nu)$, defined in (3.18), by Theorem 3.4. By Theorem 4.3, the sign of $\lambda_{\ell,0}^s(\nu)$ and its derivatives is determined by the signs of $\mathfrak{j}_\infty$ and $\mathfrak{w}_\infty$, provided $\ell > 0$ is sufficiently large. This proves the result. $\qquad\square$

We stress that the conditions in Corollary 4.7 comprise some form of nonlinear stability for the homoclinic $\phi_{\infty,\varepsilon}$ to (1.2). Indeed, these conditions imply that $\mathcal{E}_{\infty,0}$ has no zeros $\lambda \in \mathbb{C} \setminus \{0\}$ with $\mathrm{Re}(\lambda) \geq 0$, and that 0 is a simple root of $\mathcal{E}_{\infty,0}$ – see §3. Hence, the same holds for $\mathcal{E}_{\infty,\varepsilon}$, provided $\varepsilon > 0$ is sufficiently small, by Theorem 3.1. So, there exists $\beta > 0$ such that all $\lambda \in \sigma(\mathcal{L}_{\infty,\varepsilon}) \setminus \{0\}$ satisfy $\mathrm{Re}(\lambda) < -\beta$ and $\lambda = 0$ is a simple eigenvalue of $\mathcal{L}_{\infty,\varepsilon}$. The latter implies by [17, Section 5.1] nonlinear stability with asymptotic phase. On the other hand, spectral stability implies nonlinear (diffusive) stability for the *periodic* pulse solution $\phi_{\ell,\varepsilon}$ by the analysis in [6, Section 3.3]. Thus, Corollary 4.7 can be employed to test whether or not nonlinear stability of the homoclinic $\phi_{\infty,\varepsilon}$ implies nonlinear stability of the nearby periodics $\phi_{\ell,\varepsilon}$, for $\ell \gg 1$.

4.4 Hopf destabilization in the homoclinic limit

Consider the family of periodic pulse solutions $\phi_{\ell,\varepsilon}(x)$, established in Theorem 4.1, converging pointwise to the homoclinic limit $\phi_{\infty,\varepsilon}(x)$ as $\ell \to \infty$. In this section we study the character of destabilization of the periodic pulse pattern $\phi_{\ell,\varepsilon}$, when the homoclinic $\phi_{\infty,\varepsilon}$ undergoes a Hopf destabilization. In §1, we reasoned that the character of destabilization of $\phi_{\ell,\varepsilon}$ is determined by the geometry of three spectral curves: the critical spectral curve attached to the origin and the two conjugate spectral curves converging to the critical eigenvalues associated with the homoclinic. We employ Theorems 4.3 and 4.5 to

obtain information about these spectral curves.

Thus, let $\lambda_\infty \in C_\Lambda$ be a simple zero of $\mathcal{E}_{\infty,s}$ in the vicinity of the imaginary axis $i\mathbb{R} \setminus \{0\}$ such that $\lambda_\infty \notin \mathcal{E}_{\infty,f}^{-1}(0)$ and the condition (4.8) is satisfied. We infer from Theorem 4.5 – see also (4.13) – that there is a unique curve $\lambda_\ell \colon [-1, 1] \to \mathbb{C}$ of zeros of $\mathcal{E}_{\ell,s}$ shrinking to λ_∞ as $\ell \to \infty$ exponentially with rate $-2\omega_*\ell$. By (4.11), the curve λ_ℓ is to leading order a straight line that rotates with frequency $\mathrm{Im}(\omega_\infty)/\pi$ and whose length decays exponentially with rate $-2\mathrm{Re}(\omega_\infty)\ell$ as $\ell \to \infty$. Therefore, the point on λ_ℓ with largest real part will generically be one of the endpoints $\lambda_\ell(\pm 1)$. The following result shows that this is actually always the case – see Figure 5 in the Introduction.

Corollary 4.8 (Belly-dance). *Let $\lambda_\infty \in C_\Lambda \setminus \mathcal{E}_{\infty,f}^{-1}(0)$ be a simple zero of $\mathcal{E}_{\infty,s}$ satisfying (4.8). For $0 \ll \ell < \infty$ the point of largest real part on $\lambda_\ell([-1, 1])$, where $\lambda_\ell \colon [-1, 1] \to \mathbb{C}$ is established in Theorem 4.5, is always one of the endpoints $\lambda_\ell(\pm 1)$. Specifically, recall L_1 defined in (4.12), and consider the quantity*

$$\chi_\ell := L_1 e^{-2\omega_\infty \ell}. \tag{4.14}$$

If $\mathrm{Re}(\chi_\ell) \neq 0$, then $\lambda_\ell(\mathrm{sgn}(\mathrm{Re}(\chi_\ell)))$ is the point of largest real part on $\lambda_\ell([-1, 1])$.

Proof. By (4.11), the curve $\lambda_\ell(\gamma_r)$ is to leading order a straight line. Its orientation is determined by the argument of the quantity χ_ℓ. Thus, in the case $\chi_\ell \notin i\mathbb{R}$, it is clear that $\lambda_\ell(\mathrm{sgn}(\mathrm{Re}(\chi_\ell)))$ must be the endpoint of largest real part. Now suppose $\chi_\ell \in i\mathbb{R}$. Since λ_∞ is a simple zero of $\mathcal{E}_{\infty,s}$, χ_ℓ is non-zero. Thus, we have $\chi_\ell^2 < 0$. By (4.11), the quadratic deformation of the curve λ_ℓ is to leading order determined by the quantity $-2\chi_\ell^2 \ell \omega_\infty^{-1}$, which has strictly positive real part. Hence, we derive $\mathrm{Re}(\lambda_\ell(\pm 1)) \geq \mathrm{Re}(\lambda_{\ell_v}(\gamma_r))$ for all $\gamma_r \in [-1, 1]$. This concludes the proof. $\square$

Now suppose equation (1.2) depends on a real parameter μ. We make the following assumption:

(HO) There is $\mu_* \in \mathbb{R}$ and a unique pair $\pm\lambda_{\infty,*}$ with $\lambda_{\infty,*} \in i\mathbb{R} \setminus \{0\}$ satisfying $\mathcal{E}_{\infty,s,\mu_*}(\pm\lambda_{\infty,*}) = 0$ and

$$\mathrm{Re}\left[\frac{\partial_\mu \mathcal{E}_{\infty,s,\mu_*}(\lambda_{\infty,*})}{\partial_\lambda \mathcal{E}_{\infty,s,\mu_*}(\lambda_{\infty,*})}\right] < 0.$$

In addition, we have $\mathrm{i}_\infty(\mu_*) \neq 0$, $\mathrm{j}_\infty(\mu_*)\mathrm{w}_\infty(\mu_*) > 0$ and $\mathcal{E}_{\infty,s,\mu_*}(\lambda) \neq 0$ for all $\lambda \in \mathbb{C} \setminus \{\pm\lambda_{\infty,*}\}$ with $\mathrm{Re}(\lambda) \geq 0$.

The condition **(HO)** implies that the homoclinic $\phi_{\infty,\varepsilon}$ undergoes a Hopf destabilization at a μ-value close to μ_*. The assumption $\mathrm{j}_\infty(\mu_*)\mathrm{w}_\infty(\mu_*) > 0$ in **(HO)** yields that the critical spectral curve associated with $\phi_{\ell,\varepsilon}$ is confined to the left half-plane by Corollary 4.7, for $\ell > 0$ sufficiently large. Hence, the long-wavelength periodic pulse pattern $\phi_{\ell,\varepsilon}$ also undergoes a Hopf destabilization at a μ-value close to μ_*, since two spectral curves associated to $\phi_{\ell,\varepsilon}$ converge to the critical eigenvalues of the homoclinic $\phi_{\infty,\varepsilon}$ by Theorems 3.1, 3.2 and 4.5 as $\ell \to \infty$. The (leading-order) geometry of these spectral curves given in Theorem 4.5 and Corollary 4.8 determines the type of Hopf instability and whether the homoclinic pulse solution is the last (or first) periodic pulse to destabilize – see Figure 4 in the Introduction. Thus, Theorems 3.1, 3.2, 4.3 and 4.5 and Corollary 4.8 yield the following result.

Corollary 4.9. *Assume (HO) and fix $\delta > 0$. Then, there exists $\ell_0 > 0$ such that for each $\ell \in (\ell_0, \infty)$ the following holds true for $\varepsilon > 0$ sufficiently small:*

1. *The homoclinic pulse solution $\phi_{\infty,\varepsilon}$ to (1.2) undergoes a Hopf destabilization at $\mu = \mu_{\infty,\varepsilon}$ with $|\mu_{\infty,\varepsilon} - \mu_*| < \delta$.*

2. *The periodic pulse solution $\phi_{\ell,\varepsilon}$ to (1.2) undergoes a γ_ℓ-Hopf destabilization at $\mu = \mu_{\ell,\varepsilon}$ with $|\mu_{\ell,\varepsilon} - \mu_*| < \delta$. It holds either $|\gamma_\ell - 1| < \delta$ or $|\gamma_\ell + 1| < \delta$.*

3. *If the real part of $\chi_\ell = \chi_\ell(\mu_*)$, defined in (4.14), is non-zero, then we have $|\gamma_\ell - \mathrm{sgn}(\mathrm{Re}(\chi_\ell))| < \delta$.*

4. *If the quantity $L_0 = L_0(\mu_*)$, defined in (4.9), is non-zero, then it holds $\mathrm{sgn}(\mathrm{Re}(\mu_{\infty,\varepsilon} - \mu_{\ell,\varepsilon})) = \mathrm{sgn}(\mathrm{Re}(L_0))$, i.e. the homoclinic pulse solution is the last to destabilize if $\mathrm{Re}(L_0) > 0$.*

Remark 4.10. Corollary 4.9 implies that, as the wave number $k \sim \ell^{-1}$ of the periodic pulse pattern $\phi_{\ell,\varepsilon}$ decreases, the character of destabilization of $\phi_{\ell,\varepsilon}$ alternates between ± 1-Hopf instabilities in the limit $\varepsilon \to 0$. This has the following implications for the region of stable pulse solutions in (μ, k)-space, which is known as the Busse balloon – see §1. By Corollary 4.9, the boundary $\{(\ell^{-1}, \mu_{\ell,\varepsilon}) : \ell \in (\ell_0, \infty)\}$ of the Busse balloon is in the limit $\varepsilon \to 0$ given by two curves $\mathcal{H}_{\pm 1}$ corresponding to ± 1-Hopf instabilities of $\phi_{\ell,\varepsilon}$. The curves $\mathcal{H}_{\pm 1}$ intersect infinitely often as they oscillate about each other

while both are converging to the point $\lim_{\varepsilon \to 0}(\mu_{\infty,\varepsilon}, 0) = (\mu_*, 0)$ on the line $k = 0$, see Figure 2. Moreover, Corollary 4.8 implies that in the limit $\varepsilon \to 0$, the boundary of the Busse balloon is non-smooth at the intersection points of $\mathcal{H}_{+1}$ and $\mathcal{H}_{-1}$. Note that the non-smooth points in the boundary of the Busse balloon persist for $\varepsilon > 0$ sufficiently small. Indeed, by Corollary 4.9, close to an intersection point of $\mathcal{H}_+$ and $\mathcal{H}_-$ there are, on the one hand, points on the boundary of the Busse balloon that correspond to a γ_ε-Hopf destabilization where $\gamma_\varepsilon \to 1$ as $\varepsilon \to 0$, and on the other hand, there are points on the boundary of the Busse balloon that correspond to a γ_ε-Hopf destabilization where $\gamma_\varepsilon \to -1$ as $\varepsilon \to 0$.

We have thus established the occurrence of the Hopf and belly dance destabilization mechanisms for the general class (1.2) of slowly nonlinear systems – see Figure 2 in the Introduction. We refer to Sections 5.1 and 5.2 for numerical simulations of the Hopf and belly dances in the slowly nonlinear model equation (1.4).

As mentioned in the Introduction, it was conjectured by Wei-Ming Ni in the context of the Gierer-Meinhardt equations [25] that the homoclinic pulse solution is the last 'periodic' pulse to become unstable as we vary μ – see also [10, Remark 5.4] and Figure 2. Numerical simulations in the slowly nonlinear model equation (1.4) indicate that there exist parameter regimes where the real part of the quantity L_0, defined in (4.9), has negative sign upon destabilization – see Section 5.2. Hence, Ni's conjecture does not hold beyond the slowly linear Gierer-Meinhardt equations. We stress that a structural difference can be readily observed between both cases: the derivative $\partial_{uu}H_1(u_\infty(\check{x}), 0, 0)$ in (4.9) vanishes in the slowly linear case.

5 Numerical analysis in model system (1.4)

In this section we present numerical simulations – using the numerical continuation software Auto – for the slowly nonlinear model system (1.4) that corroborate and illustrate our analysis. In order to separate the parameters of the existence from the stability problem in the numerics, we consider (1.4) in the slightly different form

$$\begin{cases} \frac{1}{\mu}u_t &= u_{\check{x}\check{x}} - \sin u - \frac{1}{\tilde{\varepsilon}}v^2(\tilde{\nu}_2 - \tilde{\nu}_3 v) \\ v_t &= \tilde{\varepsilon}^2 v_{\check{x}\check{x}} - v + \frac{v^2}{\mu_2 + \mu_3 \sin u} \end{cases}, \quad u \in \mathbb{R}, v \in \mathbb{R}, \tag{5.1}$$

which relates to (1.4) – in the scaling of (1.1) – by setting,

$$\varepsilon = \frac{\tilde{\varepsilon}}{\sqrt{\mu}}, \quad \mu_1 = \mu, \quad \nu_1 = \tilde{\nu}_2 \sqrt{\mu}, \quad \nu_2 = \frac{\tilde{\nu}_3}{\tilde{\nu}_2}, \quad x = \tilde{\varepsilon}\check{x}, \tag{5.2}$$

(the remaining parameters are as in (1.4)). We consider several specific parameters choices in (5.1). In each case, μ is our main parameter (as in the preceding analysis). In Sections 5.1 and 5.2, we present simulations of the analytically predicted Hopf and belly dances and compare the outcome of the numerics to the analysis of model (1.4) in Sections 2.1 and 3.4. The examples are chosen such that the occurrence of each of the critical spectral configurations as depicted in Figure 4 is corroborated. In Section 5.1, Ni's conjecture holds, i.e. the critical spectrum is as in Figure 4(b) and the Busse balloon is thus as sketched in Figure 2(a). The case of Figures 4(c) and 2(b), where Ni's conjecture does not hold, is presented in Section 5.2 and the case with unstable small spectrum of Figure 4(a) is (briefly) considered in Section 5.3.

In this section, we denote by $\mu_H(\gamma, L)$ the critical value of μ such that the solution with parameter μ and period L lies on the Hopf stability boundary (of the Busse balloon) for $\gamma \in S^1$. We write $\lambda_H(\gamma, L) = \lambda_{\ell,\mu_H}$, where $\lambda_{\ell,\mu}$ is as in the previous sections, so that $\text{Re}(\lambda_H(\gamma, L)) = 0$ and $\text{Im}(\lambda_H(\gamma, L)) \neq 0$. The formulation for the implementation of the numerical procedure is the same as in [10], which relies on the results in [30]. Briefly, we write the existence problem (2.1), rescaled to $\check{x}$, jointly with the eigenvalue problem of its linearization in this solution as a boundary value problem. In a shorthand notation and with the linear part rescaled as $\Phi(\check{x}) = e^{\nu\check{x}}\varphi(\check{x})$ – with $\nu = \log(\gamma)/(2L)$ to achieve periodic boundary conditions – this reads

$$U_{\check{x}} = F(U), \quad \Phi_{\check{x}} = (F'(U) + \lambda B + \nu)\Phi, \quad (U, \Phi)(L) = (U, \Phi)(-L),$$

where F is the right hand side of (2.1) rescaled to $\check{x}$, and the matrix B encodes the second order structure. Since ε is fixed it is natural to replace the parameter ℓ used in the analysis by the half-period of the solutions $L = L_{\varepsilon,\ell}$ in this section . Recall from Theorem 2.1 that $\varepsilon L_{\varepsilon,\ell} \to \ell$ as $\varepsilon \to 0$. For continuation in a parameter $\mathfrak{p}$ we impose the phase condition $\langle \partial_\mathfrak{p}U, U_{\check{x}} \rangle = 0$ and the normalization constraint $\|\Phi\| = 1$. Except at bifurcation points, this leads, for instance, to a curve $\lambda(\mathfrak{p})$, when taking λ as a free (complex valued) parameter while keeping all other parameters fixed. With $\mathfrak{p} = \gamma$ this will compute a curve of essential spectrum. Having found a point of marginal stability, $\text{Re}(\lambda(\mathfrak{p}_0)) = 0$ at some value $\mathfrak{p} = \mathfrak{p}_0$, we can keep $\text{Re}(\lambda)$ fixed and compute $\mu(\mathfrak{p}), \text{Im}(\lambda)(\mathfrak{p})$ in this way. This leads to a stability boundary for the continuation of this point in the spectrum.
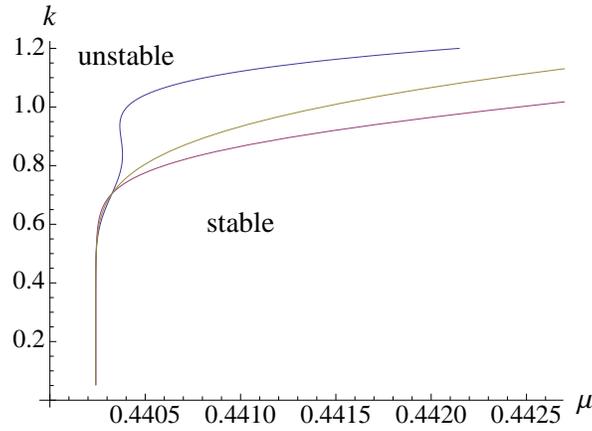
Figure 10: The spectral stability of long-wavelength patterns in model (5.1) with parameters $\tilde{\varepsilon} = 0.01, \tilde{\nu}_2 = -1.57, \tilde{\nu}_3 = -0.77, \mu_2 = 0, \mu_3 = 1$. Numerical plots in the (μ, k)-plane of the stability boundary curves $\mathcal{H}_{+1}$, i.e. $\mu = \mu_H(\gamma, L)$ for $\gamma = 1$ (blue), $\mathcal{H}_{-1}$, i.e. $\mu = \mu_H(\gamma, L)$ with $\gamma = -1$ – (red), and of $\mu = \mu_H(\gamma, L)$ with $\gamma = i$ (magenta). Ni's conjecture holds: there are no stable long-wavelength patterns for $\mu < \mu_* \approx 0.4402$.

5.1   Example 1: Ni's conjecture holds

In our first example, we consider (5.1) with parameters $\tilde{\varepsilon} = 0.01, \tilde{\nu}_2 = -1.57, \tilde{\nu}_3 = -0.77, \mu_2 = 0, \mu_3 = 1$ and varying μ around 0.44. The profile plotted in Figure 3 corresponds to one period of a marginally stable solution to (5.1) with $L = 20$; μ is chosen such that $\mu = \mu_H(1, 20) \approx 0.4402$, i.e. the critical spectral curve $\lambda_{\ell,\mu}(\gamma_r)$ has its first intersection with the imaginary axis at $\gamma_r = \gamma = 1$. Thus, the parameters and wavelength are such that the pattern depicted in Figure 3 is on the $\mathcal{H}_{+1}$ part of the boundary of the Busse balloon.

In Figure 10, we plot in the (μ, k)-plane – where $k = 1/L$ denotes the wave number – the stability boundary curves $\mathcal{H}_{\pm 1}$, which correspond to the curves $\mu_H(\gamma, L)$ for $\gamma = \pm 1$. The homoclinic limit destabilizes as μ decreases through $\mu_* \approx 0.4402$ (and clearly $\mu_* = \lim_{L \to \infty} \mu_H(\pm 1, L)$). Moreover, the homoclinic pattern is the last pattern to destabilize (as μ decreases): Ni's conjecture indeed holds (see also Figure 12(a)). Figure 10 also shows the first intersections associated with a Hopf dance. In order to illustrate both the Hopf and the belly dance, we also plot the curve $\mu_H(i, L)$ in Figure 10 and consider

$$
\begin{aligned}
r_\gamma(L) &= e^{\rho L}(\mu_H(\gamma, L) - \mu_H(i, L)), \\
s(L) &= e^{\rho L} \left(\mu_H(i, L) - \max(\mu_H(1, L), \mu_H(-1, L)) \right).
\end{aligned}
\tag{5.3}
$$

Thus, the curves $r_{\pm 1}(L)$ resolve the oscillations of the Hopf dance while the belly dance corresponds to $s(L)$ having a constant sign. In Figure 11(a) – where $\rho = 1.245$ is chosen such that the amplitude of the oscillations of $r_\gamma(L)$ remain (approximately) constant – the first 4 elements of $\mathcal{H}_{+1} \cap \mathcal{H}_{-1}$ are shown; since $s(L) < 0$, Figure 11(b) corroborates the belly dance (within numerical accuracy). To be certain that the destabilization mechanism is indeed caused by two dancing curves of Hopf destabilizations – as in Figure 2(a) – we also need to determine the small spectral curve $\lambda_{\ell,\varepsilon}^s(\nu)$ – see Figure 4(b). We refer to Figure 12 for a numerical confirmation that shows there is no unstable small spectrum.

To connect these numerical evaluations to the analysis in Sections 2.1 and 3.4, we first use (5.2) to conclude that the choice of parameters in (5.1) in this section correspond to $\nu_1 = -1.57 \sqrt{\mu}, \nu_2 \approx 0.49, \mu_1 = \mu, \mu_2 = 0, \mu_3 = 1$ and $\varepsilon = 0.01/\sqrt{\mu}$ in basic model (1.4). We consider the wave profile presented in Figure 3 for which $\mu \approx 0.44$. This pattern can be approximated by a single homoclinic pulse whose existence is established by solving (2.13) for $\kappa = 1$. Using the explicit formulation for $\mathcal{J}(u)$ in (2.12), we infer that the existence condition (2.13) is satisfied for $u_\diamond = 0.253881$. Note that, because ν_1 is scaled with $\sqrt{\mu}$, the value of $u_\diamond$ does not depend on μ. This theoretical leading-order value of the pulse amplitude corresponds very well with the numerical value of $u(0) \approx 0.25$ exhibited by the pattern in Figure 3.

Using Section 3.4, we can determine the spectral curves associated with the patterns in the equivalent models (1.4)/(5.1) with the above parameter values. The main quantity of interest is the leading-order expression of the slow Evans function (3.28). By numerical evaluation of $\mathcal{E}_{\infty,s}(\lambda)$ in MATHEMATICA for the above parameter values and varying μ, we find that the homoclinic pulse undergoes a Hopf destabilization at $\mu = \mu_* \approx 0.4308$, with Hopf eigenvalues $\lambda_H \approx \pm 0.808\,i$. For this value of μ, we have $\varepsilon = 0.01/\sqrt{0.4308} \approx 0.01524$. The difference between the numerically observed Hopf destabilization value $\mu_{*,num} \approx 0.4402$ and the theoretical leading-order value is $\left| \mu_{*,num} - \mu_* \right| \approx 0.62\,\varepsilon$, which is well within an $O(\varepsilon)$ validity

(a)   (b)
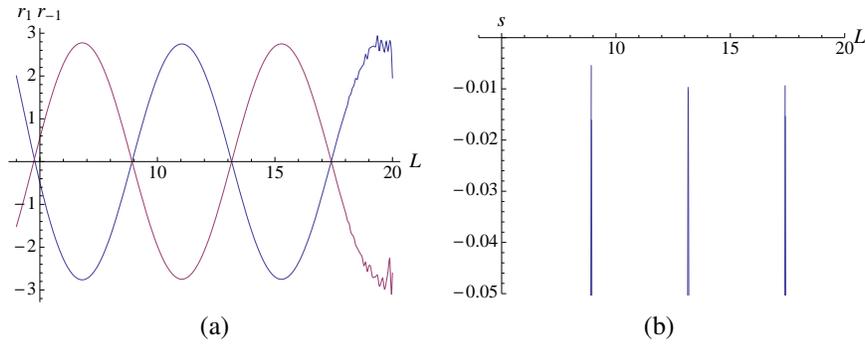
Figure 11: The first oscillations of the Hopf and belly dances in model (5.1) with parameters $\tilde{\varepsilon} = 0.01, \tilde{v}_2 = -1.57, \tilde{v}_3 = 0.77, \mu_2 = 0, \mu_3 = 1$. (a) The anti-cyclic oscillation of $r_1(L)$ (blue) versus $r_{-1}(L)$ (magenta) signifies the Hopf dance (where the numerical accuracy is insufficient to resolve the details for $L > 20$). (b) $s(L) < 0$ implies the belly dance.

(a)   (b)   (c)
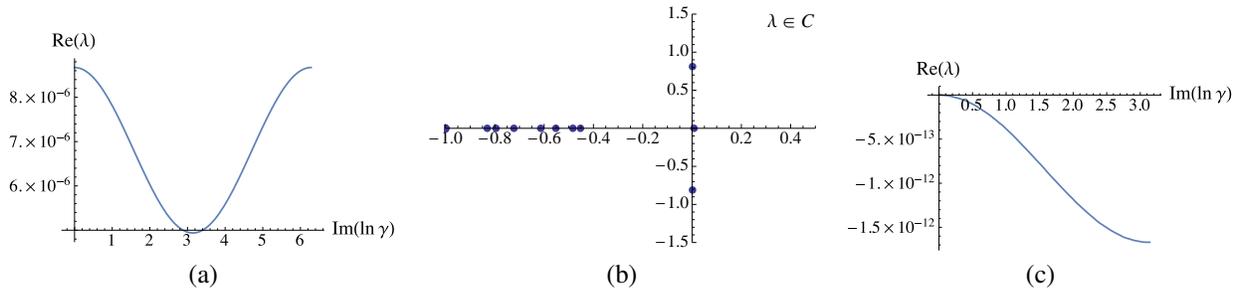
Figure 12: The spectrum for a finite difference approximation on the (periodic) domain $[-L, L]$ of a long-wavelength pattern solution to (5.1) with $L \approx 11.22, \mu = \mu_* \approx 0.4402, \tilde{\varepsilon} = 0.01, \tilde{v}_2 = -1.57, \tilde{v}_3 = -0.77, \mu_2 = 0, \mu_3 = 1$. (a) The unstable loop of critical spectrum $\lambda_{\ell,\mu}(\gamma_r)$ plotted as function of $\text{Im}(\log \gamma)$. (b) The critical finite difference spectrum on the grid from AUTO with 6400 points. (c) The small spectrum near the origin is stable.

region. Having found the leading-order values for $u_\diamond, \mu_*$ and λ_H, we can determine whether for this destabilization of the homoclinic limit pulse Ni's conjecture holds – using Corollaries 4.7 and 4.9. For the parameter values used, we calculate $j_\infty w_\infty \approx 1.281 > 0$ and $L_0 \approx 0.5138 - 1.6263\,i$. From Corollary 4.9(4), we conclude that the homoclinic pulse solution is the last 'periodic' to destabilize, as $\text{Re}(L_0) > 0$. This corroborates the above numerical observations that this is indeed a case in which Ni's conjecture holds.

5.2   Example 2: a violation of Ni's conjecture

We consider (5.1) with parameters $\tilde{\varepsilon} = 0.01, \tilde{v}_2 = 2.93, \tilde{v}_3 = 2.85, \mu_2 = 0, \mu_3 = 1$ and $\mu \in [0.27, 0.36]$. A profile of a marginally stable long-wavelength periodic pulse pattern with $L = 20$ and $\mu \approx 0.3565$ such that $(\mu, k) \in \mathcal{H}_{+1}$, is plotted in Figure 13(a). In Figure 13(b), the stability boundary curves $\mu = \mu_H(\gamma, L)$ for $\gamma = \pm 1$ – i.e. $\mathcal{H}_{\pm 1}$ – and for $\gamma = i$ are plotted in the (μ, k)-plane. As in Section 5.1, we consider $r_\pm(L)$ and $s(L)$ as defined in (5.3), now with $\rho = 1.4$ in order to demonstrate the Hopf and belly dances, see Figure 14. The numerical computation in Figure 15 shows that the small spectrum is stable, which implies that the configuration of the critical spectrum is as in Figure 4(c). We may conclude that this is an example of a case in which Ni's conjecture does not hold: the Busse balloon has the structure of Figure 2(b).

By (5.2), we find that the choice of parameters in (5.1) in this section corresponds to $v_1 = 2.93\sqrt{\mu}, v_2 \approx 0.97, \mu_1 = \mu, \mu_2 = 0, \mu_3 = 1$ in (1.4). Using condition (2.13), we calculate that $u_\diamond \approx 1.4044$, which is close to the numerical value $u(0) \approx 1.42$ – see Figure 13. The Hopf destabilization of the homoclinic pulse solution is found for $\mu_* \approx 0.30532$ with Hopf eigenvalues $\lambda_H \approx \pm 0.978\,i$. For this value of μ, we have $\varepsilon = 0.01/\sqrt{0.30532} \approx 0.0181$, so that the difference between the numerically observed Hopf destabilization value $\mu_{*,num} \approx 0.3565$ and the leading-order theoretical prediction μ_*, is $|\mu_{*,num} - \mu_*| \approx 2.83\,\varepsilon = O(\varepsilon)$. We can again use Corollaries 4.7 and 4.9 and calculate $j_\infty w_\infty \approx 0.240 > 0$ and $L_0 \approx -6.165 + 12.797\,i$. Thus, we conclude from Corollary 4.9(4) that the homoclinic pulse solution is not the last to destabilize as $\text{Re}(L_0) < 0$, and that Ni's conjecture indeed does not hold.

26

(a)   (b)
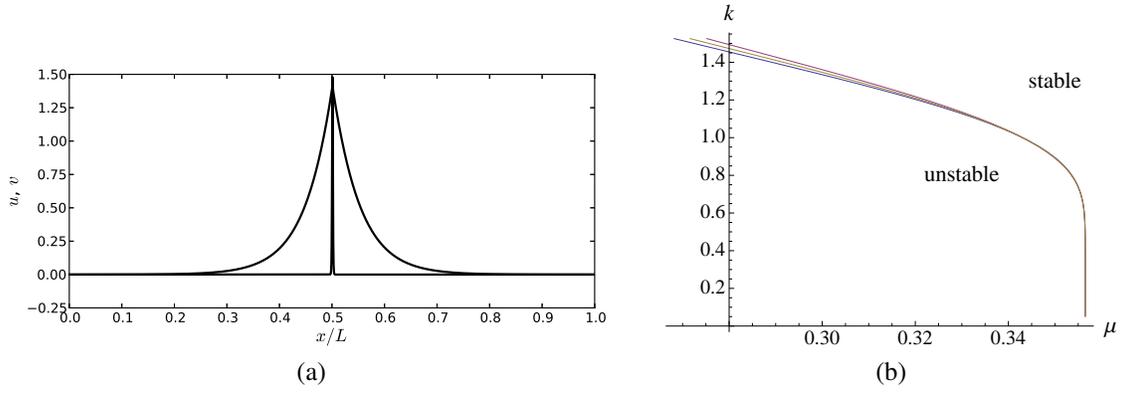
Figure 13: Long-wavelength periodic pulse solutions of (5.1) for $\tilde{\varepsilon} = 0.01, \tilde{\nu}_2 = 2.93, \tilde{\nu}_3 = 2.85, \mu_2 = 0, \mu_3 = 1$. (a) Profile of a marginally stable pattern with $L = 20$, $\mu \approx 0.3565$ and $u(0) \approx 1.42$ such that $(\mu, k) \in \mathcal{H}_{+1}$. (b) Stability boundary curves $\mu = \mu_H(\gamma, L)$ for $\gamma = 1$ ($\mathcal{H}_{+1}$; blue), -1 ($\mathcal{H}_{-1}$; red) and i (magenta) in the (μ, k)-plane.

(a)   (b)
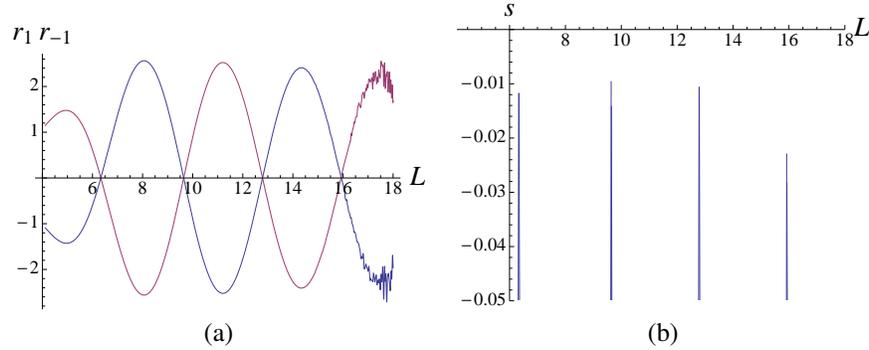
Figure 14: The first oscillations of the Hopf and belly dances in model (5.1) with parameters $\tilde{\varepsilon} = 0.01, \tilde{\nu}_2 = 2.93, \tilde{\nu}_3 = 2.85$, $\mu_2 = 0, \mu_3 = 1$. (a) The anticyclic oscillations of r_1 (blue) versus r_{-1} (magenta) signify the Hopf dance (up to $L \approx 18$) (b) The belly-dance.

5.3 Example 3: unstable small spectrum

In this section, we briefly consider spatially periodic long-wavelength pulse patterns in (5.1) with parameters $\tilde{\varepsilon} = 0.01, \tilde{\nu}_2 = 2.93, \tilde{\nu}_3 = 2.85, \mu_2 = \mu_3 = 1$ fixed and $\mu \in [0.032, 0.039]$. As in the preceding sections, we plot the stability boundary curves $\mathcal{H}_{\pm 1}$ – equivalent to $\mu_H(\pm 1, L)$ for $\gamma = \pm 1$ – and $\mu_H(i, L)$ in the (μ, k)-plane in Figure 16(a). This is a situation that strongly suggests a Busse balloon of periodic patterns near a homoclinic limit – including the familiar Hopf dance fine-structure – that violates Ni's conjecture. However, the (numerical) plot in Figure 16(b) shows that there is unstable small spectrum: the spectral configuration is as in Figure 4(a).

In the case that the critical curve of small spectrum attached to the origin is unstable, the curves $\mathcal{H}_{\pm 1}$ and the boundary of the Busse balloon may approach $(\mu_*, 0)$ from different directions in the (μ, k)-plane. In fact, the homoclinic tip $(\mu_*, 0)$ is in such a situation generically connected to the Busse-balloon boundary by a segment *on* the horizontal axis $k = 0$. Indeed, by Theorem 4.3, unstable small spectrum yields $j_\infty w_\infty \leq 0$ at $\mu = \mu_*$. In the generic situation that $j_\infty w_\infty < 0$ at $\mu = \mu_*$, we must have $j_\infty w_\infty < 0$ in a neighbourhood $M \subset \mathbb{R}$ of μ_* by continuity. Therefore, there exists by Theorem 4.3 a constant $k_0 > 0$ such that the small spectrum is unstable for any periodic pulse solution corresponding to a point $(\mu, k) \in M \times (0, k_0)$. Thus, $(\mu_*, 0)$ is connected to the boundary of the Busse balloon by a segment that lies on the axis $k = 0$. We expect that the boundary detaches from the axis $k = 0$ at a point $\mu_\diamond$ where $j_\infty w_\infty$ changes sign. The Busse-balloon boundary around the detachment point $(\mu_\diamond, 0)$ is then generically given by a curve of sideband destabilizations. Finally, in the non-generic situation that $j_\infty w_\infty = 0$ at $\mu = \mu_*$, we expect that the boundary detaches from the axis $k = 0$ *at* $(\mu_*, 0)$, although the curves $\mathcal{H}_{\pm 1}$ and the Busse-balloon boundary could still approach the homoclinic tip $(\mu_*, 0)$ from different directions in the (μ, k)-plane.
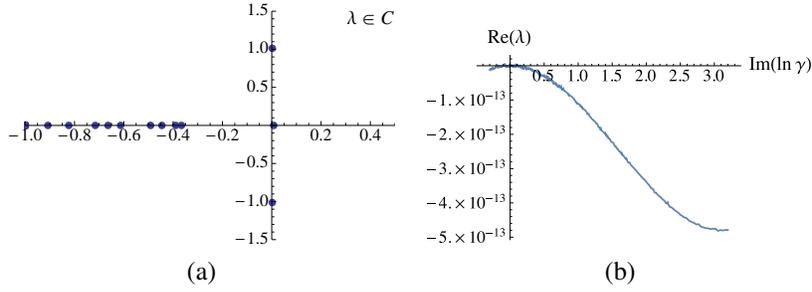
Figure 15: (a) The critical finite difference spectrum (by an adaptive grid from Auto with 6400 points) associated with the solution to (5.1) in Figure 13(a). (b) The small spectrum is stable.
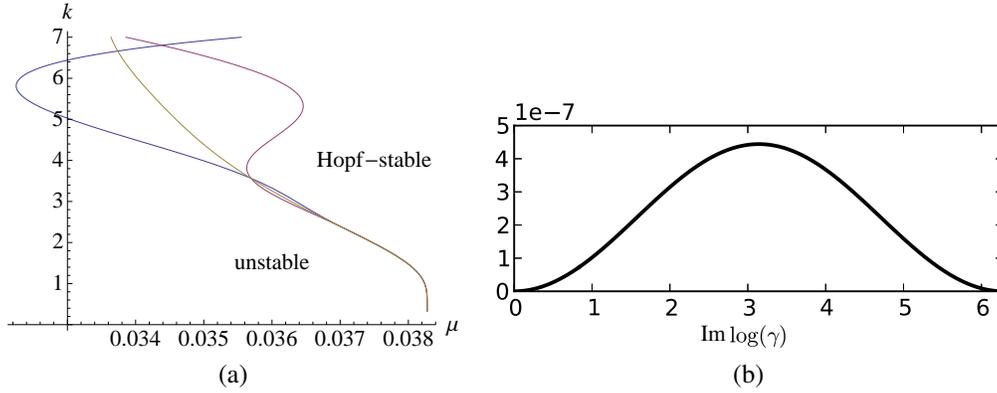
Figure 16: The stability of spatially periodic long-wavelength pulse patterns in (5.1) with parameters $\tilde{\varepsilon} = 0.01, \tilde{v}_2 = 2.93, \tilde{v}_3 = 2.85, \mu_2 = \mu_3 = 1$ fixed and vary $\mu \in [0.032, 0.039]$. (a) The stability boundary curves $\mathcal{H}_\gamma$ – or equivalently $\mu = \mu_H(\gamma, L)$ – for $\gamma = 1$ (blue), -1 (magenta), i (yellow). (b) The (unstable) small spectrum near the origin in the complex plane.

6   Proofs of key results

In this section we prove Theorems 4.3 and 4.5. Our approach is as follows. Let λ_∞ be a simple root of $\mathcal{E}_{\infty,s}$ satisfying (4.8). We want to understand the geometry of the critical curve $\lambda^s_{\ell,0}(\nu)$, defined in (3.18), and of the unique solution curve $\lambda_\ell(\gamma)$, satisfying $\mathcal{E}_{\ell,s}(\lambda_\ell(\gamma), \gamma) = 0$ for each $\gamma \in S^1$, which converges to λ_∞ as $\ell \to \infty$. By Proposition 3.3 and Theorem 3.4 we have

$$\lambda^s_{\ell,0}(\nu) = \mathfrak{a}_\ell \mathfrak{w}_\ell \frac{\cos(\nu) - 1}{2e^{-i\nu}\mathcal{E}_{\ell,s}(0, e^{i\nu})}, \tag{6.1}$$

where

$$\mathfrak{a}_\ell := \mathcal{J}'(u_\ell(0))\mathcal{J}(u_\ell(0)) - H_1(u_\ell(0), 0, 0),$$

$$\mathfrak{w}_\ell := -\frac{\int_{-\infty}^{\infty} \frac{\partial G}{\partial u}(u_\ell(0), v_{\mathrm{h}}(x, u_\ell(0)), 0)\partial_x v_{\mathrm{h}}(x, u_\ell(0))x dx}{\int_{-\infty}^{\infty} [\partial_x v_{\mathrm{h}}(x, u_\ell(0))]^2 dx}.$$

One readily observes $\mathfrak{a}_\ell \to \mathfrak{a}_\infty$ and $\mathfrak{w}_\ell \to \mathfrak{w}_\infty$ as $\ell \to \infty$ by Theorem 4.1. Thus, to prove Theorems 4.3 and 4.5, we need to relate the periodic slow Evans function $\mathcal{E}_{\ell,s}$ to the homoclinic slow Evans function $\mathcal{E}_{\infty,s}$. The homoclinic slow Evans function $\mathcal{E}_{\infty,s}$ is defined in terms of the unique solution $\varphi_\infty(\check{x}, \lambda)$ to the *homoclinic slow eigenvalue problem* (4.10) that satisfies (3.10). Our approach is to find an analytic solution $\varphi_\ell(\check{x}, \lambda)$ to the *periodic slow eigenvalue problem*,

$$\varphi_{\check{x}} = \mathcal{A}_\ell(\check{x}, \lambda)\varphi, \quad \varphi \in \mathbb{C}^2, \quad \mathcal{A}_\ell(\check{x}, \lambda) := \begin{pmatrix} 0 & 1 \\ \partial_u H_1(u_\ell(\check{x}), 0, 0) + \lambda & 0 \end{pmatrix}, \tag{6.2}$$

that is (pointwise) close to $\varphi_\infty(\check{x}, \lambda)$ and decays exponentially on $[0, 2\ell]$. Recall that system (6.2) is R_s-reversible at $\check{x} = \ell$, i.e. the evolution $\mathcal{T}_\ell(\check{x}, \check{y}, \lambda)$ of (6.2) satisfies $R_s\mathcal{T}_\ell(\check{x}, \check{y}, \lambda)R_s = \mathcal{T}_\ell(2\ell - \check{x}, 2\ell - \check{y}, \lambda)$ for $\check{x}, \check{y} \in [0, 2\ell]$. In particular,

$\varphi_\ell^r(\check{x}, \lambda) := R_s \varphi_\ell(2\ell - \check{x}, \lambda)$ is also a solution to (6.2). Now, to relate the periodic slow Evans function $\mathcal{E}_{\ell,s}$ to $\mathcal{E}_{\infty,s}$, we multiply $\mathcal{E}_{\ell,s}(\lambda, \gamma)$ with the ($\check{x}$-independent) Wronskian $\mathcal{W}_\ell(\lambda) := \det(\varphi_\ell(\check{x}, \lambda) \mid \varphi_\ell^r(\check{x}, \lambda))$. Using the bilinearity of the determinant and the fact that $\det(\Upsilon(u, \lambda)), \det(\mathcal{T}_\ell(\check{x}, \check{y}, \lambda)) = 1$ for all $\check{x}, \check{y} \in [0, 2\ell]$, $\lambda \in C_\Lambda$ and $u \in U_h$, we derive the key identity

$$\gamma^{-1} \mathcal{E}_{\ell,s}(\lambda, \gamma) \mathcal{W}_\ell(\lambda) := 2\mathrm{Re}(\gamma) \mathcal{W}_\ell(\lambda) - \mathcal{K}_\ell(\lambda), \tag{6.3}$$

where $\mathcal{K}_\ell \colon C_\Lambda \to \mathbb{C}$ is defined by

$$\begin{aligned} \mathcal{K}_\ell(\lambda) = \det\left(\varphi_\ell(0, \lambda) \mid \Upsilon(u_\ell(0), \lambda) R_s \varphi_\ell(0, \lambda)\right) \\ + \det\left(\Upsilon(u_\ell(0), \lambda) \varphi_\ell(2\ell, \lambda) \mid R_s \varphi_\ell(2\ell, \lambda)\right). \end{aligned} \tag{6.4}$$

Since $\varphi_\ell(2\ell, \lambda)$ decays exponentially as $\ell \to \infty$, one observes that the right hand side of (6.3) converges to the homoclinic slow Evans function $\mathcal{E}_{\infty,s}(\lambda)$ as $\ell \to \infty$. This leads to the desired approximation (4.6) of $\lambda_{0,\ell}(\nu)$ in Theorem 4.3.

To prove Theorem 4.5, we apply the implicit function theorem to (6.3). This yields the existence of a curve $\lambda_\ell \colon [-1, 1] \to \mathbb{C}$ such that for each $\gamma \in S^1$, the point $\lambda_\ell(\mathrm{Re}(\gamma))$ is the unique zero of $\mathcal{E}_{\ell,s}(\cdot, \gamma)$ converging to λ_∞ as $\ell \to \infty$. To calculate the leading-order difference $\lambda_\ell(\mathrm{Re}(\gamma)) - \lambda_\infty$ in order to prove (4.9), we need the leading-order expressions of the differences $\varphi_\ell(\check{x}, \lambda) - \varphi_\infty(\check{x}, \lambda)$ and $\psi_\ell(\check{x}) - \psi_\infty(\check{x})$ of the solutions to the slow eigenvalue problems and the slow reduced system, respectively. Finally, identity (4.11) is proved by implicit differentiation of identity (6.3).

Thus, the set-up of this section is as follows. First, we will establish a leading-order expression for the difference $\psi_\ell(\check{x}) - \psi_\infty(\check{x})$ of the solutions to the slow reduced system (2.3). This allows us to approximate $u_\ell(0)$ by $u_\infty(0)$ in (6.4). Second, we construct the desired solution $\varphi_\infty(\check{x}, \lambda)$ to (6.2) that is close to the solution $\varphi_\infty(\check{x}, \lambda)$ to (4.10) and decays exponentially on $[0, 2\ell]$. At the same time, we establish a leading-order expression for the difference $\varphi_\ell(\check{x}, \lambda) - \varphi_\infty(\check{x}, \lambda)$. Finally, we provide the proofs of Theorems 4.3 and 4.5 using the approach described above.

6.1 Approximations in the slow reduced subsystem

We start by collecting some basic facts for the situation described in §4.1. Recall the definition of ς_* and ω_* provided in Theorems 4.3 and 4.5. Since $\psi_* = (u_*, 0)$ is a hyperbolic saddle in (2.3) by (**E2**), we have

$$\|\psi_\infty(\check{x}) - \psi_*\| \le C e^{-\varsigma_* \check{x}}, \quad \check{x} \ge 0, \tag{6.5}$$

where $C > 0$ is a constant. The eigenvectors of the linearization of (2.3) about ψ_* are given by $w_\pm := (1, \pm\omega_*)$. We obtain by the stable manifold theorem:

$$\left\| e^{\omega_* \check{x}}(\psi_\infty(\check{x}) - \psi_*) - \alpha_* w_- \right\|, \left\| e^{\omega_* \check{x}} \psi_\infty'(\check{x}) + \alpha_* \omega_* w_- \right\| \le C e^{-\varsigma_* \check{x}}, \quad \check{x} \ge 0, \tag{6.6}$$

where $\alpha_* \in \mathbb{R} \setminus \{0\}$ is given by

$$\alpha_* := \lim_{\check{x} \to \infty} e^{\omega_* \check{x}}(u_\infty(\check{x}) - u_*).$$

It is well known that in a neighborhood of the point ψ_*, one can give growth and decay rates of solutions to the (un)stable manifolds, see for example [19, Proposition 3.1]. Using these bounds, one can estimate the distance between ψ_ℓ and ψ_∞ in terms of the 'time of flight' ℓ. Indeed, it holds for $0 \ll \ell < \infty$ that

$$\|\psi_\ell(\check{x}) - \psi_\infty(\check{x})\| \le C e^{-\varsigma_*(2\ell - \check{x})}, \quad \check{x} \in [0, 2\ell], \tag{6.7}$$

with $C > 0$ a constant independent of ℓ.

We need a leading-order expression for the difference $\psi_\ell(\check{x}) - \psi_\infty(\check{x})$. Identity (6.7) gives an a priori estimate for this quantity, which is used in the proof of the next proposition.

Proposition 6.1. *For $0 \ll \ell < \infty$ we have the following expansion:*

$$\psi_\ell(\check{x}) = \psi_\infty(\check{x}) - \frac{2\omega_*^2 \alpha_*^2 e^{-2\omega_* \ell}}{\mathfrak{a}_\infty} \Phi_\infty(\check{x}, 0) \begin{pmatrix} 1 \\ \mathcal{J}'(u_\infty(0)) \end{pmatrix} + \mathcal{R}_{1,\ell}(\check{x}), \quad \check{x} \in [0, \ell], \tag{6.8}$$

where $\mathfrak{a}_\infty$ is defined in (3.15), the remainder $\mathcal{R}_\ell \colon [0, \ell] \to \mathbb{C}^2$ is bounded by $\|\mathcal{R}_\ell(\check{x})\| \le C e^{-\varsigma_*(3\ell - \check{x})}$ with $C > 0$ independent of ℓ, and where $\Phi_\infty(\check{x}, \check{y})$ denotes the evolution operator of the variational equation of (2.3) about ψ_∞,

$$\theta_{\check{x}} = \mathcal{A}_\infty(\check{x})\theta, \quad \theta \in \mathbb{R}^2, \qquad \mathcal{A}_\infty(\check{x}) := \begin{pmatrix} 0 & 1 \\ \partial_u H_1(u_\infty(\check{x}), 0, 0) & 0 \end{pmatrix}. \tag{6.9}$$

Proof. In the following, we denote by $C > 0$ a constant independent of ℓ.

Define $\theta_\ell(\check{x}) = \psi_\ell(\check{x}) - \psi_\infty(\check{x})$ for $\check{x} \in [0, \ell]$. Our approach is to obtain a leading-order expression for $\theta_\ell(\check{x})$ using Lin's method [23, 44]. Note that θ_ℓ solves the boundary value problem

$$\theta_{\check{x}} = \mathcal{A}_\infty(\check{x})\theta + g_0(\theta, \check{x}),$$

$$\theta(0) + \psi_\infty(0) \in T_+, \tag{6.10}$$

$$\theta(\ell) + \psi_\infty(\ell) \in \ker(I - R_s), \tag{6.11}$$

where $g_0 \colon \mathbb{R}^3 \to \mathbb{R}^2$ is defined by

$$g_0(\theta, \check{x}) := f(\psi_\infty(\check{x}) + \theta) - f(\psi_\infty(\check{x})) - \mathcal{A}_\infty(\check{x})\theta.$$

Our plan is to study the inhomogeneous equation,

$$\theta_{\check{x}} = \mathcal{A}_\infty(\check{x})\theta + g(\check{x}), \quad \theta \in \mathbb{R}^2. \tag{6.12}$$

with $g \in C([0, \ell], \mathbb{R}^2)$ first. Using the exponential dichotomy of the variational equation, we construct a solution operator to (6.12). Subsequently, we substitute $g_0(\theta, \check{x})$ for $g(\check{x})$ and formulate an integral formulation for $\theta_\ell(\check{x})$ that is of fixed point type. This enables us to obtain a leading-order expression for $\theta_\ell(\check{x})$.

We establish an exponential dichotomy for the variational equation (6.9). First, the matrix function $\mathcal{A}_\infty(\check{x})$ converges as $\check{x} \to \infty$ to the asymptotic matrix $\mathcal{A}_*$. More precisely, by (6.5) it holds for $\check{x} \geq 0$ that

$$\|\mathcal{A}_\infty(\check{x}) - \mathcal{A}_*\| \leq Ce^{-\varsigma_*\check{x}}.$$

Second, the derivative $\psi'_\infty(\check{x})$ is a solution to (6.9), which is bounded as $\check{x} \to \infty$. Combining these items with Proposition A.3 yields an exponential dichotomy of (6.9) on $[0, \infty)$ with constants $C, \varsigma_* > 0$ and projections $P_\infty(\check{x})$. By Lemma A.5 we may, without loss of generality, assume that $P_\infty(0)$ is the projection on $\mathrm{Sp}(\psi'_\infty(0))$ along $\mathrm{Sp}(1, \mathcal{J}'(u_\infty(0)))$, since the stable manifold $W^s(\psi_*)$ intersects the touch-down curve $\mathcal{T}_+$ transversally in $\psi_\infty(0)$ by **(E2)**. In addition, Lemma A.4 yields the estimate

$$\|P_\infty(\check{x}) - P_*\| \leq Ce^{-\varsigma_*\check{x}}, \quad \check{x} \geq 0, \tag{6.13}$$

where P_* denotes the spectral projection of $\mathcal{A}_*$ on $\mathrm{Sp}(w_-)$ along $\mathrm{Sp}(w_+)$.

We proceed by constructing a solution operator to the boundary value problem (6.10)-(6.11). Denote by $\Phi_\infty^{u,s}(\check{x}, \check{y})$ the (un)stable evolution operator of (6.9) under the exponential dichotomy. The bounded, linear solution operator $W_\ell \colon \ker(P_*) \times P_\infty(0)[\mathbb{R}^2] \times C([0, \ell], \mathbb{R}^2) \to C([0, \ell], \mathbb{R}^2)$ given by

$$W_\ell(a, b, g)[\check{x}] = \Phi_\infty^u(\check{x}, \ell)a + \Phi_\infty^s(\check{x}, 0)b + \int_0^{\check{x}} \Phi_\infty^s(\check{x}, z)g(z)dz - \int_{\check{x}}^\ell \Phi_\infty^u(\check{x}, z)g(z)dz,$$

solves (6.12). Since G is C^3 on its domain by **(S1)**, the homoclinic solution $\kappa_h(x, u) = (v_h(x, u), q_h(x, u))$ to (2.4) is C^3 on its domain $\mathbb{R} \times U_h$. Therefore, $\mathcal{J}$ is C^3 on U_h. We expand $\mathcal{J}(u)$ in the neighborhood U_h of $u_\infty(0)$ with Taylor's Theorem as

$$\mathcal{J}(u) = \mathcal{J}(u_\infty(0)) + \mathcal{J}'(u_\infty(0))(u - u_\infty(0)) + h(u - u_\infty(0)), \quad u \in U_h,$$

where $h(u - u_\infty(0)) \leq C|u - u_\infty(0)|^2$. Since $\psi_\infty(0)$ equals $(u_\infty(0), \mathcal{J}(u_\infty(0))) \in T_+$, we have that $\theta(\check{x}) = W_\ell(a, b, g)[\check{x}]$ satisfies condition (6.10) if and only if there exists $\rho \in U_h - u_\infty(0)$ such that

$$\Phi_\infty^u(0, \ell)a + b - \int_0^\ell \Phi_\infty^u(0, z)g(z)dz = \rho\begin{pmatrix} 1 \\ \mathcal{J}'(u_\infty(0)) \end{pmatrix} + \begin{pmatrix} 0 \\ h(\rho) \end{pmatrix}. \tag{6.14}$$

For a vector $w := (w_1, w_2) \in \mathbb{R}^2$ we denote by $w^\perp$ the vector $(-w_2, w_1)$, which is perpendicular to w. Taking the inner product on both sides of (6.14) with $\psi'_\infty(0)^\perp$ yields

$$\left\langle \Phi_\infty^u(0, \ell)a - \int_0^\ell \Phi_\infty^u(0, z)g(z)dz, \psi'_\infty(0)^\perp \right\rangle = \rho\mathfrak{a}_\infty + h(\rho)u'_\infty(0). \tag{6.15}$$

Since $\mathcal{T}_+$ intersects the stable manifold $W^s(\psi_*)$ transversally by **(E2)**, the quantity $\mathfrak{a}_\infty$ is non-zero. Therefore, the right hand side of (6.15) defines an invertible function in ρ on a neighborhood of 0. Hence, there exists an ℓ-independent neighborhood A_0 of $0 \in \ker(P_0) \times C([0, \ell], \mathbb{R}^2)$ and a Lipschitz continuous map $\rho \colon A_0 \to \mathbb{R}$ such that $\rho(a, g)$ satisfies (6.15) and is bounded by

$$|\rho(a, g)| \le C(e^{-\varsigma_* \ell} \|a\| + \|g\|). \tag{6.16}$$

Now substitute $\rho(a, g)$ in (6.14) and apply $P_\infty(0)$ on both sides. This gives rise to Lipschitz continuous map $b \colon A_0 \to P_\infty(0)[\mathbb{R}^2]$ satisfying

$$b(a, g) = \frac{-h(\rho(a, g))}{\mathfrak{a}_\infty} \psi'_\infty(0), \quad \|b(a, g)\| \le C(e^{-\varsigma_* \ell} \|a\| + \|g\|)^2, \tag{6.17}$$

using that $P_\infty(0)$ projects on $\mathrm{Sp}(\psi'_\infty(0))$ along $\mathrm{Sp}(1, \mathcal{J}'(u_\infty(0)))$. By construction, $\theta[\check{x}] = W_\ell(a, b(a, g), g)[\check{x}]$ satisfies (6.14) and thus (6.10). Similarly, $\theta[\check{x}] = W_\ell(a, b(a, g), g)[\check{x}]$ satisfies condition (6.11) if there exists $\beta \in \mathbb{R}$ such that

$$(I - P_\infty(\ell))a + \Phi^s_\infty(\ell, 0)b(a, g) + \int_0^\ell \Phi^s_\infty(\ell, z)g(z)dz + \psi_\infty(\ell) - \psi_* = \beta \begin{pmatrix} 1 \\ 0 \end{pmatrix}. \tag{6.18}$$

By estimate (6.13) it holds

$$\|(I - P_\infty(\ell))w_+ - w_+\| \le Ce^{-\varsigma_* \ell}. \tag{6.19}$$

Estimate (6.19) shows that the inner product $\langle \begin{pmatrix} 1 \\ 0 \end{pmatrix}, [(I - P_\infty(\ell))w_+]^\perp \rangle$ is to leading order given by the non-zero quantity $-\omega_*$. Thus, taking the inner product on both sides of (6.18) with $[(I - P_\infty(\ell))w_+]^\perp$ yields a Lipschitz continuous map $\beta \colon A_0 \to \mathbb{R}$ given by

$$\beta(a, g) = \frac{\left\langle \Phi^s_\infty(\ell, 0)b(a, g) + \int_0^\ell \Phi^s_\infty(\ell, z)g(z)dz + \psi_\infty(\ell) - \psi_*, [(I - P_\infty(\ell))w_+]^\perp \right\rangle}{\left\langle \begin{pmatrix} 1 \\ 0 \end{pmatrix}, [(I - P_\infty(\ell))w_+]^\perp \right\rangle},$$

satisfying for $(a, g), (a_1, g) \in A_0$

$$|\beta(a, g)| \le C(e^{-\varsigma_* \ell} + \|g\| + e^{-2\varsigma_* \ell} \|a\|), \quad |\beta(a, g) - \beta(a_1, g)| \le Ce^{-\varsigma_* \ell} \|a - a_1\|, \tag{6.20}$$

by estimate (6.5). Now substitute $\beta(a, g)$ in (6.18) and apply $I - P_\infty(\ell)$ on both sides. This yields

$$a = (P_\infty(\ell) - P_*)a - (I - P_\infty(\ell))\left[\psi_\infty(\ell) - \psi_* - \beta(a, g)\begin{pmatrix} 1 \\ 0 \end{pmatrix} \right] \tag{6.21}$$

One readily verifies that the right hand side of (6.21) defines a contraction mapping in a for $\ell > 0$ sufficiently large, using estimates (6.13) and (6.20). Therefore, there exists, by the Banach fixed point theorem, an ℓ-independent neighborhood A_b of $0 \in C([0, \ell], \mathbb{R}^2)$ and a Lipschitz continuous map $a \colon A_b \to \ker(P_*)$, such that $a(g)$ satisfies equation (6.21) for each $g \in A_b$. The map a enjoys the bound

$$\|a(g)\| \le C(e^{-\varsigma_* \ell} + \|g\|). \tag{6.22}$$

We conclude that the Lipschitz continuous map $W_{1,\ell} \colon A_b \to C([0, \ell], \mathbb{R}^2)$ given by $W_{1,\ell}(g) = W_\ell(a(g), b(a(g), g), g)$ satisfies (6.10)-(6.12). Therefore, θ_ℓ is the unique solution to the fixed point problem

$$\theta = W_{1,\ell}(g_0(\theta, \cdot)). \tag{6.23}$$

By shrinking A_b if necessary, it is not difficult to verify that the right hand side of (6.23) defines indeed a contraction mapping in $\theta \in C([0, \ell], \mathbb{R}^2)$.

Finally, the above fixed point arguments provide a mechanism to expand θ_ℓ in terms of $\ell \gg 1$. The first observation is that, a priori, the norm of $\theta_\ell(\check{x})$ is bounded by $Ce^{-\varsigma_*(2\ell - \check{x})}$ by estimate (6.7). Thus, the map $\hat{g} \colon [0, \ell] \to \mathbb{R}^2$ defined by $\hat{g}(\check{x}) = g_0(\theta_\ell(\check{x}), \check{x})$ is bounded by $Ce^{-2\varsigma_*(2\ell - \check{x})}$. We invoke the bounds (6.16), (6.17), (6.20) and (6.22) on the maps ρ, b, β and a to obtain the estimates

$$\|a(\hat{g})\| \le Ce^{-\varsigma_* \ell}, \quad |\rho(a(\hat{g}), \hat{g})| \le Ce^{-2\varsigma_* \ell},$$

$$\|b(a(\hat{g}), \hat{g})\| \le Ce^{-4\varsigma_* \ell}, \quad |\beta(a(\hat{g}), \hat{g})| \le Ce^{-\varsigma_* \ell}.$$

Combining the latter estimates with (6.6), (6.13) and (6.19) yields the expansions

$$\beta(a(\hat{g}), \hat{g}) = \frac{\alpha_* \langle w_-, w_+^\perp \rangle e^{-\omega_* \ell}}{\left\langle \binom{1}{0}, w_+^\perp \right\rangle} + O\left(e^{-2\varsigma_* \ell}\right) = 2\alpha_* e^{-\omega_* \ell} + O\left(e^{-2\varsigma_* \ell}\right),$$

$$a(\hat{g}) = (I - P_*)\left[\beta(a(\hat{g}), \hat{g})\binom{1}{0}\right] + O\left(e^{-2\varsigma_* \ell}\right) = \alpha_* w_+ e^{-\omega_* \ell} + O\left(e^{-2\varsigma_* \ell}\right).$$

Substituting these expansions in $\theta_\ell = W_\ell(a(\hat{g}), b(a(\hat{g}), \hat{g}), \hat{g})$ yields

$$\psi_\ell(\check{x}) = \psi_\infty(\check{x}) + \alpha_* \Phi_\infty^u(\check{x}, \ell) w_+ e^{-\omega_* \ell} + O\left(e^{-\varsigma_*(3\ell - \check{x})}\right), \quad \check{x} \in [0, \ell]. \tag{6.24}$$

Note that $P_\infty(\check{x})$ is the projection on $\mathrm{Sp}(\psi'_\infty(\check{x}))$ along $\mathrm{Sp}\left(\Phi_\infty(\check{x}, 0)\binom{1}{\mathcal{J}'(u_\infty(0))}\right)$. Thus, we estimate with the aid of (6.6)

$$\begin{aligned}
\Phi_\infty^u(\check{x}, \ell) w_+ &= \frac{\langle w_+, \psi'_\infty(\ell)^\perp \rangle}{\mathfrak{a}_\infty} \Phi_\infty(\check{x}, 0)\begin{pmatrix} 1 \\ \mathcal{J}'(u_\infty(0)) \end{pmatrix} \\
&= \frac{-2\omega_*^2 \alpha_* e^{-\omega_* \ell}}{\mathfrak{a}_\infty} \Phi_\infty(\check{x}, 0)\begin{pmatrix} 1 \\ \mathcal{J}'(u_\infty(0)) \end{pmatrix} + O\left(e^{-\varsigma_*(2\ell - \check{x})}\right),
\end{aligned} \tag{6.25}$$

for $\check{x} \in [0, \ell]$. Combining (6.24) and (6.25) yields (6.8). $\qquad\square$

Remark 6.2. The proof of Proposition 6.1 is based on [44, Theorem 6]. The fundamental difference with [44] is that it is not the existence of θ_ℓ that is of our interest, but the leading-order behavior. Moreover, in contrast to [44], we have to consider nonlinear boundary conditions.

6.2 Approximation in slow eigenvalue problems

We proceed by constructing an analytic solution $\varphi_\ell(\check{x}, \lambda)$ to (6.2) that is close to the solution $\varphi_\infty(\check{x}, \lambda)$ to (4.10) and decays exponentially on $[0, 2\ell]$. At the same time, we establish a leading-order expression for the difference $\varphi_\ell(\check{x}, \lambda) - \varphi_\infty(\check{x}, \lambda)$. We start by collecting some facts about the solution $\varphi_\infty(\check{x}, \lambda)$ to (4.10). Recall that the coefficient matrix of (4.10) converges as $\check{x} \to \infty$ to the asymptotic matrix $\mathcal{A}_*(\lambda)$, defined in (3.9), which is hyperbolic on C_Λ. The eigenvalues of $\mathcal{A}_*(\lambda)$ are given by $\pm\omega(\lambda)$ and corresponding eigenvectors are $v_\pm(\lambda) := (1, \pm\omega(\lambda))$, where

$$\omega(\lambda) := \sqrt{\partial_u H_1(u_*, 0, 0) + \lambda}$$

denotes the principal square root. Note that both $\omega(\lambda)$ and $v_\pm(\lambda)$ are analytic on C_Λ. Choose an open and bounded subset $C_{b,\Lambda} \subset C_\Lambda$. An application of Proposition A.1 yields the estimate

$$\|e^{\omega(\lambda)\check{x}} \varphi_\infty(\check{x}, \lambda) - v_-(\lambda)\| \le Ce^{-\varsigma_* \check{x}}, \quad \check{x} \ge 0, \lambda \in C_{b,\Lambda}, \tag{6.26}$$

where $C > 0$ is a constant independent of λ.

We are now ready to prove the existence of the desired solution $\varphi_\ell(\check{x}, \lambda)$ to (6.2). To state the result, we take $\delta > 0$ such that we have

$$\mu(\lambda) := \mathrm{Re}(\omega(\lambda)) - \delta > 0,$$

for all λ in the bounded set $C_{b,\Lambda}$.

Proposition 6.3. *For $0 \ll \ell < \infty$, there exists a solution $\varphi_\ell : [0, 2\ell] \times C_{b,\Lambda} \to \mathbb{C}^2$ to the periodic slow eigenvalue problem (6.2), satisfying the bounds*

$$\begin{aligned}
\|\varphi_\ell(\check{x}, \lambda)\| &\le Ce^{-\mu(\lambda)\check{x}}, \\
\|\varphi_\ell(0, \lambda) - \varphi_\infty(0, \lambda)\| &\le Ce^{-2\min\{\varsigma_*, \mu(\lambda)\}\ell}, \\
\|\varphi_\ell(\ell, \lambda) - \varphi_\infty(\ell, \lambda)\| &\le Ce^{-(\varsigma_* + \mu(\lambda))\ell},
\end{aligned} \qquad \begin{aligned} \check{x} &\in [0, 2\ell], \\ \lambda &\in C_{b,\Lambda}, \end{aligned} \tag{6.27}$$

where $C > 0$ is a constant independent of ℓ and λ. Moreover, $\varphi_\ell(\check{x}, \cdot)$ is analytic on $C_{b,\Lambda}$ for each $\check{x} \in [0, 2\ell]$. Finally, we have for $\lambda \in C_{b,\Lambda}$ the expansion

$$\begin{aligned}
\varphi_\ell(0, \lambda) - \varphi_\infty(0, \lambda) = \\
\int_0^\ell Q_\infty(\lambda) \mathcal{T}_\infty(0, \check{y}, \lambda) \left[\mathcal{A}_\ell(\check{x}, \lambda) - \mathcal{A}_\infty(\check{x}, \lambda)\right] \varphi_\infty(\check{y}, \lambda) d\check{y} + \mathcal{R}_{1,\ell}(\lambda),
\end{aligned} \tag{6.28}$$

where $\mathcal{T}_\infty(\check{x}, \check{y}, \lambda)$ denotes the evolution operator of system (4.10), $Q_\infty(\lambda)$ *is an analytic projection along* $\mathrm{Sp}(\varphi_\infty(0, \lambda))$ *and the remainder* $\mathcal{R}_{1,\ell} \colon C_{b,\Lambda} \to \mathbb{C}^2$ *is bounded as* $\|\mathcal{R}_{1,\ell}(\lambda)\| \le C \max\left\{e^{-3\varsigma_*\ell}, e^{-2\mu(\lambda)\ell}\right\}$.

Proof. In the following, we denote by $C > 0$ a constant independent of ℓ and λ.

Our approach is to regard the periodic slow eigenvalue problem (6.2) as the perturbation

$$\varphi_{\check{x}} = (\mathcal{A}_\infty(\check{x}, \lambda) + \mathcal{H}_\ell(\check{x}))\,\varphi, \quad \varphi \in \mathbb{C}^2$$

of system (4.10) on $[0, \ell]$ and as the perturbation

$$\varphi_{\check{x}} = (\mathcal{A}_\infty(-\check{x}, \lambda) + \mathcal{H}_\ell(\check{x}))\,\varphi, \quad \varphi \in \mathbb{C}^2$$

of system

$$\varphi_{\check{x}} = \mathcal{A}_\infty(-\check{x}, \lambda)\varphi, \quad \varphi \in \mathbb{C}^2 \tag{6.29}$$

on $[-\ell, 0)$, where $\mathcal{H}_\ell \colon [-\ell, \ell] \to \mathrm{Mat}_2(\mathbb{C})$ is given by

$$\mathcal{H}_\ell(\check{x}) := \begin{cases} \mathcal{A}_\ell(\check{x}, \lambda) - \mathcal{A}_\infty(\check{x}, \lambda), & \check{x} \in [0, \ell] \\ \mathcal{A}_\ell(2\ell + \check{x}, \lambda) - \mathcal{A}_\infty(-\check{x}, \lambda), & \check{x} \in [-\ell, 0) \end{cases}.$$

By estimate (6.7), the norm of $\mathcal{H}_\ell$ satisfies

$$\|\mathcal{H}_\ell\| \le Ce^{-\varsigma_*\ell}. \tag{6.30}$$

Let X_b be the space of bounded functions $[-\ell, \ell] \to \mathbb{C}^2$ that are continuous, except for a possible discontinuity at 0. Our plan is to obtain exponential dichotomies for equations (4.10) and (6.29) first. The exponential dichotomies yield a solution operator to the inhomogeneous problem

$$\varphi_{\check{x}} = \mathcal{A}_\infty(|\check{x}|, \lambda)\varphi + G(\check{x}), \quad \varphi \in \mathbb{C}^2, \tag{6.31}$$

with $G \in X_b$, using the variation of constants formula. Then, using Lin's method [23, 36], we construct a solution operator to (6.31) that satisfies a matching condition at the endpoints $\check{x} = \ell$ and $\check{x} = -\ell$. Finally, we substitute $\mathcal{H}_\ell(\check{x})\varphi$ for $G(\check{x})$ in (6.31) and obtain a solution operator to (6.2). We apply the latter solution operator to the initial condition $\varphi_\infty(0, \lambda)$ to establish the existence of the desired solution $\varphi_\ell(\check{x}, \lambda)$.

We establish exponential dichotomies for the homoclinic slow eigenvalue problems (4.10) and (6.29). By Proposition A.3 and estimate (6.7), system (4.10) has for $\lambda \in C_{b,\Lambda}$ an exponential dichotomy on $[0, \infty)$ with constants $C, \mu(\lambda) > 0$. The corresponding projections $\mathcal{P}_\infty(\check{x}, \lambda)$ can be chosen to be analytic on $C_{b,\Lambda}$. Moreover, since $\mathcal{A}_*(\lambda)$ is hyperbolic with spectral gap larger than $\mu(\lambda) \ge \varsigma_*$ and $\mathcal{A}_*$ is bounded on $C_{b,\Lambda}$, Lemma A.4 and (6.7) yield

$$\|\mathcal{P}_\infty(\check{x}, \lambda) - \mathcal{P}_*(\lambda)\| \le Ce^{-\varsigma_*\check{x}}, \quad \check{x} \ge 0, \lambda \in C_{b,\Lambda}, \tag{6.32}$$

where $\mathcal{P}_*(\lambda)$ denotes the analytic spectral projection of $\mathcal{A}_*(\lambda)$ on $\mathrm{Sp}(v_-(\lambda))$ along $\mathrm{Sp}(v_+(\lambda))$. Moreover, since we have $R_s v_-(\lambda) = v_+(\lambda)$, the identity

$$R_s \mathcal{P}_*(\lambda) R_s = I - \mathcal{P}_*(\lambda) \tag{6.33}$$

holds for each $\lambda \in C_\Lambda$. Denote by $\mathcal{T}_\infty(\check{x}, \check{y}, \lambda)$ the evolution operator of system (4.10). By [20, Lemma 2.1.4], $\mathcal{T}_\infty(\check{x}, \check{y}, \cdot)$ is analytic on C_Λ, since $\mathcal{A}_\infty(\check{x}, \cdot)$ is analytic on C_Λ.

Using the reversibility symmetry R_s, system (6.29) can be fully described in terms of system (4.10). Indeed, for the evolution $\mathcal{T}_{\infty,r}(\check{x}, \check{y}, \lambda)$ of system (6.29), we have $\mathcal{T}_{\infty,r}(\check{x}, \check{y}, \lambda) = R_s \mathcal{T}_{\infty,r}(-\check{x}, -\check{y}, \lambda)R_s$. Consequently, system (6.29) has for any $\lambda \in C_{b,\Lambda}$ an exponential dichotomy on $(-\infty, 0]$ with constants $C, \mu(\lambda) > 0$. The corresponding projections $\mathcal{P}_{\infty,r}(\check{x}, \lambda)$ satisfy $\mathcal{P}_{\infty,r}(\check{x}, \lambda) = I - R_s \mathcal{P}_\infty(-\check{x}, \lambda)R_s$ for $\check{x} \le 0$. Moreover, by (6.33), it holds that

$$\|\mathcal{P}_{\infty,r}(\check{x}, \lambda) - \mathcal{P}_*(\lambda)\| \le Ce^{\varsigma_*\check{x}}, \quad \check{x} \le 0, \lambda \in C_{b,\Lambda}. \tag{6.34}$$

We proceed by constructing a solution operator to the periodic slow eigenvalue problem (6.2). Consider $W_\ell(\lambda)\colon \mathbb{C}^2 \times \mathbb{C}^2 \times X_b \to X_b$ to (6.31), given by

$$W_\ell(\lambda)(a,b,G)[\check{x}] = \mathcal{T}_\infty^u(\check{x},\ell,\lambda)a + \mathcal{T}_\infty^s(\check{x},0,\lambda)b + \int_0^{\check{x}} \mathcal{T}_\infty^s(\check{x},\check{y},\lambda)G(\check{y})d\check{y}$$

$$- \int_{\check{x}}^{\ell} \mathcal{T}_\infty^u(\check{x},\check{y},\lambda)G(\check{y})d\check{y}, \qquad \check{x} \in [0,\ell],$$

$$W_\ell(\lambda)(a,b,G)[\check{x}] = -\mathcal{T}_{\infty,r}^s(\check{x},-\ell,\lambda)a - \int_{\check{x}}^0 \mathcal{T}_{\infty,r}^u(\check{x},\check{y},\lambda)G(\check{y})d\check{y}$$

$$+ \int_{-\ell}^{\check{x}} \mathcal{T}_{\infty,r}^s(\check{x},\check{y},\lambda)G(\check{y})d\check{y}, \qquad \check{x} \in [-\ell,0),$$

where $\mathcal{T}_\infty^{u,s}(\check{x},\check{y},\lambda)$ and $\mathcal{T}_{\infty,r}^{u,s}(\check{x},\check{y},\lambda)$ denote the (un)stable evolution operators of systems (4.10) and (6.29) under the exponential dichotomies established above. Note that W_ℓ is an analytic operator on $C_{b,\Lambda}$, since the evolutions $\mathcal{T}_\infty(\check{x},\check{y},\cdot)$ and the projections $\mathcal{P}_\infty(\check{x},\cdot)$ are analytic. By (6.32) and (6.34), it holds that

$$\|\mathcal{P}_\infty(\ell,\lambda) - \mathcal{P}_{\infty,r}(-\ell,\lambda)\| \le Ce^{-\varsigma_*\ell}, \quad \lambda \in C_{b,\Lambda}. \tag{6.35}$$

We can conclude that the analytic linear operator $A_{1,\ell}(\lambda) := I - \mathcal{P}_\infty(\ell,\lambda) + \mathcal{P}_{\infty,r}(-\ell,\lambda)$ is invertible for $\ell > 0$ sufficiently large. Now define the analytic linear operator $A_{2,\ell}(\lambda)\colon \mathbb{C}^2 \times X_b \to \mathbb{C}^2$ by

$$A_{2,\ell}(\lambda)(b,G) = A_{1,\ell}(\lambda)^{-1}\left(W_\ell(\lambda)(0,b,G)[-\ell] - W_\ell(\lambda)(0,b,G)[\ell]\right).$$

One readily verifies that the analytic linear operator $W_{2,\ell}(\lambda)\colon \mathbb{C}^2 \times X_b \to X_b$ defined by $W_{2,\ell}(\lambda)(b,G) = W_\ell(\lambda)(A_{2,\ell}(\lambda)(b,G),b,G)$ is linear and satisfies

$$W_{2,\ell}(\lambda)(b,G)[-\ell] = W_{2,\ell}(\lambda)(b,G)[\ell], \quad b \in \mathbb{C}^2, G \in X_b, \lambda \in C_{b,\Lambda}. \tag{6.36}$$

Moreover, we have the estimates

$$\|A_{2,\ell}(\lambda)(b,G)\| \le C(e^{-\mu(\lambda)\ell}\|b\| + \|G\|),$$

$$\|W_{2,\ell}(\lambda)(b,G)[\check{x}]\| \le \begin{cases} C(e^{-\mu(\lambda)\check{x}}\|b\| + \|G\|), & \check{x} \in [0,\ell], \\ C(e^{-\mu(\lambda)(2\ell+\check{x})}\|b\| + \|G\|), & x \in [-\ell,0), \end{cases} \tag{6.37}$$

for $b \in \mathbb{C}^2, G \in X_b, \lambda \in C_{b,\Lambda}$. Denote by $W_{3,\ell}(\lambda)\colon X_b \to X_b$ the analytic linear map $W_{3,\ell}(\lambda)(w) = W_{2,\ell}(\lambda)(0,\mathcal{H}_\ell \cdot w)$, where $\cdot$ denotes pointwise multiplication, i.e. $(\mathcal{H}_\ell \cdot w)[\check{x}] = \mathcal{H}_\ell(\check{x})w(\check{x})$. By (6.30), we have the estimate,

$$\|W_{3,\ell}(\lambda)\| \le Ce^{-\varsigma_*\ell}, \quad \lambda \in C_{b,\Lambda}.$$

Hence for $\ell > 0$ sufficiently large, the map $I - W_{3,\ell}(\lambda)$ is invertible. Finally, consider the analytic linear map $W_{4,\ell}(\lambda)\colon \mathbb{C}^2 \to X_b$ given by $W_{4,\ell}(\lambda)(b) = (I - W_{3,\ell}(\lambda))^{-1}(W_{2,\ell}(\lambda)(b,0))$. One readily checks that

$$W_{4,\ell}(\lambda)(b) = W_{2,\ell}(\lambda)(b,\mathcal{H}_\ell \cdot W_{4,\ell}(\lambda)(b)), \quad b \in \mathbb{C}^2, \lambda \in C_{b,\Lambda} \tag{6.38}$$

is satisfied. Define the map $\zeta\colon [0,2\ell] \to [-\ell,\ell]$ by

$$\zeta(\check{x}) = \begin{cases} \check{x}, & \check{x} \in [0,\ell] \\ \check{x} - 2\ell, & \check{x} \in (\ell,2\ell) \end{cases}.$$

By identities (6.36) and (6.38), we have $W_{4,\ell}(\lambda)(b)[\ell] = W_{4,\ell}(\lambda)(b)[-\ell]$. We conclude that, for every $\lambda \in C_{b,\Lambda}, b \in \mathbb{C}^2$ and $\ell > 0$ sufficiently large, $W_{4,\ell}(\lambda)(b)[\zeta(\check{x})]$ is a solution to (6.2) on $[0,2\ell]$ that can be extended to $[0,2\ell]$.

Next, we apply the solution operator $W_{4,\ell}$ to initial condition $b_\lambda := \varphi_\infty(0,\lambda) \in \mathbb{C}^2$ and consider the solution

$$\varphi_\ell(\check{x},\lambda) := W_{4,\ell}(\lambda)(b_\lambda)[\zeta(\check{x})]$$

to (6.2). Note that $\varphi_\ell(\check{x},\cdot)$ is analytic on $C_{b,\Lambda}$, since both $W_{4,\ell}$ and $\varphi_\infty(0,\lambda)$ are analytic on $C_{b,\Lambda}$. Using (6.30), (6.37) and identity (6.38), we estimate

$$\|\varphi_\ell(\check{x},\lambda)\| \le \|W_{2,\ell}(\lambda)(b_\lambda,0)[\zeta(\check{x})]\| + \|W_{2,\ell}(\lambda)(0,\mathcal{H}_\ell \cdot W_{4,\ell}(\lambda)(b_\lambda))[\zeta(\check{x})]\|$$

$$\le C\left[e^{-\mu(\lambda)\check{x}} + e^{-\varsigma_*\ell}\int_0^{2\ell}\left(e^{-\mu(\lambda)|\check{x}-\check{y}|} + e^{-\mu(\lambda)(|\ell-\check{x}|+|\ell-\check{y}|)}\right)\|\varphi_\ell(\check{y},\lambda)\|d\check{y}\right], \tag{6.39}$$

for $\check{x} \in [0, 2\ell]$, $\lambda \in C_{b,\Lambda}$. Application of [4, Lemma III.2.1] on the integral inequality (6.39) yields

$$\|\varphi_\ell(\check{x}, \lambda)\| \leq Ce^{-\mu(\lambda)\check{x}}, \quad \check{x} \in [0, 2\ell], \lambda \in C_{b,\Lambda}, \tag{6.40}$$

provided $\ell > 0$ is sufficiently large. Moreover, we approximate with the aid of (6.35)

$$\begin{aligned}
\|A_{2,\ell}(\lambda)&(b_\lambda, 0) - T_\infty^s(\ell, 0, \lambda)b_\lambda\| \\
&= \|(\mathcal{P}_\infty(\ell, \lambda) - \mathcal{P}_{\infty,r}(-\ell, \lambda))A_{1,\ell}(\lambda)^{-1}T_\infty^s(\ell, 0, \lambda)b_\lambda\| \leq Ce^{-(\mu(\lambda)+\varsigma_*)\ell}
\end{aligned} \tag{6.41}$$

for $\lambda \in C_{b,\Lambda}$. On the other hand, using (6.30) and (6.40), we estimate

$$\begin{aligned}
\|W_{2,\ell}(\lambda)(0, \mathcal{H}_\ell \cdot W_{4,\ell}(\lambda)(b_\lambda))[\ell]\| &\leq Ce^{-\varsigma_*\ell} \int_0^{2\ell} e^{-\mu(\lambda)|\ell-\check{y}|}\|\varphi_\ell(\check{y}, \lambda)\|d\check{y} \\
&\leq Ce^{-(\mu(\lambda)+\varsigma_*)\ell}
\end{aligned} \tag{6.42}$$

for $\lambda \in C_{b,\Lambda}$. Using identity (6.38) and estimates (6.41) and (6.42), we expand $\varphi_\ell(\check{x}, \lambda)$ at $\check{x} = \ell$ as follows:

$$\begin{aligned}
\varphi_\ell(\ell, \lambda) &= W_{2,\ell}(\lambda)(b_\lambda, 0)[\ell] + W_{2,\ell}(\lambda)(0, \mathcal{H}_\ell \cdot W_{4,\ell}(\lambda)(b_\lambda))[\ell] \\
&= T_\infty^s(\ell, 0, \lambda)b_\lambda + O\left(e^{-(\mu(\lambda)+\varsigma_*)\ell}\right) \\
&= \varphi_\infty(\ell, \lambda) + O\left(e^{-(\mu(\lambda)+\varsigma_*)\ell}\right)
\end{aligned}$$

for $\lambda \in C_{b,\Lambda}$. Similarly, using identity (6.38) and estimates (6.7), (6.30) and (6.41), we expand $\varphi_\ell(\check{x}, \lambda)$ at $\check{x} = 0$ as follows for $\lambda \in C_{b,\Lambda}$:

$$\begin{aligned}
\varphi_\ell(0, \lambda) &= W_{2,\ell}(\lambda)(b_\lambda, \mathcal{H}_\ell \cdot W_{2,\ell}(\lambda)(b_\lambda, 0))[0] \\
&\quad + W_{2,\ell}(\lambda)(0, \mathcal{H}_\ell \cdot W_{2,\ell}(\lambda)(0, \mathcal{H}_\ell \cdot W_{4,\ell}(\lambda)(b_\lambda)))[0] \\
&= \mathcal{P}_\infty(0, \lambda)b_\lambda - \int_0^\ell \mathcal{T}_\infty^u(0, \check{y}, \lambda)\mathcal{H}_\ell(\check{y})\mathcal{T}_\infty^s(\check{y}, 0, \lambda)b_\lambda d\check{y} + O\left(e^{-3\varsigma_*\ell}, e^{-2\mu(\lambda)\ell}\right) \\
&= \varphi_\infty(0, \lambda) - \int_0^\ell \mathcal{T}_\infty^u(0, \check{y}, \lambda)\mathcal{H}_\ell(\check{y})\varphi_\infty(\check{y}, \lambda)d\check{y} + O\left(e^{-3\varsigma_*\ell}, e^{-2\mu(\lambda)\ell}\right) \\
&= \varphi_\infty(0, \lambda) + O\left(e^{-2\varsigma_*\ell}\right),
\end{aligned}$$

where we used that $\mu(\lambda) > \varsigma_*$. $\qquad\square$

Since system (6.2) is R_s-reversible at $\check{x} = \ell$, $\varphi_\ell^r(\check{x}, \lambda) = R_s\varphi_\ell(2\ell - \check{x}, \lambda)$ is a also solution to (6.2). The next proposition shows that $\varphi_\ell(\check{x}, \lambda)$ and $\varphi_\ell^r(\check{x}, \lambda)$ are linearly independent, and provides an approximation for their Wronskian $\mathcal{W}_\ell(\lambda)$.

Corollary 6.4. *For $0 \ll \ell < \infty$, the ($\check{x}$-independent) Wronskian $\mathcal{W}_\ell(\lambda) = \det(\varphi_\ell(\check{x}, \lambda) \mid \varphi_\ell^r(\check{x}, \lambda))$ is approximated by*

$$\|\mathcal{W}_\ell(\lambda) - E_\ell(\lambda)\| \leq Ce^{-(2\mu(\lambda)+\varsigma_*)\ell}, \quad \lambda \in C_{b,\Lambda}, \tag{6.43}$$

where $C > 0$ is a constant independent of ℓ and λ and $E_\ell \colon C_{b,\Lambda} \to \mathbb{C}$ is the non-zero analytic map given by $E_\ell(\lambda) = 2\omega(\lambda)e^{-2\omega(\lambda)\ell}$.

Proof. Combining estimates (6.26) and (6.27) yields

$$\left|\det\left(\varphi_\ell(\ell, \lambda) \mid R_s\varphi_\ell(\ell, \lambda)\right) - e^{-2\omega(\lambda)\ell}\det\left(v_-(\lambda) \mid R_sv_-(\lambda)\right)\right| \leq Ce^{-(2\mu(\lambda)+\varsigma_*)\ell},$$

which concludes the proof. $\qquad\square$

6.3 Conclusion

With the preparatory work done in the previous sections, we are able to prove Theorems 4.3 and 4.5 using the aforementioned approach.

Proof of Theorem 4.3. In the following, we denote by $C > 0$ a constant independent of ℓ. First, using (6.7) and (6.27), we approximate

$$\left| \mathcal{K}_\ell(0) - \mathcal{E}_{\infty,s}(0) \right| \le C e^{-2\varsigma_* \ell},$$

where $\mathcal{K}_\ell(\lambda)$ is defined in (6.4). Combining the latter with (6.3) and (6.43) yields

$$\left| e^{-i\nu} \mathcal{E}_{\ell,s}(0, e^{i\nu}) \mathcal{W}_\ell(0) - \mathcal{E}_{\infty,s}(0) \right| \le C e^{-2\varsigma_* \ell}, \quad \nu \in \mathbb{R}. \tag{6.44}$$

On the other hand, by (6.7) it holds that

$$|\mathfrak{a}_\ell - \mathfrak{a}_\infty|, |\mathfrak{w}_\ell - \mathfrak{w}_\infty| \le C e^{-2\varsigma_* \ell}. \tag{6.45}$$

Finally, applying Proposition 3.3, (6.43), (6.44) and (6.45) on identity (6.1) establishes the desired approximation (4.6). □

Proof of Theorem 4.5. In the following, we denote by $C > 0$ a constant independent of ℓ and λ. Let $\lambda_\infty \in C_\Lambda$ be a simple zero of $\mathcal{E}_{\infty,s}$ satisfying (4.8). Then, we take $C_{b,\Lambda} \subset C_\Lambda$ an open and bounded neighborhood of λ_∞ of $\mathcal{E}_{\infty,s}$ such that it holds $\mathrm{Re}(\omega(\lambda)) > \omega_*$ for all $\lambda \in C_{b,\Lambda}$. We chose $\delta > 0$ such that

$$2\delta < \varsigma_*, \quad \mu(\lambda) := \mathrm{Re}(\omega(\lambda)) - \delta > \omega_*,$$

for all λ in $C_{b,\Lambda}$.

We are looking for zeros of $\mathcal{E}_{\ell,s}(\cdot, \gamma)$ close to λ_∞ for $0 \ll \ell < \infty$ and $\gamma \in S^1$. In other words, we are looking for solutions $\lambda \in C_{b,\Lambda}$ in a neighborhood of λ_∞, to the equation

$$0 = \mathcal{E}_{\ell,s}(\lambda, \gamma). \tag{6.46}$$

By multiplying (6.46) with the non-zero (see Corollary 6.4) quantity $\gamma^{-1} \mathcal{W}_\ell(\lambda)$ on both sides, we obtain the equivalent equation

$$0 = 2\mathrm{Re}(\gamma) \mathcal{W}_\ell(\lambda) - \mathcal{K}_\ell(\lambda), \quad \lambda \in C_{b,\Lambda}, \quad \gamma \in S^1, \tag{6.47}$$

see also (6.3). Using (6.7) and (6.27) we approximate

$$\left| \mathcal{K}_\ell(\lambda) - \mathcal{E}_{\infty,s}(\lambda) \right| \le C e^{-2\varsigma_* \ell}, \quad \lambda \in C_{b,\Lambda}. \tag{6.48}$$

Note that both $\mathcal{W}_\ell$ and $\mathcal{K}_\ell$ are analytic on $C_{b,\Lambda}$, since $\varphi_\ell(\check{x}, \cdot)$ and $\Upsilon(u, \cdot)$ are analytic. By shrinking $C_{b,\Lambda}$ if necessary, the approximations (6.43) and (6.48) provide bounds for the derivatives of the analytic maps $\mathcal{W}_\ell$ and $\mathcal{K}_\ell$ via the estimates

$$\begin{aligned}
\left| \frac{\partial^i}{\partial \lambda^i} \left(\mathcal{K}_\ell(\lambda) - \mathcal{E}_{\infty,s}(\lambda) \right) \right| &\le C e^{-2\varsigma_* \ell}, \\
\left| \frac{\partial^i}{\partial \lambda^i} \left(\mathcal{W}_\ell(\lambda) - E_\ell(\lambda) \right) \right| &\le C e^{-(2\mu(\lambda)+\varsigma_*)\ell},
\end{aligned} \quad i = 0, 1, 2, \quad \lambda \in C_{b,\Lambda}. \tag{6.49}$$

Consider the analytic function $\eta_\ell \colon C_{b,\Lambda} \times \mathbb{C} \to \mathbb{C}$ given by $\eta_\ell(\lambda, \gamma_r) = 2\gamma_r \mathcal{W}_\ell(\lambda) - \mathcal{K}_\ell(\lambda)$. Let $\mathcal{D} \subset \mathbb{C}$ be open and bounded such that it contains the closed unit circle. Provided $\ell > 0$ is sufficiently large, we have by (6.43) and (6.48)

$$|\eta_\ell(\lambda, \gamma_r) + \mathcal{E}_{\infty,s}(\lambda)| < |\mathcal{E}_{\infty,s}(\lambda)|,$$

for each $\gamma_r \in \mathcal{D}$ and λ on the boundary of some sufficiently small disk $\mathcal{B} \subset C_{b,\Lambda}$ around λ_∞. Thus, by Rouché's Theorem, there exists for each $\gamma_r \in \mathcal{D}$ a unique zero $\lambda_\ell(\gamma_r) \in \mathcal{B}$ of $\eta_\ell(\cdot, \gamma_r)$, which satisfies

$$|\lambda_\ell(\gamma_r) - \lambda_\infty| \le C e^{-2\varsigma_* \ell}. \tag{6.50}$$

By estimate (6.49), it holds that

$$\left| \partial_\lambda \eta_\ell(\lambda, \gamma_r) - \mathcal{E}'_{\infty,s}(\lambda) \right| \le C e^{-2\varsigma_* \ell}, \quad \lambda \in \mathcal{B}, \gamma_r \in \mathcal{D}.$$

Hence, using the (analytic) Implicit Function Theorem and the fact that $\mathcal{E}'_{\infty,s}(\lambda_\infty) \neq 0$, we conclude that the map $\lambda_\ell \colon \mathcal{D} \to \mathbb{C}$ is analytic. Implicit differentiation of identity (6.47) yields the derivatives

$$\lambda'_\ell(\gamma_r) = \frac{2\mathcal{W}_\ell(\lambda_\ell(\gamma_r))}{\mathcal{K}'_\ell(\lambda(\gamma_r)) - 2\gamma_r\mathcal{W}'_\ell(\lambda(\gamma_r))},$$

$$\lambda''_\ell(\gamma_r) = \lambda'_\ell(\gamma_r)\frac{4\mathcal{W}'_\ell(\lambda_\ell(\gamma_r)) - \left[\mathcal{K}''_\ell(\lambda(\gamma_r)) - 2\gamma_r\mathcal{W}''_\ell(\lambda(\gamma_r))\right]\lambda'_\ell(\gamma_r)}{\mathcal{K}'_\ell(\lambda(\gamma_r)) - 2\gamma_r\mathcal{W}'_\ell(\lambda(\gamma_r))}, \qquad \gamma_r \in \mathcal{D}.$$

Approximating these derivatives with (6.50) and (6.49) leads to (4.11). Next, we expand $\mathcal{K}_\ell$ in an ℓ-independent neighborhood V_∞ of λ_∞ with Taylor's Theorem as

$$\mathcal{K}_\ell(\lambda) = \mathcal{K}_\ell(\lambda_\infty) + (\lambda - \lambda_\infty)\mathcal{K}'_\ell(\lambda_\infty) + \hat{\mathcal{K}}_\ell(\lambda - \lambda_\infty), \quad \lambda \in V_\infty, \tag{6.51}$$

with $\|\hat{\mathcal{K}}_\ell(\lambda - \lambda_\infty)\| \leq C|\lambda - \lambda_\infty|^2$. By (6.50) and the ℓ-independence of V_∞, we can substitute $\lambda_\ell(\gamma_r)$ for λ in (6.51) for $\ell > 0$ sufficiently large. Thus, using estimates (6.43), (6.50) and (6.49), we arrive at

$$\begin{aligned}
0 &= 2\gamma_r\mathcal{W}_\ell(\lambda_\ell(\gamma_r)) - \mathcal{K}_\ell(\lambda_\ell(\gamma_r)) \\
&= -\mathcal{K}_\ell(\lambda_\infty) - (\lambda_\ell(\gamma_r) - \lambda_\infty)\mathcal{E}'_{\infty,s}(\lambda_\infty) + O\left(e^{-4\varsigma_*\ell}, e^{-2\omega(\lambda_\infty)\ell}\right).
\end{aligned} \tag{6.52}$$

Hence, we obtain the desired leading-order expression for $\lambda_\ell(\gamma_r) - \lambda_\infty$ by calculating the leading order of $\mathcal{K}_\ell(\lambda_\infty)$. First, since G is C^3 on its domain by **(S1)**, the solutions $\kappa_{\mathrm{h}}(x, u)$ and $\mathcal{X}_{in}(x, u, \lambda)$ to (2.4) and to (3.7) are C^2 on their domains $\mathbb{R} \times U_{\mathrm{h}}$ and $\mathbb{R} \times U_{\mathrm{h}} \times C_{b,\Lambda}$. Therefore, Υ is C^2 on $U_{\mathrm{h}} \times C_{b,\Lambda}$. Thus, by shrinking the $\ell-$ and λ-independent neighborhood U_∞ of $u_\infty(0)$ if necessary, we expand

$$\Upsilon(u, \lambda) = \Upsilon(u_\infty(0), \lambda) + \partial_u\Upsilon(u_\infty(0), \lambda)(u - u_\infty(0)) + \tilde{\Upsilon}(u, \lambda), \quad u \in U_\infty, \tag{6.53}$$

where $\|\tilde{\Upsilon}(u, \lambda)\| \leq C|u - u_\infty(0)|^2$. With the aid of identities (6.8), (6.27) and (6.53), we expand

$$\begin{aligned}
\mathcal{K}_\ell(\lambda) &= \det\left(\varphi_\ell(0, \lambda) - \varphi_\infty(0, \lambda) \mid \Upsilon(u_\infty(0), \lambda)R_s\varphi_\infty(0, \lambda)\right) \\
&\quad + \det\left(\varphi_\infty(0, \lambda) \mid \Upsilon(u_\infty(0), \lambda)R_s\left(\varphi_\ell(0, \lambda) - \varphi_\infty(0, \lambda)\right)\right) \\
&\quad + (u_\ell(0) - u_\infty(0))\det\left(\varphi_\infty(0, \lambda) \mid \partial_u\Upsilon(u_\infty(0), \lambda)R_s\varphi_\infty(0, \lambda)\right) \\
&\quad + \mathcal{E}_{\infty,s}(\lambda) + O\left(e^{-4\varsigma_*\ell}\right) \\
&= 2\det\left(\varphi_\ell(0, \lambda) - \varphi_\infty(0, \lambda) \mid \Upsilon(u_\infty(0), \lambda)R_s\varphi_\infty(0, \lambda)\right) + \mathcal{E}_{\infty,s}(\lambda) \\
&\quad - \frac{2\omega_*^2\alpha^2 e^{-2\omega_*\ell}}{\mathfrak{a}_\infty}\det\left(\varphi_\infty(0, \lambda) \mid \partial_u\Upsilon(u_\infty(0), \lambda)R_s\varphi_\infty(0, \lambda)\right) + O\left(e^{-3\varsigma_*\ell}\right),
\end{aligned} \tag{6.54}$$

where we used $[\Upsilon(u_\infty(0), \lambda)]^{-1} = \Upsilon(u_\infty(0), \lambda)R_s$, $\det(\Upsilon(u_\infty(0), \lambda)) = 1$, $\det(R_s) = -1$ and the bilinearity of the determinant. Our aim is to approximate $\varphi_\ell(0, \lambda_\infty) - \varphi_\infty(0, \lambda_\infty)$ in (6.54). First, recall that H_1 is C^3 on its domain. Fix $\check{x} \in [0, \ell]$. Using Taylor's Theorem and estimate (6.7), we approximate

$$|\partial_u H_1(u_\ell(\check{x}), 0, 0) - \partial_u H_1(u_\infty(\check{x}), 0, 0) - \partial_{uu}H_1(u_\infty(\check{x}), 0, 0)(u_\ell(\check{x}) - u_\infty(\check{x}))| \leq Ce^{-2\varsigma_*(2\ell - \check{x})}. \tag{6.55}$$

By estimate (6.8) and (6.55), we obtain

$$\begin{aligned}
&\mathcal{A}_\ell(\check{x}, \lambda) - \mathcal{A}_\infty(\check{x}, \lambda) \\
&= -\frac{2\omega_*^2\alpha_*^2 e^{-2\omega_*\ell}\partial_{uu}H_1(u_\infty(\check{x}), 0, 0)\tilde{u}_\infty(\check{x})}{\mathfrak{a}_\infty}\begin{pmatrix} 0 & 0 \\ 1 & 0 \end{pmatrix} + O\left(e^{-\varsigma_*(3\ell - \check{x})}\right)
\end{aligned} \tag{6.56}$$

for $\check{x} \in [0, \ell]$. Subsequently, we combine (6.28) and (6.56) to obtain a leading-order approximation of $\varphi_\ell(0, \lambda) - \varphi_\infty(0, \lambda)$ for $\lambda \in C_{b,\Lambda}$:

$$\begin{aligned}
\varphi_\ell(0, \lambda) - \varphi_\infty(0, \lambda) &= -\int_0^\ell \mathcal{Q}_\infty(\lambda)\mathcal{T}_\infty(0, \check{y}, \lambda)\left(\mathcal{A}_\ell(\check{x}, \lambda) - \mathcal{A}_\infty(\check{x}, \lambda)\right)\varphi_\infty(\check{y}, \lambda)d\check{y} \\
&\quad + O\left(e^{-3\varsigma_*\ell}, e^{-2\mu(\lambda)\ell}\right) \\
&= \frac{2\omega_*^2\alpha_*^2 e^{-2\omega_*\ell}}{\mathfrak{a}_\infty}\int_0^\infty \mathcal{Q}_\infty(\lambda)\mathcal{T}_\infty(0, \check{y}, \lambda)\mathcal{Z}(\check{y}, \lambda)d\check{y} + O\left(e^{-3\varsigma_*\ell}, e^{-2\mu(\lambda)\ell}\right),
\end{aligned} \tag{6.57}$$

37

where we denote

$$\mathcal{Z}(\check{x}, \lambda) := \begin{pmatrix} 0 \\ \partial_{uu} H_1(u_\infty(\check{x}), 0, 0)\tilde{u}_\infty(\check{x})\hat{u}_\infty(\check{x}, \lambda) \end{pmatrix}, \quad \check{x} \geq 0.$$

Since the determinant $\mathcal{E}_{\infty,s}(\lambda_\infty) = \det(\varphi_\infty(0, \lambda) \mid \Upsilon(u_\infty(0), \lambda)R_s\varphi_\infty(0, \lambda))$ equals 0, the vectors $\Upsilon(u_\infty(0), \lambda_\infty)R_s\varphi_\infty(0, \lambda_\infty)$ and $\varphi_\infty(0, \lambda_\infty)$ are scalar multiples of each other. As the u-coordinate of both vectors are equal, we have in fact $\varphi_\infty(0, \lambda_\infty) = \Upsilon(u_\infty(0), \lambda_\infty)R_s\varphi_\infty(0, \lambda_\infty)$. Moreover, $Q_\infty(\lambda)$ is a projection along $\mathrm{Sp}(\varphi_\ell(0, \lambda))$. Therefore, the determinant $\det(Q_\infty(\lambda)w \mid \varphi_\ell(0, \lambda))$ equals $\det(w \mid \varphi_\ell(0, \lambda))$ for any vector $w \in \mathbb{C}^2$ and $\lambda \in \mathcal{C}_{b,\Lambda}$. Using the latter two observations and the equality $\det(\mathcal{T}_\infty(0, \check{y}, \lambda)) = 1$, we simplify the determinant

$$\det\left(Q_\infty(\lambda_\infty)\mathcal{T}_\infty(0, \check{y}, \lambda_\infty)\mathcal{Z}(\check{y}, \lambda_\infty) \mid \Upsilon(u_\ell(0), \lambda_\infty)R_s\varphi_\ell(0, \lambda_\infty)\right)$$
$$= \det\left(\mathcal{T}_\infty(0, \check{y}, \lambda_\infty)\mathcal{Z}(\check{y}, \lambda_\infty) \mid \varphi_\ell(0, \lambda_\infty)\right) = \det\left(\mathcal{Z}(\check{y}, \lambda_\infty) \mid \varphi_\ell(\check{y}, \lambda_\infty)\right). \tag{6.58}$$

Finally, using (6.54), (6.57) and (6.58), we rewrite (6.52) as

$$\begin{aligned}
\lambda_\ell(\gamma_r) - \lambda_\infty &= -\frac{\mathcal{K}_\ell(\lambda_\infty)}{\mathcal{E}'_{\infty,s}(\lambda_\infty)} + O\left(e^{-4\varsigma_* \ell}\right) \\
&= \frac{2\omega_*^2\alpha_*^2 e^{-2\omega_*\ell}}{\mathfrak{a}_\infty \mathcal{E}'_{\infty,s}(\lambda_\infty)}\left(\det\left(\varphi_\infty(0, \lambda_\infty) \mid \partial_u\Upsilon(u_\infty(0), \lambda_\infty)R_s\varphi_\infty(0, \lambda_\infty)\right)\right. \\
&\qquad\left. -2\int_0^\infty \det\left(\mathcal{Z}(\check{y}, \lambda_\infty) \mid \varphi_\ell(\check{y}, \lambda_\infty)\right) d\check{y}\right) + O\left(e^{-3\varsigma_*\ell}, e^{-2\mu(\lambda_\infty)\ell}\right) \\[2mm]
&= \frac{2\omega_*^2\alpha^2 e^{-2\omega_*\ell}}{\mathfrak{a}_\infty \mathcal{E}'_{\infty,s}(\lambda_\infty)}\left(2\int_0^\infty \partial_{uu} H_1(u_\infty(\check{x}), 0, 0)\tilde{u}_\infty(\check{x})\left[\hat{u}_\infty(\check{x}, \lambda_\infty)\right]^2 d\check{x}\right. \\
&\qquad\left. + \left[\hat{u}_\infty(0, \lambda_\infty)\right]^2 \partial_u\mathcal{G}(u_\infty(0), \lambda_\infty)\right) + O\left(e^{-3\varsigma_*\ell}, e^{-2\mu(\lambda_\infty)\ell}\right),
\end{aligned}$$

which concludes the proof of identity (4.9). □

7 Discussion and Outlook

Busse balloons have first been introduced as central 'bridge' towards complex pattern dynamics in the context fluid mechanics [2]. Being defined as the region in (parameter, wave number)-space in which stable spatially periodic patterns exist, it thus is a priori a relevant concept in any spatially extended and thus potentially pattern forming evolutionary system. In fact, in recent years, Busse balloons appeared as organizing center in the literature on desertification dynamics in spatial ecosystems as modeled by reaction-diffusion systems: it serves as a guide for the evolution of vegetation patterns from a homogeneously vegetated state to the bare soil 'catastrophe' under worsening climatological circumstances [37, 39, 40, 43]. Moreover, it was found in these papers that the final ecological catastrophe takes place amid long-wavelength patterns, i.e. near the homoclinic limit – the (idealized) ecological oasis state – considered in this work. These simulations corroborated earlier observations in the literature on spatially periodic patterns in classical reaction-diffusion systems as the Gray-Scott and Gierer-Meinhard models [10, 42]: the homoclinic $k \downarrow 0$ limit – i.e. the 'homoclinic tip' of the Busse balloon – comes up as the most stable spatially 'periodic' pattern, in the sense that it is the last 'periodic' pattern to destabilize as parameters vary. This phenomenon was first noted in simulations and subsequently conjectured as driving mechanism by Wei-Ming Ni in [25] in the context of the Gierer-Meinhardt model. Although this was not yet noticed in [25], later work/simulations also indicated that the destabilization of the limiting homoclinic pattern always is of Hopf type. Here, we have included this in our formulation of Ni's conjecture.

In this paper we have investigated Ni's conjecture in full analytical detail in a broad class of (singularly perturbed, 2-component, slowly nonlinear) reaction-diffusion equations. We have shown that a Hopf destabilization of a the homoclinic $k = 0$ pattern necessarily induces a fine-structure of the boundary of the Busse balloon near the homoclinic limit – called the 'Hopf dance' [10, 43] – formed by successive pieces of two countably many times intersecting curves of distinct Hopf bifurcations, $\mathcal{H}_{+1}$ and $\mathcal{H}_{-1}$. Moreover, we have established by further refined asymptotic expansions – based on the analytical methods developed in [7, 11] – that this Hopf dance must be accompanied by a 'belly dance', which means that all intersections of $\mathcal{H}_{+1}$ and $\mathcal{H}_{-1}$ induce co-dimension 2 points on the boundary of the Busse balloon. Especially this latter finding is surprising, as it implies a correlation of two geometrically independent characteristics, here in the form of natural

orientation of the leading order shape of the critical destabilizing spectral curve, which is counter-intuitive.

The stability analysis presented in this paper is a spectral analysis, which implies that our findings only provide linear mechanisms by which near homoclinic spatially periodic patterns are destabilized. Of course, the simulations of reaction-diffusion models that inspired our work show – better: approximate – the nonlinear dynamics of the system beyond these destabilizations, i.e. these simulations follow the bifurcations induced by the linear mechanisms established here. In other words, our analysis – for instance – shows that spatially periodic patterns are destabilized by perturbations with approximately twice the wavelength of the pattern itself if the boundary of the Busse balloon is crossed through the curve $\mathcal{H}_{-1}$ and thus that neighboring pulses initially evolve out of phase.

However, to understand the full long-term dynamics, i.e. to track the bifurcations induced by crossing $\mathcal{H}_{-1}$ in the full nonlinear PDE, a nonlinear analysis is required, because the dominant behavior of a destabilized system in the long run is not dictated by its linear part. At present this is a very open, challenging – and also extremely relevant – line of research. The literature by which the long-term behavior of a bifurcation of nearly homoclinic patterns can be explicitly determined is strongly limited, but a deeper understanding of the bifurcations associated to crossing the boundary of the Busse balloon could have a direct ecological interpretation: the simulations of [1, 39, 40] show that spatially periodic patterns have a remarkable tendency to evolve towards patterns with only half the number of pulses (with double wavelength) as the boundary of the Busse balloon is crossed. This dominance of the 'period doubling bifurcation' is yet in essence not understood and our present analysis only provides the very first step towards a deeper understanding.

Finally, we note that we have focused in this work on reversibly symmetric pulse solutions to the general class of singularly perturbed 2-component reaction-diffusion systems (1.1). As already mentioned in the introduction, our choice to study singularly perturbed systems is partly motivated by the fact that many models in the literature have this singularly perturbed nature and partly by the fact that this nature enables us to perform the (detailed) analysis necessary for understanding destabilization mechanisms near the homoclinic limit. However, we have thus also restricted our analysis to the class of *symmetric* solutions in *2-component* systems, which induces two natural questions: are the structures uncovered here special for N-component models with necessarily $N = 2$ and/or for periodic patterns that are necessarily symmetric?

Without going into any further details, we conjecture that the Hopf and belly dance mechanisms will appear naturally near a Hopf-type homoclinic tip of a Busse balloon in any *reversible* $N \geq 2$-component reaction-diffusion system. In fact, we expect that this could be worked out in full analytical detail by application of the methods developed in [7] that work for multi-component systems.

On the other hand, the Hopf-dance mechanism in the form presented here is expected to break down – or better: to change significantly – as soon as the reversible symmetry of reaction-diffusion model (1.1) is broken. This happens for instance as an advection term is included in the model (which appears naturally in ecosystems, where the advection term models the impact of non-flat terrains on the vegetation dynamics [1, 21, 37, 39, 40, 43]). In general, the spectrum associated with periodic wave trains to reaction-advection-diffusion systems consists of continuous images of the unit circle S^1 [14]. The presence of a reversibility symmetry in the eigenvalue problem yields degenerate spectrum: the image of S^1 covers each curve of spectrum twice. This degeneracy drives the Hopf dance and the non-degeneracy induced by advection terms is thus expected to affect the destabilization mechanisms discussed here. Numerical investigations in the extended Klausmeier system [43] indicate that the Hopf and belly dance destabilization mechanisms indeed break down in the presence of $O(1)$-advection: the boundary of the Busse balloon near the homoclinic tip consists no longer of curves $\mathcal{H}_{\pm 1}$ of ± 1-Hopf instabilities in the limit $\varepsilon \to 0$ and the codimension 2 points disappear. Instead, the boundary is smooth in the limit $\varepsilon \to 0$ and consists of oscillating curves of γ-Hopf instabilities, where γ can be *any* Floquet multiplier in S^1. However, this has not been investigated analytically. It is expected to be especially interesting to understand and follow the transition from the reversible case to the non-reversible case by the introduction of small advective – reversibility breaking – effects.

A   Prerequisites

A.1   Asymptotically constant systems

The eigenvalue problems arising in our analysis are non-autonomous linear systems of the form

$$\varphi_x = A(x, \lambda)\varphi, \quad \varphi \in \mathbb{C}^n, \tag{A.1}$$

depending analytically on a spectral parameter λ. Often we are looking for the eigenvalues $\lambda \in \mathbb{C}$ for which (A.1) admits a non-trivial bounded (or exponentially localized) solution. Therefore, we are interested in the asymptotic behavior of

solutions to (A.1).

Linearizing about pulse type solutions leads to eigenvalue problems (A.1) that have an asymptotically constant coefficient matrix. In such systems, the asymptotics of solutions to (A.1) is dictated by the behavior of the constant coefficient system at $\pm\infty$ – see also Proposition A.3. The following result concerns the construction of a unique solution with the highest decay rate to an asymptotically constant system.

Proposition A.1. *[28, Proposition 1.2] Let $n \in \mathbb{Z}_{>0}, \Omega \subset \mathbb{C}$ open and $A \in C([0,\infty) \times \Omega, \mathrm{Mat}_{n\times n}(\mathbb{C}))$ such that $A(x,\cdot)$ is analytic on Ω for each $x \geq 0$. Suppose that there exists $\mu, K > 0$ and $A_\infty : \Omega \to \mathrm{Mat}_{n\times n}(\mathbb{C})$ analytic such that*

$$\|A(x,\lambda) - A_\infty(\lambda)\| \leq Ke^{-\mu x}, \quad x \geq 0, \lambda \in \Omega. \tag{A.2}$$

Furthermore, suppose that the eigenvalue $\mu(\lambda)$ of $A_\infty(\lambda)$ of smallest real part is simple for all $\lambda \in \Omega$. Denote by $v(\lambda)$ an analytic eigenvector of A_∞ corresponding to $\mu(\lambda)$. For any compact subset $\Omega_b \subset \Omega$, there exists $C > 0$, independent of λ, and a unique solution $y(x,\lambda)$ to (A.1) satisfying

$$\left\|e^{-\mu(\lambda)x}y(x,\lambda) - v(\lambda)\right\| \leq Ce^{-\mu x}, \quad x \geq 0, \lambda \in \Omega_b.$$

The solution $y(x,\cdot)$ is analytic on the interior of Ω_b for each $x \geq 0$.

A.2 Exponential dichotomies

Exponential dichotomies enable us to track solutions in linear systems by separating the solution space in solutions that either decay exponentially in forward time or else in backward time. Moreover, their associated projections inherit analytic dependence of the problem on a spectral parameter λ. Therefore, they provide a natural framework [34] to capture the linear dynamics of eigenvalue problems of the form (A.1) arising in our analysis.

Definition A.2. Let $n \in \mathbb{Z}_{>0}$, $J \subset \mathbb{R}$ an interval and $A \in C(J, \mathrm{Mat}_{n\times n}(\mathbb{C}))$. Denote by $T(x,y)$ the evolution operator of

$$\varphi_x = A(x)\varphi, \quad \varphi \in \mathbb{C}^n. \tag{A.3}$$

Equation (A.3) has *an exponential dichotomy on J with constants $K, \mu > 0$ and projections $P(x) \colon \mathbb{C}^n \to \mathbb{C}^n$* if for all $x, y \in J$ it holds that

- $P(x)T(x,y) = T(x,y)P(y)$;

- $\|T(x,y)P(y)\| \leq Ke^{-\mu(x-y)}$ for $x \geq y$;

- $\|T(x,y)(I - P(y))\| \leq Ke^{-\mu(y-x)}$ for $y \geq x$.

Let $P(x)$ be the family of projections associated with an exponential dichotomy on J. For each $x, y \in J$, we denote by $T^s(x,y) = T(x,y)P(y)$ and $T^u(x,y) = T(x,y)(I - P(y))$ the *stable and unstable evolution* of system (A.3), leaving the projection $P(y)$ implicit.

An autonomous linear system $\varphi_x = A_0\varphi$, where $A_0 \in \mathrm{Mat}_{n\times n}(\mathbb{C})$ is hyperbolic, admits an exponential dichotomy on $\mathbb{R}$. This result can be extended to non-autonomous systems (A.3). If the coefficient matrix $A(x)$ converges to a hyperbolic matrix $A_{\pm\infty}$ as $x \to \pm\infty$, then exponential dichotomies for (A.3) on the half-lines $[0,\infty)$ and $(-\infty, 0]$ can be constructed from the exponential dichotomies of the asymptotic systems $\varphi_x = A_{\pm\infty}\varphi$.

Proposition A.3. *[26, Lemma 3.4], [35, Theorem 1] Let $n \in \mathbb{Z}_{>0}$, $\Omega \subset \mathbb{C}$ open and $A \in C([0,\infty) \times \Omega, \mathrm{Mat}_{n\times n}(\mathbb{C}))$ such that $A(x,\cdot)$ is analytic on Ω for each $x \geq 0$. Suppose that there exist constants $\mu, K, \alpha > 0$ and an analytic map $A_\infty : \Omega \to \mathrm{Mat}_{n\times n}(\mathbb{C})$ such that*

i. Identity (A.2) is satisfied for each $x \geq 0$ and $\lambda \in \Omega$;

ii. For any $\lambda \in \Omega$ the matrix $A_\infty(\lambda)$ is hyperbolic with spectral gap larger than α.

Then, system (A.1) admits for any $\lambda \in \Omega$ an exponential dichotomy on $[0,\infty)$ with constants $C(\lambda), \alpha > 0$ and projections $P(x,\lambda)$, whose rank equals the dimension of the stable eigenspace of $A_\infty(\lambda)$. The projections $P(x,\cdot)$ are analytic on Ω for each $x \geq 0$. Moreover, the map $\lambda \mapsto C(\lambda)$ is continuous.

In addition, we have that the associated dichotomy projections converges to the spectral projection of the hyperbolic matrix $A_\infty(\lambda)$.

Lemma A.4. *[26, Lemma 3.4] Let $n \in \mathbb{Z}_{>0}$ and $A \in C([0, \infty), \mathrm{Mat}_{n \times n}(\mathbb{C}))$. Suppose equation* (A.3) *admits an exponential dichotomy on* $[0, \infty)$ *with constants $K, \mu > 0$ and projections $P(x)$. In addition, suppose there exists a hyperbolic matrix $A_0 \in \mathrm{Mat}_{n \times n}(\mathbb{C})$ with spectral gap larger than μ such that*

$$\|A_0\| \le K, \quad \|A(x) - A_0\| \le Ke^{-\mu x}, \quad x \ge 0.$$

Then, there exists a constant $C > 0$, depending on n, μ and K only, such that

$$\|P(x) - P_0\| \le Ce^{-\mu x}, \quad x \ge 0,$$

where P_0 is the spectral projection onto the stable eigenspace of A_0.

Exponential dichotomies on an interval $J \subset \mathbb{R}$ are in general not unique. If $J = [0, \infty)$, then the range of the dichotomy projection corresponds to the space of solutions decaying in forward time and is therefore uniquely determined, whereas its kernel can be any complement.

Lemma A.5. *[33, Lemma 1.2(ii)] Let $n \in \mathbb{Z}_{>0}$ and $A \in C([0, \infty), \mathrm{Mat}_{n \times n}(\mathbb{C}))$. Suppose equation* (A.3) *admits an exponential dichotomy on* $[0, \infty)$ *with projections $P(x)$. If $Y \subset \mathbb{C}^n$ satisfies $Y \oplus P(0)[\mathbb{C}^n] = \mathbb{C}^n$, then* (A.3) *admits an exponential dichotomy on* $[0, \infty)$ *with projections $Q(x)$, where $Q(0)$ is the projection on $P(0)[\mathbb{C}^n]$ along Y.*

References

[1] R. Bastiaansen and A. Doelman. Pulse dynamics in an extended-klausmeier model with parameters that vary in time and space. *in preparation*, 2017.

[2] F. H. Busse. Non-linear properties of thermal convection. *Rep. Prog. Phys.*, 41(12):1929–1967, 1978.

[3] W. Chen and Ward M. J. Oscillatory instabilities and dynamics of multi-spike patterns for the one-dimensional gray-scott model. *Europ. J. Appl. Math.*, 20(2):187–214, 2009.

[4] Ju. L. Dalec′kiĭ and M. G. Kreĭn. *Stability of solutions of differential equations in Banach space*. American Mathematical Society, Providence, R.I., 1974. Translated from the Russian by S. Smith, Translations of Mathematical Monographs, Vol. 43.

[5] B. de Rijk. Spectra and stability of spatially periodic pulse patterns: the critical spectral curve. *accepted*.

[6] B. de Rijk. *Periodic pulse solutions to slowly nonlinear reaction-diffusion systems*. PhD thesis, Leiden University, 2016.

[7] B. de Rijk, A. Doelman, and J. D. M. Rademacher. Spectra and stability of spatially periodic pulse patterns: Evans function factorization via Riccati transformation. *SIAM J. Math. Anal.*, 48(1):61–121, 2016.

[8] A. Doelman and T. J. Kaper. Semistrong pulse interactions in a class of coupled reaction-diffusion equations. *SIAM J. Appl. Dyn. Syst.*, 2(1):53–96 (electronic), 2003.

[9] A. Doelman, T. J. Kaper, and H. van der Ploeg. Spatially periodic and aperiodic multi-pulse patterns in the one-dimensional Gierer-Meinhardt equation. *Methods Appl. Anal.*, 8(3):387–414, 2001.

[10] A. Doelman, J. D. M. Rademacher, and S. van der Stelt. Hopf dances near the tips of Busse balloons. *Discrete Contin. Dyn. Syst. Ser. S*, 5(1):61–92, 2012.

[11] A. Doelman and F. Veerman. An explicit theory for pulses in two component, singularly perturbed, reaction-diffusion equations. *J. Dynam. Differential Equations*, 27(3-4):555–595, 2015.

[12] W. Eckhaus. *Studies in non-linear stability theory*, volume 6 of *Springer Tracts in Natural Philosophy*. Springer, New York, 1965.

[13] N. Fenichel. Geometric singular perturbation theory for ordinary differential equations. *J. Differential Equations*, 31(1):53–98, 1979.

[14] R. A. Gardner. On the structure of the spectra of periodic travelling waves. *J. Math. Pures Appl. (9)*, 72(5):415–439, 1993.

[15] R. A. Gardner. Spectral analysis of long wavelength periodic waves and applications. *J. Reine Angew. Math.*, 491:149–181, 1997.

[16] A. Gierer and H. Meinhardt. A theory of biological pattern formation. *Kybernetik*, 12(1):30–39, 1972.

[17] D. Henry. *Geometric theory of semilinear parabolic equations*, volume 840 of *Lecture Notes in Mathematics*. Springer-Verlag, Berlin-New York, 1981.

[18] D. Iron, M. J. Ward, and J. Wei. The stability of spike solutions to the one-dimensional Gierer-Meinhardt model. *Phys. D*, 150(1-2):25–62, 2001.

[19] C. K. R. T. Jones and N. Kopell. Tracking invariant manifolds with differential forms in singularly perturbed systems. *J. Differential Equations*, 108(1):64–88, 1994.

[20] T. Kapitula and K. Promislow. *Spectral and dynamical stability of nonlinear waves*, volume 185 of *Applied Mathematical Sciences*. Springer, New York, 2013.

[21] C. A. Klausmeier. Regular and irregular patterns in semiarid vegetation. *Science*, 284(5421):1826–1828, 1999.

[22] J. J. Kovacic. An algorithm for solving second order linear homogeneous differential equations. *J. Symbolic Comput.*, 2(1):3–43, 1986.

[23] X. B. Lin. Using Mel′nikov's method to solve Šilnikov's problems. *Proc. Roy. Soc. Edinburgh Sect. A*, 116(3-4):295–325, 1990.

[24] A. Mielke. The Ginzburg-Landau equation in its role as a modulation equation. In *Handbook of dynamical systems, Vol. 2*, pages 759–834. North-Holland, Amsterdam, 2002.

[25] W. M. Ni. Diffusion, cross-diffusion, and their spike-layer steady states. *Notices Amer. Math. Soc.*, 45(1):9–18, 1998.

[26] K. J. Palmer. Exponential dichotomies and transversal homoclinic points. *J. Differential Equations*, 55(2):225–256, 1984.

[27] J. E. Pearson. Complex patterns in a simple system. *Science*, 261(5118):189–192, 1993.

[28] R. L. Pego and M. I. Weinstein. Eigenvalues, and instabilities of solitary waves. *Philos. Trans. Roy. Soc. London Ser. A*, 340(1656):47–94, 1992.

[29] J. D. M. Rademacher. First and second order semistrong interaction in reaction-diffusion systems. *SIAM J. Appl. Dyn. Syst.*, 12(1):175–203, 2013.

[30] J. D. M. Rademacher, B. Sandstede, and A. Scheel. Computing absolute and essential spectra using continuation. *Phys. D*, 229(2):166–183, 2007.

[31] J. D. M. Rademacher and A. Scheel. Instabilities of wave trains and Turing patterns in large domains. *Internat. J. Bifur. Chaos Appl. Sci. Engrg.*, 17(8):2679–2691, 2007.

[32] *NIST Digital Library of Mathematical Functions*. http://dlmf.nist.gov/, Release 1.0.14 of 2016-12-21. F. W. J. Olver, A. B. Olde Daalhuis, D. W. Lozier, B. I. Schneider, R. F. Boisvert, C. W. Clark, B. R. Miller and B. V. Saunders, eds.

[33] B. Sandstede. *Verzweigungstheorie homokliner Verdopplungen*. PhD thesis, University of Stuttgart, 1993.

[34] B. Sandstede. Stability of travelling waves. In *Handbook of dynamical systems, Vol. 2*, pages 983–1055. North-Holland, Amsterdam, 2002.

[35] B. Sandstede and A. Scheel. Absolute and convective instabilities of waves on unbounded and large bounded domains. *Phys. D*, 145(3-4):233–277, 2000.

[36] B. Sandstede and A. Scheel. On the stability of periodic travelling waves with large spatial period. *J. Differential Equations*, 172(1):134–188, 2001.

[37] J. A. Sherratt. History-dependent patterns of whole ecosystems. *Ecological Complexity*, 14:8–20, 2013.

[38] J. A. Sherratt and G. J. Lord. Nonlinear dynamics and pattern bifurcations in a model for vegetation stripes in semi-arid environments. *Theor. Popul. Biol.*, 71:1–11, 2007.

[39] E. Siero, A. Doelman, M. B. Eppinga, J. D. M. Rademacher, M. Rietkerk, and K. Siteur. Striped pattern selection by advective reaction-diffusion systems: resilience of banded vegetation on slopes. *Chaos*, 25(3):036411, 2015.

[40] K. Siteur, E. Siero, M. B. Eppinga, J. D. M. Rademacher, A. Doelman, and M. Rietkerk. Beyond Turing: The response of patterned ecosystems to environmental change. *Ecological Complexity*, 20:81–96, 2014.

[41] A. M. Turing. The chemical basis of morphogenesis. *Phil. Trans. R. Soc. B*, 237(641):37–72, 1952.

[42] H. van der Ploeg and A. Doelman. Stability of spatially periodic pulse patterns in a class of singularly perturbed reaction-diffusion equations. *Indiana Univ. Math. J.*, 54(5):1219–1301, 2005.

[43] S. van der Stelt, A. Doelman, G. Hek, and J. D. M. Rademacher. Rise and fall of periodic patterns for a generalized Klausmeier-Gray-Scott model. *J. Nonlinear Sci.*, 23(1):39–95, 2013.

[44] A. Vanderbauwhede and B. Fiedler. Homoclinic period blow-up in reversible and conservative systems. *Z. Angew. Math. Phys.*, 43(2):292–318, 1992.

[45] F. Veerman. Breathing pulses in singularly perturbed reaction-diffusion systems. *Nonlinearity*, 28(7):2211–2246, 2015.

[46] F. Veerman and A. Doelman. Pulses in a Gierer-Meinhardt equation with a slow nonlinearity. *SIAM J. Appl. Dyn. Syst.*, 12(1):28–60, 2013.

[47] M. J. Ward and J. Wei. Hopf bifurcations and oscillatory instabilities of spike solutions for the one-dimensional Gierer-Meinhardt model. *J. Nonlinear Sci.*, 13(2):209–264, 2003.